TOWARD HIGH-THROUGHPUT ZEOLITIC IMIDAZOLATE FRAMEWORK ZIF-8 MEMBRANES FOR PROPYLENE/PROPANE SEPARATION

A Dissertation

by

MOON JOO LEE

Submitted to the Office of Graduate and Professional Studies of
Texas A&M University
in partial fulfillment of the requirements for the degree of

DOCTOR OF PHILOSOPHY

Chair of Committee,	Hae-Kwon Jeong
Committee Members,	Hongcai Joe Zhou
	Yossef Elabd
	Benjamin Wilhite
Head of Department,	M. Nazmul Karim

May 2018

Major Subject: Chemical Engineering

ABSTRACT

Separations of light olefin/paraffin, e.g., ethylene/ethane and propylene/propane, are crucial in the petrochemical industries. However, conventional separation processes, e.g., cryo-distillation, require tremendous amounts of energy and high capital cost. Membrane-based separations are a promising alternative to conventional separation processing, however, because of the limited separation capability of current membrane materials, such as polymers, the development of advanced membrane materials is highly desirable.

Zeolitic-imidazolate frameworks (ZIFs) are nanoporous crystalline materials with well-defined ultramicropores (< 5 Å), thereby attractive for membrane-based gas separations. A prototypical ZIF-8 have shown unprecedented propylene/propane separation capabilities because of its effective aperture size of ca. 4 Å, which is in between the sizes of propylene and propane. However, some challenges are impeding their commercial applications; slow batch processes, expensive and fragile ceramic supports, long-term stability, lack of general processing methods. A significant improvement in the productivity (*i.e.*, throughput) of polycrystalline ZIF-8 membranes is required to overcome the current challenges of membrane processing. Therefore, the membrane productivity can be enhanced by increasing membrane area and substantially reducing membrane thickness.

In this dissertation, advanced membrane processing techniques toward high flux ZIF-8 membranes for their practical propylene/propane separation are proposed. Two unique membrane fabrication methods, *in situ* counter diffusion method and microwave-seeding and secondary growth method, previously developed from our group were chosen and thoroughly studied in the overall study. Firstly, the separation performances of ZIF-8 membranes depend on

synthesis method, for propylene/propane separation, are studied. Defect-density of ZIF-8 powders and membranes were characterized with a series of characterizations. Post-synthetic treatments effectively stabilized less stable membranes. Secondly, high propylene-throughput ZIF-8 membrane was prepared by a novel approach for propylene/propane separation. Propylene-selective layer thickness was systematically reduced via post-synthetic linker exchange of ZIF-8 membranes. The resulting linker-exchanged ZIF-8 membranes exhibited significant increase in propylene permeance by four times. Lastly, scalable ZIF-8 membrane processing method on polymeric hollow fiber substrates is introduced. The unique microwave-assisted seeding prepared was capable of ultrathin ZIF-8 membranes formation. Propylene/propane separation performance of resulting ZIF-8 membranes was performed.

To my loving husband for his loving support and patience
To my parents for their endless love and prayers
And to God

ACKNOWLEDGEMENTS

I would like to thank my committee chair, Prof. Jeong, for his endless support and guidance in research and friendly advice on career and personal life. Without his guidance and consistent help this dissertation would not have been possible. I would like to thank my committee members, Prof. Zhou, Prof. Elabd, and Prof. Wilhite, for their precious guidance and sincere support throughout the course of this research.

Thanks also go to my friends and colleagues, Hyuk Taek, for his valuable works which greatly ease my research, Rezi, for his friendship and great talents for making essentially anything, Yu-Chen, for his hardworking, creativity, humor and kindness, Stephanie, for her caring heart, friendship and hardworking. I would also like to thank Jingze, Febrian, Sungwhan, Dr. Kie-Yong, Chen, Prof. Lim, Prof. Bae, Jaemin and and the department faculty and staff for making my time at Texas A&M University a great experience.

Finally, I give my thankful heart to my father, mother, father-in-law, and mother-in-law for their prayer, support, and encouragement and to my husband for his support, encouragement and love.

CONTRIBUTORS AND FUNDING SOURCES

This work was supported by a dissertation committee consisting of Professor Hae-Kwon Jeong [advisor] and Professor Yoseef Elabd and Professor Benjamin Wilhite of the Department of Chemical Engineering and Professor Hongcai Joe Zhou of Department of Chemistry.

The data analyzed for Chapter III were conducted in part by Dr. Albert S. Lee at the Korea Institute of Science and Technology (KIST) for taking solid-state NMR spectra and by Mr. Touseef Habib at Texas A & M University for taking TGA data. In Chapter IV, the propylene/propane separation data of CD-ZIF-8 and Ica-exchanged CD-ZIF-8 membranes were done by Dr. Hyuk-Taek Kwon who graduated Texas A&M University. The analyses depicted in Chapter IV were conducted in part Dr.Jun Kyun Oh, Joshua Weatherston, and Tzu-Ling Cheng at Texas A&M University for performing contact angle measurements, Raman spectroscopy, and ATR-FTIR analyses, respectively. The hollow fiber substrates used in Chapter V was prepared by Dr. Jongmyeong Lee and Mr. Jusung Kim at Hanyang University. The ZIF-8 membrane syntheses and measurements performed in Chapter V were done equally by Mohammed Rezi Abdul Hamid at Texas A&M University. All other work conducted for the dissertation was completed by the student independently.

Graduate study was supported by in parts from the National Science Foundation (CBET-1510530), the Qatar National Research Fund (NPRP 7-042-2-021 and NPRP 8-001-2-001), the R & D Convergence Program of MSIP (Ministry of Science, ICT and Future Planning), NST (National Research Council of Science & Technology) of the Republic of Korea (CRC-14-1-KRICT).

TABLE OF CONTENTS

LIST OF FIGURES

LIST OF TABLES

CHAPTER I
INTRODUCTION

Light olefins, e.g., ethylene and propylene, are essential starting materials and, therefore, separation of these olefins from paraffins is one of the most significant separations in the petrochemical industries. However, the olefin/paraffin separation processes are challenging because of their similar physicochemical properties (*i.e.*, boiling points and size).[1-3] Conventional separation processes depend on thermally-driven processes to bring down the temperature, e.g., cryo-distillation, thereby consuming significant amounts of operating energy and requiring high capital cost.[2-3] Membrane-based gas separations[4-5] have drawn massive interest as promising alternative non-thermally driven processes. Membrane separations rely on materials' properties, such as separation performances, and operational conditions. For propylene/propane separation, the range of membrane materials have been widely studied, e.g., polymers,[3, 6] carbon molecular sieves,[7-8] and zeolites.[9] However, no membranes are commercially available for the separation of light olefin/paraffin molecules[2], mainly because of the limited separation capability of current membrane materials[3] and their processing techniques, thereby the development of advanced membrane materials is highly desirable.

Zeolitic-imidazolate frameworks (ZIFs) are a subclass of metal-organic frameworks (MOFs), composed of divalent metal cations (usually Zn^{2+} or Co^{2+}) and bidentate imidazolates. ZIFs exhibit well-defined ultramicropores (< 5 Å) with relatively robust chemical and thermal stabilities in comparison to other MOFs,[10] thereby attractive for their commercial applications. Unlike other MOFs, ZIFs possess unique zeolite topologies because of the metal-ligand-metal bond angle (145 °) that are similar to the Si-O-Si bond angle in zeolites (145 °).[11] A prototypical

ZIF-8, composed of zinc cations coordinated with 2-methylimidazoles forming sodalite (SOD) topology, is a promising material for gas separations[12-15], such as CO_2/CH_4 separation[16-18], H_2 separation from small hydrocarbons[19]. In particular, ZIF-8 showed impressive kinetic separation capability of propylene/propane[20-21] because of its effective aperture size of ca. 4 Å,[22] which is in between the sizes of propylene and propane. Lately, several pure polycrystalline ZIF-8 and ZIF-67 (Co-substituted ZIF-8) membranes reported propylene/propane separation factors above 150.[23-24] Lee et al.[24] reported ZIF-8 membranes synthesized by using microwave-seeding and secondary growth on alumina discs with the separation factor (hereafter, SF) of 203 with the propylene permeance of 55 GPU (gas permeation unit, 1 GPU = 3.348×10^{-10} mol m^{-2} s^{-1} Pa^{-1}). Kwon et al.[25] reported ZIF-67 membranes heteroepitaxially grown on ZIF-8 seeded alumina disc. Resulting membrane showed the SF of 209 and propylene permeance of 111 GPU.

ZIFs have shown unprecedented propylene/propane separation capabilities than other membrane materials. However, some challenges are impeding their commercial applications; slow batch processes, expensive and fragile ceramic supports, long-term stability, lack of general processing methods.[12] A significant improvement in the productivity (*i.e.*, throughput) of polycrystalline ZIF-8 membranes is required to overcome the current challenges of membrane processing. The membrane productivity is given by the following equation [Eq. (1-1)]:

$$Q_i = -P_i\,(\Delta\rho_i/l)A \qquad (1\text{-}1)$$

where P_i, $\Delta\rho_i$, l, and A are the permeability and partial pressure difference of gas i between feed and permeate sides, membrane thickness, and membrane area, respectively. Therefore, the membrane productivity can be enhanced by increasing membrane area and substantially reducing membrane thickness.

In this regards, the dissertation is focusing on the development of membrane processing techniques toward high flux ZIF-8 membranes for their practical propylene/propane separation. Two unique membrane fabrication methods, *in situ* counter diffusion method (hereafter, CD method) and microwave-seeding and secondary growth method (hereafter, MW method), previously developed from our group were chosen and thoroughly studied in the overall study.

This dissertation is composed of six chapters, including a literature review on Chapter II. The results are presented and discussed in Chapter III through V, the study of ZIF-8 synthesis methods in the effect of long-term separation stability and their post-synthetic modification to engineer high propylene throughput ZIF-8 membranes. Chapter III is dedicated to the long-term propylene/propane separation stability of ZIF-8 membranes depend on the fabrication conditions, CD and MW methods. A range of characterization tools thoroughly studied Defect-density of ZIF-8 membranes. Post-synthetic treatments effectively stabilized kinetically unstable membranes. In Chapter IV, a novel method is studied that can reduce the effective thickness of ZIF-8 membranes for high-throughput propylene/propane separation. The physical membrane thickness remained intact; however, effective membrane thickness that can separate propylene/propane was reduced via post-synthetic linker exchange of ZIF-8 with different organic linkers. The linker-exchanged ZIF-8 membranes showed a dramatic increase in propylene permeance by four times. Chapter V is introducing new and scalable ZIF-8 membrane processing technique on polymeric hollow fiber substrates. Our unique microwave-assisted seeding prepared ultrathin ZIF-8 membranes under the microfluidic condition, followed by microfluidic secondary growth. Propylene/propane separation performance of resulting ZIF-8 membranes was conducted.

Finally, the conclusion of the dissertation and the suggestion of future works are described in Chapter VI.

CHAPTER II
BACKGROUNDS AND LITERATURE REVIEWS

2.1. Light olefin/paraffin separation

2.1.1. Current light olefin markets

Light olefins (e.g., ethylene and propylene) are the most demanding starting materials in the petrochemical industry. Propylene is the second most crucial material after ethylene, and their global demand in 2015 was estimated at 94.2 million tons. As can be seen in Figure 2-1, propylene is used to produce intermediate petrochemical feedstocks, such as polypropylene, which are used to fabricate a range of consumer products, such as plastics, resins, adhesives, and coatings.

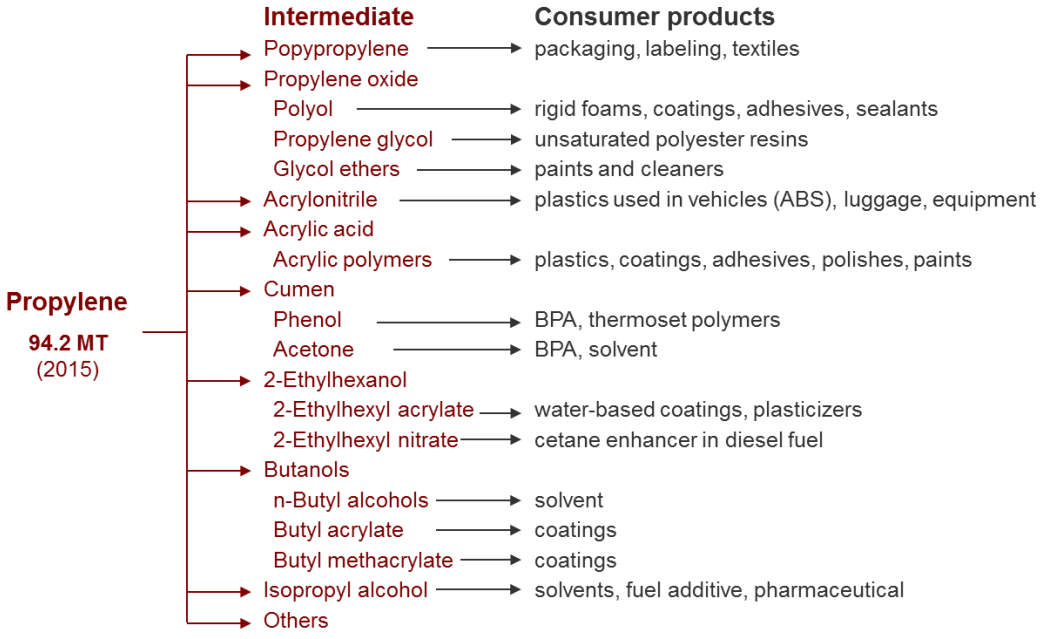

Figure 2-1 Petrochemicals produced from propylene as feedstock. Reprinted with permission.[26]

Conventional propylene productions are naphtha-fed steam crackers, and the fluid catalytic cracking (FCC) units of oil refineries and together dominates 90 % of the market. Notably, propylene is a secondary product in both cases. According to Bricker[27-28], there is a growing gap of propylene in the supply-demand curve (see Figure 2-2). This is mainly because 1) petrochemical industry (*i.e.*, steam cracker) is turning to lighter feedstock (*i.e.*, ethane) since ethane is the cheapest feedstock and 2) gasoline is not much interesting in which limited the amount of propylene produced during the oil-refining process. As conventional propylene production is declining and impossible to meet market demands, the importance of on-purpose production techniques is drawing attention and expected to supply one-quarter of the demand by 2021.

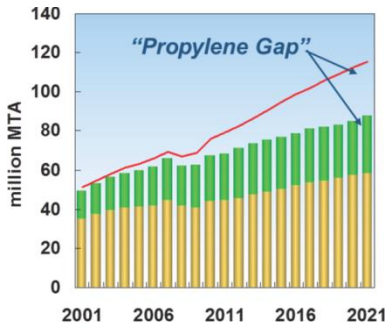

Figure 2-2 Schematic diagram depicts growing gap between propylene supply from (—) refinery FCCs and (—) steam crackers and (—) demand. Noted, FCC refers fluid catalytic cracking and MTA denotes million tons annually. Reprinted with permission.[28] Copyright 2016 by National Academies Press.

2.1.2. Conventional separation processes

Propylene/propane separation is essential for propylene production since propylene is a secondary product of propane production, *i.e.*, FCC and steam cracking processes. It is challenging to separate light olefins from paraffins due to their similar physicochemical

properties, such as boiling point. Therefore, thermally-driven separation processes are frequently used, which require significant energy to bring down the temperature to distillate (*i.e.*, cryogenic distillation).

As shown in Figure 2-3, industrial energy sector consumed ~ 30 % of total US energy consumption in 2016. 45 ~ 55 % of the industrial energy sector was consumed by separation processes, meaning that chemical separation consumed up to 13~16 % of total energy, and distillation separation used ~ 50 %.[4] Developing alternative techniques, *i.e.*, non-thermally-driven separation processing, that can reduce energy consumption and operational costs is necessary. There are three quality grades of propylene: refinery (minimum 70% propylene), chemical (minimum 92%-96%) and polymer (minimum 99.5%). Obtaining high purity propylene (> 99.5 %) makes the alternative energy saving processes a lot more challenging.

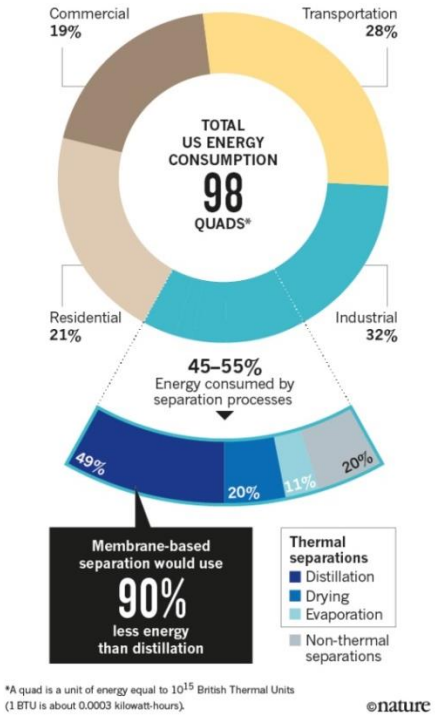

Figure 2-3 The total U.S. energy consumption by sector, 2016 and energy usage in chemical separations by thermal and non-thermal processes. 1 Quad BTU is equivalent to 1.055×10^{18} joules. Reprinted with permission.[29] Copyright 2016 by Nature.

2.1.3. Membrane separation

Membrane-based separations are a promising alternative to thermally-driven separation processes that can save significant amounts of energy by the hybrid system (~ 50 %) or by independent process (~ 90%).

The membrane-based gas separation performance is commonly expressed with two materials' intrinsic properties, permeability and selectivity. The permeability of gas A, P_A, is a quantity of gas A transport through membrane and described as following equation [Eq. (2-1)]:

$$P_A = \frac{N_A}{driving\ force} \tag{2-1}$$

where N_A is flux of gas A through membrane and driving force is expressed as differences of concentration or pressure across membrane. Gas transport through membranes may follow different mechanisms depends on gas and membranes, such as bulk flow for large pores and Knedsen diffusion for intermediate size pores. For membrane-gas separation, in general, the solution-diffusion model described as following equation is used [Eq. (2-2)]:

$$P_A = S_A \times D_A \tag{2-2}$$

where P, S, and D are the permeability, solubility, and diffusivity of gas A through membrane, respectively. Therefore, the membrane selectivity of gas mixture is as following equation [Eq. (2-3)].

$$S_{A,B} = \frac{P_A}{P_B} = \frac{S_A}{S_B} \times \frac{D_A}{D_B} \tag{2-3}$$

where $S_{A,B}$ is the ratio of permeability of gas A and permeability of gas B through membrane. The separation performances of membranes also dependes on processing techniques, which is permeance of gas A, $\wp_A$, is permeability of gas A divided by the membrane thickness, L.

Several types of materials are studied for propylene/propane separation, such as polymers[3, 6, 30-37] and carbon molecular sieves[8, 37-39]. Polymers dominate in a range of separation processes including gas separations mainly due to excellent processing techniques that can engineer polymers into high surface area per unit volume modules at low cost. However, in the case of propylene/propane separation, polymers have shown limited separation capabilities mainly due to their flexible nature. Figure 2-4 is a so-called Robeson plot of propylene/propane separation. Colling et al. claimed that the separation performance of the membrane with separation factor above 35 and permeability over 1 Barrer could be considered commercially viable materials and is shown in the blue box. Polymeric membranes have shown performances mostly limited to polymeric upper bound and this is mainly due to their solution-diffusion based separation. Whereas, carbon molecular sieve membranes exhibited higher upper bounds and some membranes have shown commercially viable separation performances. Carbon membranes showed better performances than polymers due to their molecular sieving selectivity. Moreover, ZIFs, which are advanced sieving materials, membranes[23-25, 40-53] have shown impressive separation performances.

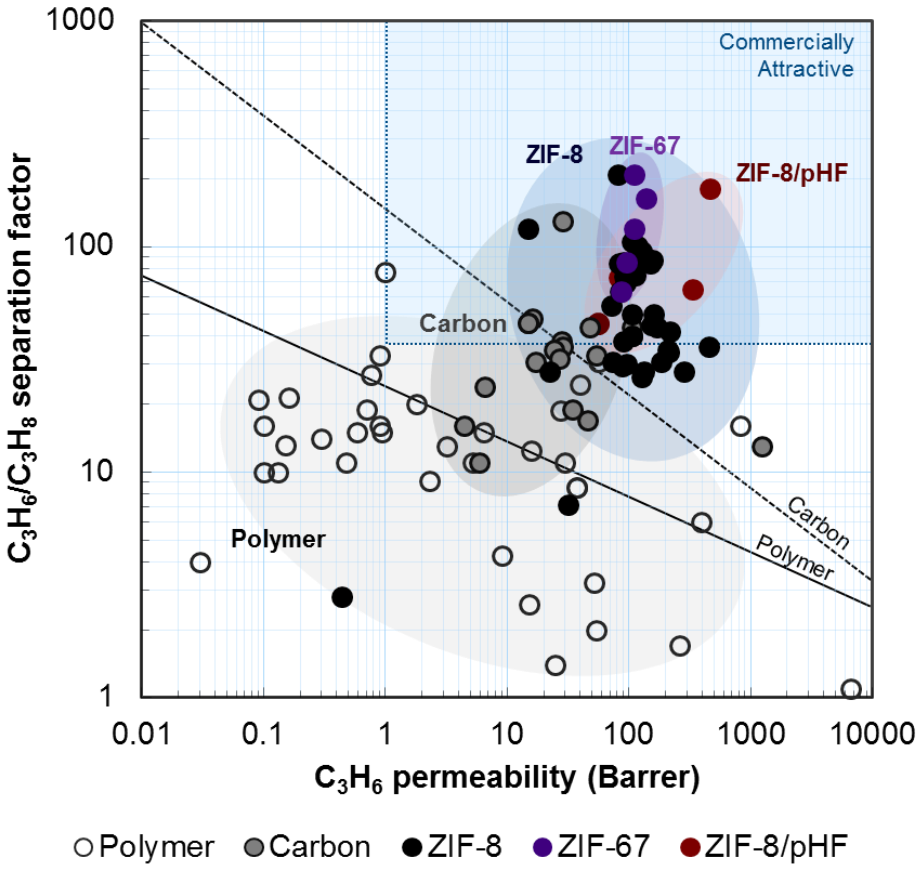

Figure 2-4 Propylene/propane separation performances of polymer, carbon, ZIF-8, ZIF-67[25, 53], and ZIF-8/pHF membranes from the literature. Data for some polymer and carbon membranes were based on single gas measurements. The upper bounds for polymer[3] (solid line) and carbon[8] (dotted line) are shown as well as the commercially attractive performances[54]. 1 Barrer = 3.348×10^{-16} mol·m·m^{-2}·s^{-1}·Pa^{-1}.

2.2. Zeolitic-Imidazolate Frameworks (ZIFs)

Zeolitic-imidazolate frameworks (ZIFs)[10-11, 55-57] are a subclass of metal-organic frameworks (MOFs)[58-60] and are composed of divalent metal nodes (e.g., Zn^{2+} and Co^{2+}) and bidentate imidazole-derived organic linkers. Similar to MOFs, ZIFs possess high crystallinity, uniformly distributed porosity, ultra-microporosity (generally less than 5.0 Å), and high surface area. The unique metal-linker-metal bond angle of ZIFs resembles Si-O-Si bond angle of zeolites, thus showing zeolitic topologies (see Figure 2-5). ZIFs exhibit higher thermal, mechanical and chemical stability compared to other MOFs[11], thus making ZIFs attractive for practical applications, such as catalysis[61], drug delivery[62-63], separation[12, 14, 64], and adsorption[65].

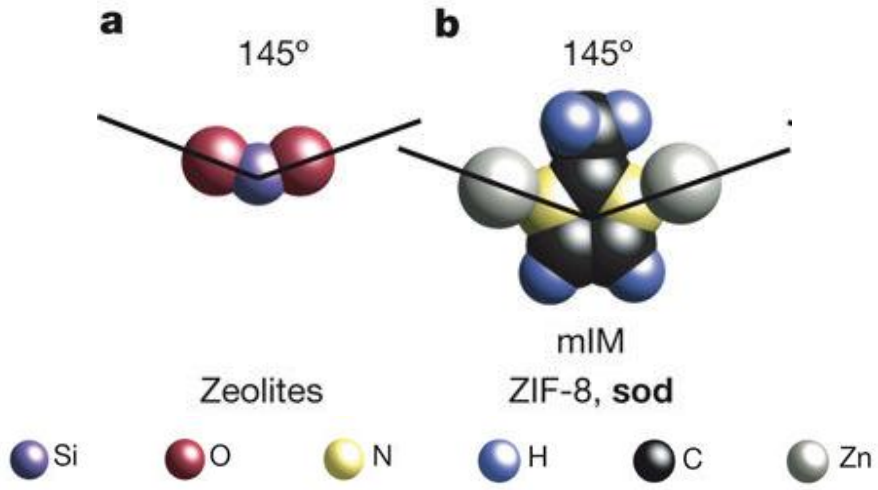

Figure 2-5 The bridging angles in metal ZIFs (a) and zeolites (b). Reprinted with permission.[57] Copyright 2008 by Nature.

2.2.1. Formation chemistry

The bonding between metal nodes and organic linkers is coordination bonding, which is kinetically weaker than covalent bonding in zeolites. The simple acid-base reaction and their formation mechanism, in the case of ZIF-8, are previously proposed by Cravillon *et al.*[66] which is again claimed later by other groups,[67-68] as shown in Figure 2-6. The organic linkers in solution phase donate lone pair electrons to metal ions and form a metal-ligand coordinated complex. The coordination can propagate once the organic ligand of the complex is deprotonated, which is capable only by the more basic molecules than the complex. In this aqueous reaction, 2-methylimidazole (H-mIm) itself has higher pK_a than the pK_a of the complex, indicating is more basic than the complex, the H-mIm can deprotonate the imidazole of the complex. Cravillon *et al.* proposed that the deprotonation step is the rate-determining step in the crystal formation, and the crystal size decreases as the deprotonation step is favored, meaning that the nucleation step is favored than the growth condition. Therefore, the higher the ligand-to-metal molar ratio, the smaller crystal size is obtained.

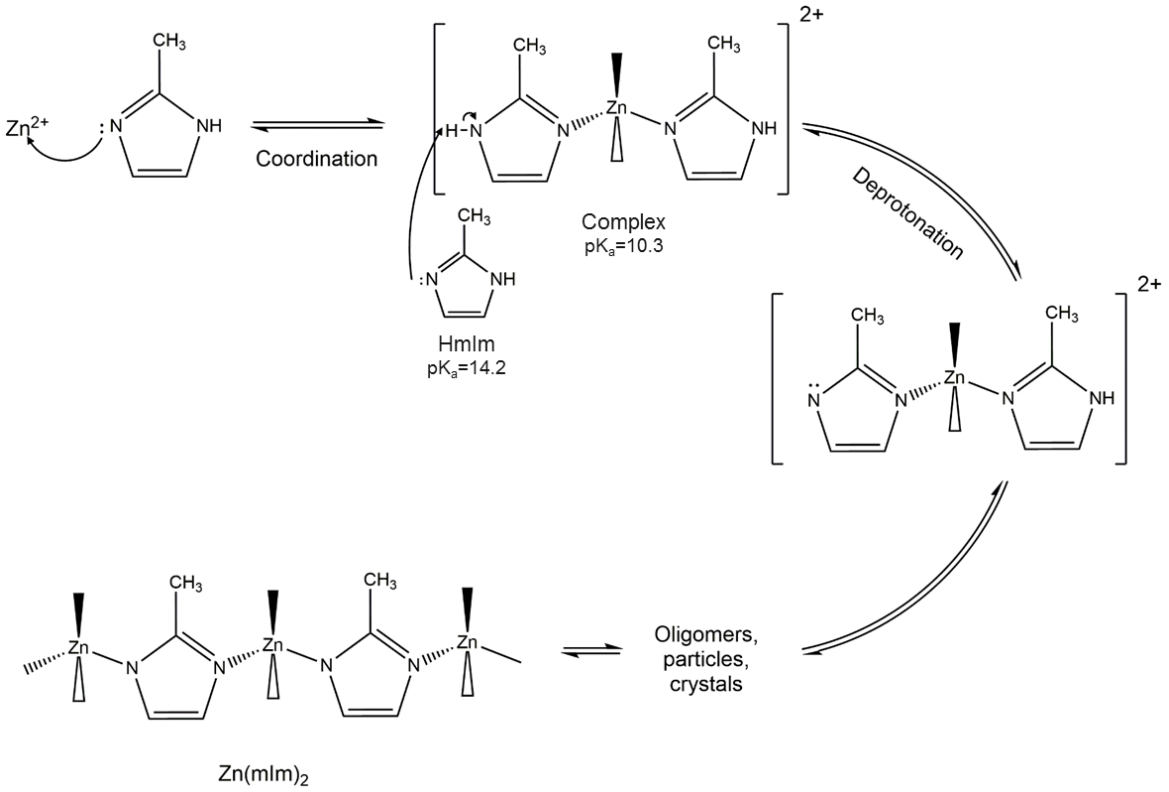

Figure 2-6 Proposed mechanism of ZIF-8 crystal formation chemistry in aqueous solution.

2.2.2. Gas transport through SOD ZIFs

2.2.2.1. ZIFs with SOD topology

Figure 2-7 illustrates sodalite (hereafter, SOD) zeolitic topology and ZIFs exhibit SOD ntes of which are preferred in gas separation application. One SOD cage is shown in Figure 2-7a, which consists of six 4-membered rings (4MR), eight 6-membered rings (6MR), and one large cavity which depicts the volume of the cage by a yellow sphere. As shown in figure 2-7b, nine SOD cages are interconnected to neighboring cages through 6MRs where guest molecules can enter to and diffuse through the frameworks. One SOD cages of different ZIFs structures containing zinc and cobalt ions are shown in Figures 2-7c and d, respectively. The prototypical ZIF-8 is composed of zinc and 2-methylimidazole with large cavity diameter of 11.0 Å and 6MR apertures diameters defined by crystallography of 3.4 Å.[11]

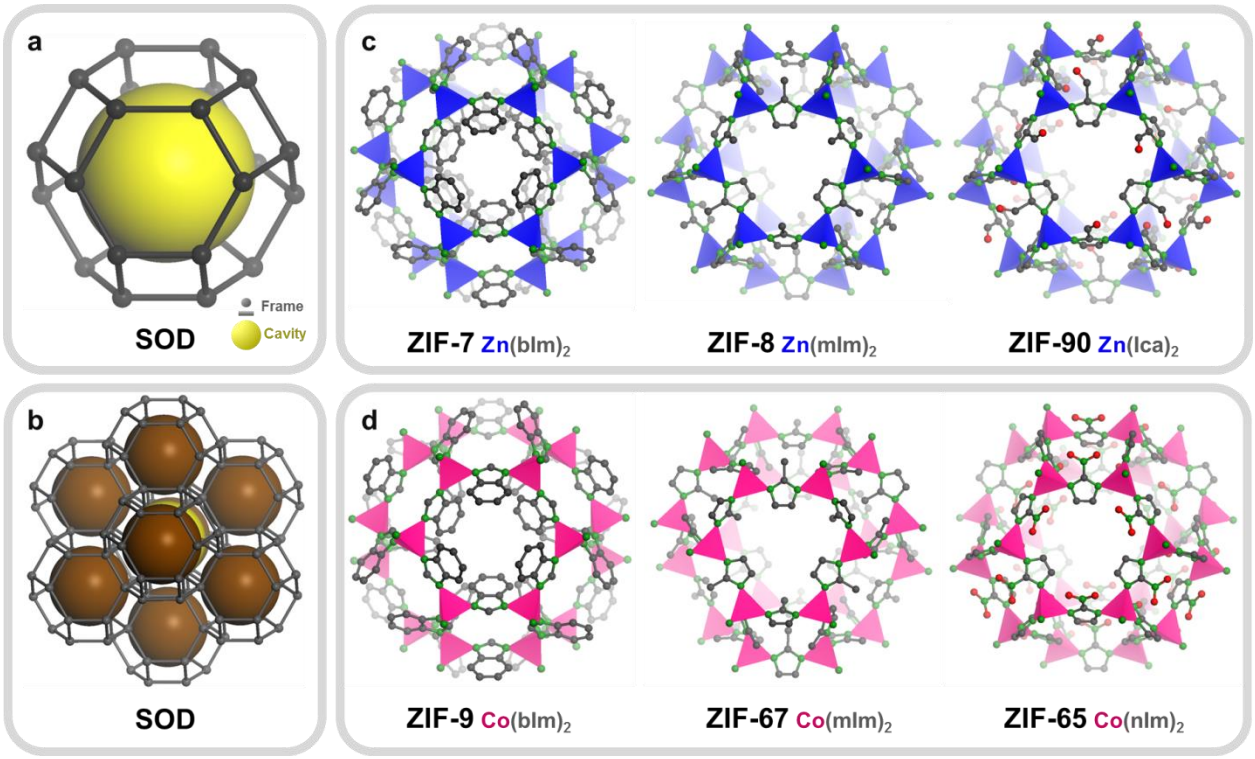

Figure 2-7 Schematics of (a, b) sodalite nets and (c, d) sodalite ZIFs with 6-membered rings located on the center are presented. The net shown in (a) describe the large cavity in yellow spheres and (d) indicate nine SOD cages interconnected, by which depicting eight cavities of the interconnected cages in brown spheres. The single-crystal XRD structures of ZIFs are shown with tetrahedral Zn in blue and Co in pink. The structures have been simplified by omitting H atoms. Linkers are shown in ball and stick illustration (C: dark grey, N: green, O: red). Note: bIm = benzimidazole, mIm = 2-methylimidazole, Ica = 2-imidazolecarboxaldehyde, nIm = 2-nitroimidazole.

2.2.2.2. Propylene-selective ZIFs: ZIF-8 and ZIF-67

As shown in Figure 2-4, ZIF-8 and ZIF-67 (*i.e.*, Co-substituted ZIF-8) have shown exceptional propylene-selectivity, though aperture size of 6 MR, *i.e.*, 3.4 Å, is smaller than the diameter of propylene (4.0 Å) and propane (4.3 Å). This unexpected allowance of guest molecules larger than the aperture size[16, 69] was explained by organic ligands flip-flop motions evidenced by experiments[70-71] and simulations.[72-74] The effective aperture size of ZIF-8 is, therefore, claimed ca. 4.0 Å based on the sharp decrease corrected diffusivities observed between

propylene and propane.[22] As can be seen in Table 2-1, the propylene/propane separation through ZIF-8 is kinetic separation. Activation energy of diffusion of propane is greater than propylene, meaning that propylene has to overcome greater energy barrier to diffuse through ZIF-8 crystals due to the restricted pore size. On the other hand, the isosteric heats of adsorption of propylene and propane are comparable, which means similar solution affinity of guest molecules to ZIF-8 crystals. Therefore, propylene/propane separation is diffusion-based sieving mechanism.

Table 2-1 Summary of activation energy of diffusion of propylene and propane through ZIF-8 and isosteric heats of adsorption of propylene and propane to ZIF-8 data calculated by molecular dynamic simulations and by experiments reported previously from other groups.

ZIF-8	Activation energy of diffusion (KJ/mol)		Isosteric heats of adsorption (KJ/mol)	
	C_3H_8	C_3H_6	C_3H_8	C_3H_6
MD simulations[75]	31 ± 2	17 ± 2	25.9	26.3
Experiments[40]	38.8	12.7	N/A	N/A
Experiments[76]	26.6	15.1	18.9	12.7
Experiments[20]	N/A	N/A	30	34

2.2.2.3. Pore tuning of SOD ZIFs

Sodalite ZIFs (e.g., ZIF-7, -8, -67, -90), which are desirable in gas separation, and have diverse aperture diameters with different combination of metal ions and organic linkers. Notably, discrete number of aperture diameters allows sieving separations of limited gas pairs, e.g. propylene/propane by ZIF-8. Therefore, tuning aperture size of SOD-ZIFs is highly attractive. In this regard, isostructural ZIFs with mixed-linkers and/or mixed-metals can provide a continuous range of aperture size, furthermore, can implement new chemical and physical properties. For example, ZIF-8 and ZIF-90 exhibit crystallographically defined aperture size of 3.4 Å[11] and 3.5 Å[56], respectively. However, their effective aperture size is 4.0[22] and 5.0 Å[77] due to different

combination of metal and ligands. Eum et al.[77] reported mixed-linker approach for tunable aperture size of ZIF-8. Hybrid ZIF-8-90 powders were prepared by *de novo* mixed-linker approach and n-butane and i-butane corrected diffusivities were obtained. The more the 2-imidazolecarboxaldehyde (i.e., ZIF-90 linker, hereafter, Ica) is added to ZIF-8, the greater the diffusivities of n-butane and i-butane were observed. Similarly, ZIF-67 exhibits tighter aperture than ZIF-8,[75] thereby higher separation capability.[25] Hillman et al.[53] prepared hybrid ZIF-8-67 by de novo approach and observed enhanced propylene/propane separation performance. As shown in Figure 2-8, hybrid ZIFs approach can provide a wide range of aperture size. Careful addition of ZIF-7 linker to ZIF-8 frameworks can provide small gas separations, such as CO_2 separation.

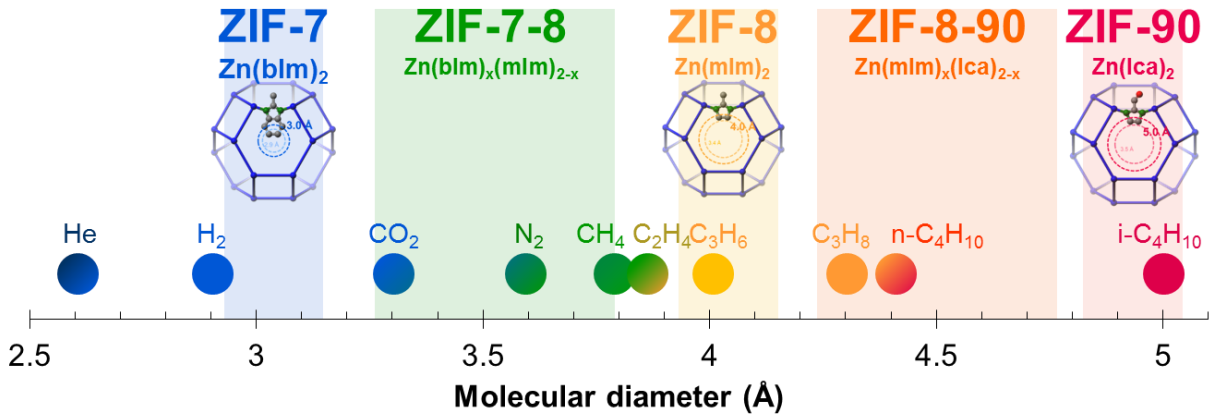

Figure 2-8 Schematic diagram of tuning aperture size of ZIFs by the post-synthetic hybrid-linker approach. The range of ZIFs apertures openings are based on their effective aperture sizes from the literature, in the case of ZIF-8[22] and ZIF-90[77] and their mixed linker ZIFs, and assumed in the case of ZIF-7.

2.2.3. Synthesis of polycrystalline membranes:

Fabrication of crystalline materials in the form of membranes is mainly divided in two types: pure polycrystalline membranes supported on porous substrates and mixed matrix membranes. In this chapter, synthesis of pure polycrystalline membranes will be discussed.

2.2.3.1. Criteria of polycrystalline membranes

Characteristics of polycrystalline membranes required for gas separation application is described in Figure 2-9. Membranes of crystalline materials are composed of numerous crystal grains that are continuously intergrown with each other. Quality of grain boundary, which is interlayers of grains, is a critical factor determines the separation performance of selective layer. Strong adhesion between selective layer and supporting layer is essential. The thickness of membrane and the surface area to volume ratio of support affect the separation productivity of membranes. Defect-free and smooth surface of supporting layer is necessary to ensure the quality of grain boundary structure.

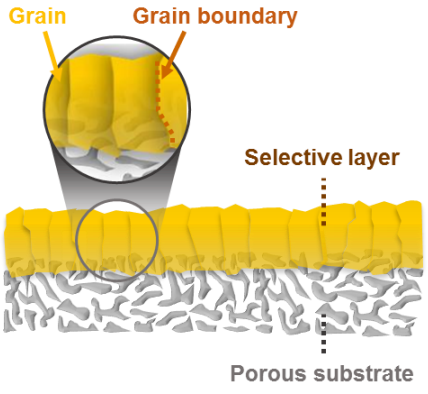

- **Selective polycrystalline layer**
  1. Perfect grain boundary structure
  2. Good adhesion with supporting layer
  3. Thin selective layer
- **Porous substrate**
  1. High surface area to volume ratio
  2. Porous asymmetric fiber
  3. Smooth surface without skin layer
  4. Economical polymer
  5. Excellent mechanical strength
  6. Good chemical strength

Figure 2-9 Schematic illustration of polycrystalline membrane supported on porous substrate and required characteristics for gas separation applications.

2.2.3.2. Conventional solvothermal and hydrothermal synthesis

Conventional fabrication of polycrystalline membranes are solvothermal and hydrothermal synthesis methods, which are broadly categorized by *in situ* and seeded (secondary) growth methods. As shown in Figure 2-10, in situ method is one step simple method, therefore economical method. On the other hand, seeded secondary growth requires additional seeding step followed by secondary growth. Although the seeding step adds complexity and increase costs, decoupling nucleation and growth leads to better control of grain boundary structure. With the high quality seed layer, the high quality selective layer with thinner thickness can be readily prepared.

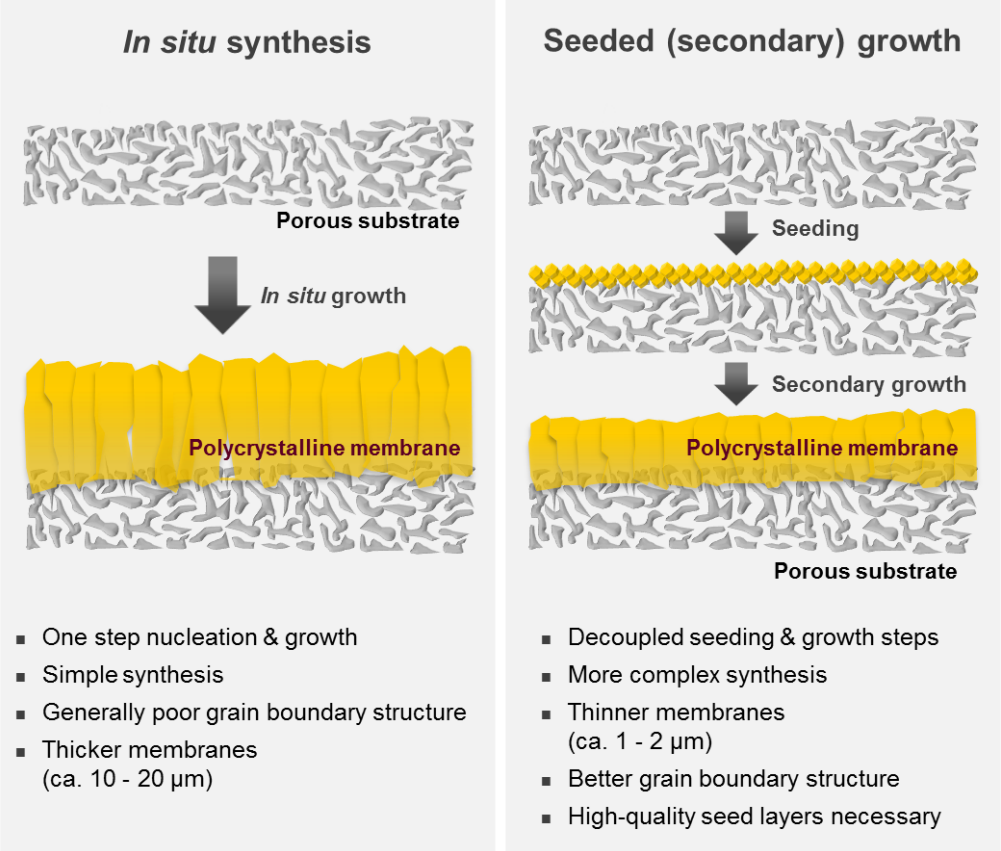

Figure 2-10 Schematic illustration of (left) *in situ* and (right) seeded secondary growth synthesis of polycrystalline membranes on porous alumina substrates and pros/cons of each method.

2.2.3.2.1. *In situ* synthesis

Conventional in situ solvothermal or hydrothermal synthesis is a method where a porous substrate is immersed in a mixture of a precursor solution of metal and ligand and heated until crystal formed. Bux et al.[16] reported defect-free ZIF-8 membranes (ca. 30 μm) synthesized on porous titania supports for hydrogen separation under microwave-assisted heating. Huang et al.[78] fabricated ZIF-22 membranes on surface modified TiO_2 porous substrate by *in situ* solvothermal method for hydrogen separation. Prior to crystal growth, the surface of TiO_2 support was chemically modified by 3-aminopropyltriethoxysilane (APTES), where APTES is serving as a covalent linker. ZIF-22 membranes (ca. 40 μm) were prepared on the APTES-functionalized support. Huang et al.[79] fabricated ZIF-90 membranes (ca. 20 μm thick) on APTES modified α-alumina support by solvothermal synthesis method. The APTES-modification was successfully applied to the preparation of ZIF-8 membranes on tubular α-alumina substrates for CO_2/CH_4 separation.[80] Well-intergrown ZIF-8 membranes (ca. 25 μm thick) were fabricated on the APTES-functionalized tubular support by microwave-assisted solvothermal method. ZIF-8 membranes were prepared by polydopamine-modified α-alumina discs[81] and stainless-steel-nets[82]. Shah et al.[83] reported a new chemical modification α-alumina discs with zinc and sodium formate to prepare continuous and well-intergrown ZIF-8 membranes (ca. 25 μm). During the in situ growth step, zinc salts and sodium formate leads to the formation of zinc oxide which acts not only as a heterogeneous nucleation sites but also secondary zinc sources for crystal growth.

Surface modification of supports is required to provide heterogeneous nucleation sites and to ensure strong adhesion of a crystalline layer with a supporting layer. However, this additional step is not desirable. Yao et al.[84] prepared ZIF-8 film on porous nylon support by contra-diffusion in situ method. The nylon membrane was placed in a diffusion cell where a

precursor solution of zinc salts and ligands are supplied from each side. Defect-free ZIF-8 membranes (ca. 16 μm thick) was tested for hydrogen separation. Kwon et al.[45] reported well-intergrown ZIF-8 membrane by in situ solvothermal synthesis on α-alumina disc for propylene/propane separation. As shown in Figure 2-11, ZIF-8 membrane was prepared by immersion of an α-alumina disc, which was saturated with metal ions, in a precursor solution of organic linker followed by solvothermal growth. This so-called counter-diffusion *in situ* method leads to the formation of continuous and well-intergrown thin ZIF-8 membranes (ca. 1 μm) with propylene/propane separation factor of 55. The ZIF-8 crystals are formed in the vicinity of the counter-diffusion of precursors, thus leading to the physical locking of ZIF-8 selective layer to the supporting porous alumina discs. Hara et al. successfully prepared ZIF-8 membranes on α-alumina capillary tubes by counter-diffusion *in situ* method[76] and interfacial *in situ* method[85] for propylene/propane separation.

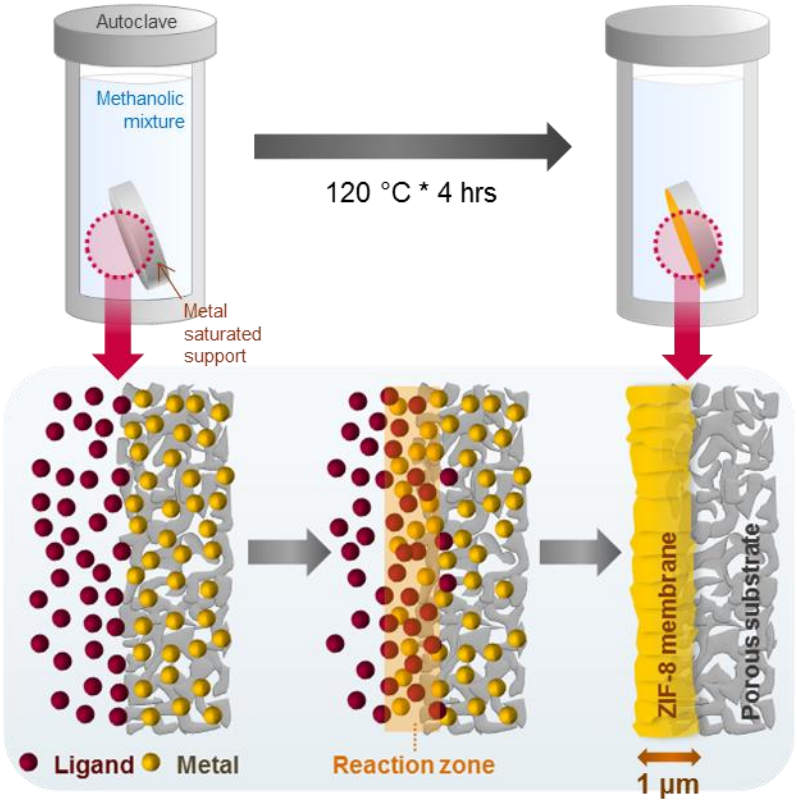

Figure 2-11 Schematic illustration of *in situ* counter-diffusion ZIF-8 membrane synthesis.

2.2.3.2.2. Seeded (secondary) growth

It is, in general, challenging to fabricate polycrystalline MOFs membranes on ceramic substrates by *in situ* synthesis method due to the low available MOFs nucleation sites on ceramic substrates.[86-88] The seeded growth method is well-established technique in zeolite membranes.[89] It is worth mentioning that the quality of membrane performance is highly dependent on the quality of seed layers. As seen in Figure 2-12, the high-quality seed layers are those nano-sized seed crystals are densely packed, uniformly covered, and strongly attached on substrates. The higher number of small seed crystals will provide the greater number of nucleation sites for crystal growth, as opposed to the poor-quality seed layers.

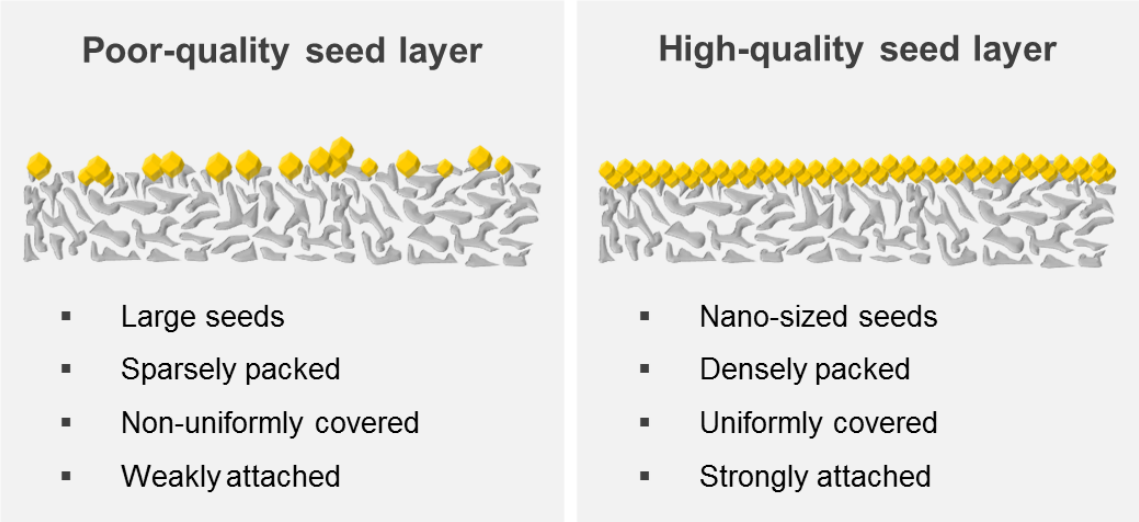

Figure 2-12 Schematic illustration of (left) poor-quality and (right) high-quality seed layers supported on porous substrates and distinctive properties of each case.

Li et al.[90] reported molecular sieving ZIF-7 membrane by seeding and secondary growth method for hydrogen separation. ZIF-7 nanocrystals, which were prepared at room temperature with excess benzimidazoles (*i.e.*, ZIF-7 linker), were dispersed in *N*,*N*-dimethylformamide (DMF). The ZIF-7 nanocrystals were deposited on porous alumina support by a conventional dip-coating method and subsequent microwave-assisted solvothermal synthesis was carried out to prepare well-intergrown ZIF-7 membranes (ca. 1 μm thick). Bux et al.[19] synthesized ZIF-8 membranes (ca. 12 μm thick) on α-alumina discs by dip-coating seeding and subsequent solvothermal growth for hydrogen separation. Pan et al.[42] synthesized propylene-selective ZIF-8 membranes on alumina discs by a slip-coating seeding followed by hydrothermal secondary growth. Thin and continuous ZIF-8 membranes (ca. 2.2 μm thick) were obtained and showed propylene/propane separation factor of ~ 50. Liu et al.[40] reported ZIF-8 membranes synthesized on alumina disc by double dip-coatings seeding and subsequent hydrothermal growth method. ZIF-8 membranes (ca. 2.5μm thick) showed propylene/propane separation factor of ~30 and

stable separation performances up to 40 days. Kwon et al.[46] synthesized thin and well-intergrown ZIF-8 membranes supported on alumina discs by microwave-assisted seeding and secondary growth. The resulting ZIF-8 membranes (ca. 1.5μm thick) exhibited propylene/propane separation factor of ~ 40. The unique microwave-assisted seeding in combination with the concept of counter-diffusion and subsequent hydrothermal growth is described in Figure 2-13. The high-quality ZIF-8 seed layers are obtained by the immersion of metal saturated porous alumina discs in a ligand precursor solution followed by microwave irradiation for a few minutes. Subsequent hydrothermal growth leads to the formation of thin and well-intergrown ZIF-8 membranes. Later, the ZIF-8 membranes synthesized by the same method showed enhanced propylene/propane separation performance, separation factor of ~ 200.[24]

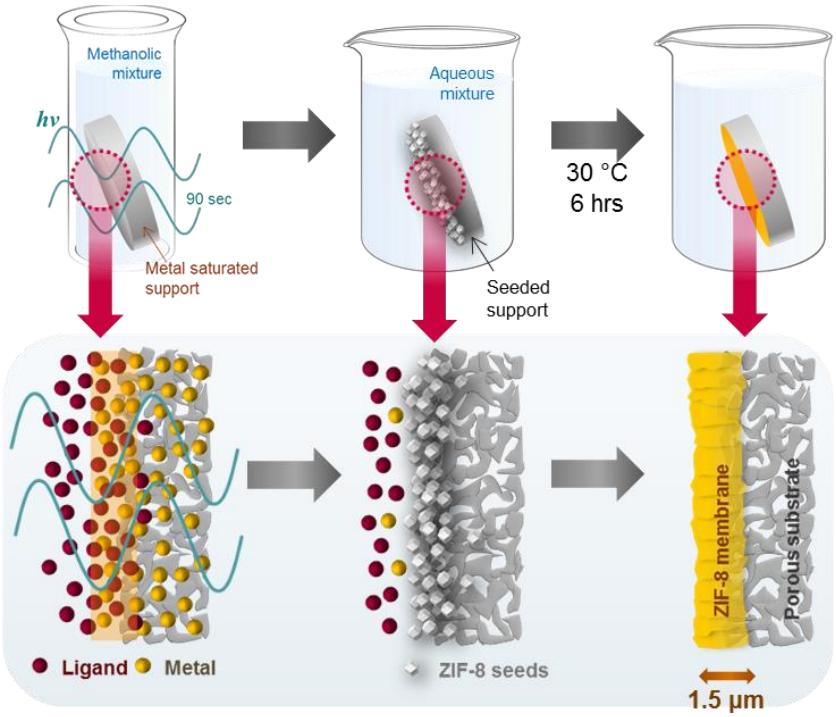

Figure 2-13 Schematic illustration of ZIF-8 membrane processing on α-alumina disc via microwave-assisted seeding and secondary growth method.[24, 46]. High-quality seed layers strongly attached to the substrates were formed in a few minutes under the microwave.

2.2.3.3. Ultrathin polycrystalline membrane synthesis methods

Conventional solvothermal or hydrothermal synthesis can prepare MOFs polycrystalline membranes successfully, however, bring down the membrane thickness to sub-micrometers is critical for their commercial separation application. It is because gas separation productivity is inversely proportional to membrane thickness. The layer-by-layer synthesis methods are utilized for the preparation of MOFs crystalline membranes, however, their application for gas separation is limited. Shekhah et al.[91] reported ultrathin ZIF-8 membranes (0.5 – 1 μm thick) on alumina substrates by layer-by-layer technique. Resulting ultrathin membranes were carried out for single gas measurements with significantly low gas permeances (ca. 100 times), given the thickness. Shamsaei et al.[92] synthesized defect-free ZIF-8 membrnaes via chemical vapor modification of polymeric support for hydrogen separation. Ultrathin ZIF-8 membranes (ca. 200 nm thick) were formed on chemical-vapor modification of an asymmetric bromomethylated poly(2,6-dimethyl-1,4-phenylene oxide) (BPPO) support followed by facile in situ growth. Kwon et al.[48] synthesized ultrathin ZIF-8 membranes (ca. 300 – 400 nm thick) via solvent-assisted recrystallization method. The defective ZIF-8 nanocrystals deposited on alumina disc by a facile microwave-assisted seeding[46] underwent ripening-like process in the presence of ligand vapor at elevated temperature (145 °C). The resulting membranes showed propylene/propane separation factor of ~ 122. Li et al. [51] fabricated ultrathin ZIF-8 membranes supported on ammoniated poly(vinylidene fluoride) (PVDF) hollow fiber supports via gel-vapor deposition technique. The propylene-selective ultrathin membranes (ca. 87 nm thick) showed the propylene/propane separation factor of 73 with the exceptional propylene permeance of 840 GPU (gas permeation unit, 1 GPU = 3.348×10^{-10} mol m^{-2} s^{-1} Pa^{-1}).

2.3. Post-synthetic modification methods of ZIFs

The coordinated organic-inorganic hybrid MOFs are available for interesting post-synthesis chemistry. The coordination bonds of metal anions and the organic linkers are labile, which means the bonds are readily dissociated and associated, in solution states. Therefore, the linkers and the metal anions in the frameworks of preformed-crystals can be post-synthetically replaced by new linkers and metals, respectively. Post-synthetic modifications (hereafter, PSMs) include 1) post-synthetic linker exchange, 2) post-synthetic metal exchange, 3) post-synthetic thermal exchange, and 4) post-synthetic chemical modifications (see Figure 2-14). Direct synthesis of MOFs with linkers having typical functional groups may produce undesired products. Therefore, it is challenging. However, PSMs can be used in MOFs synthesis, as useful tools to get MOFs as designed. PSMs can be used to change pore environments (such as pore size, pore volumes, and chemistry) and imparting new functionality (such as improve hydrothermal stability and catalytic effects). ZIFs were considered as inert materials compared to MOFs due to its strong metal to ligand bonds[93-94]. However, since Karagiaridi et al. reported the first solvent-assisted linker exchanged ZIFs[94-95], there are growing interests in PSMs to ZIFs.

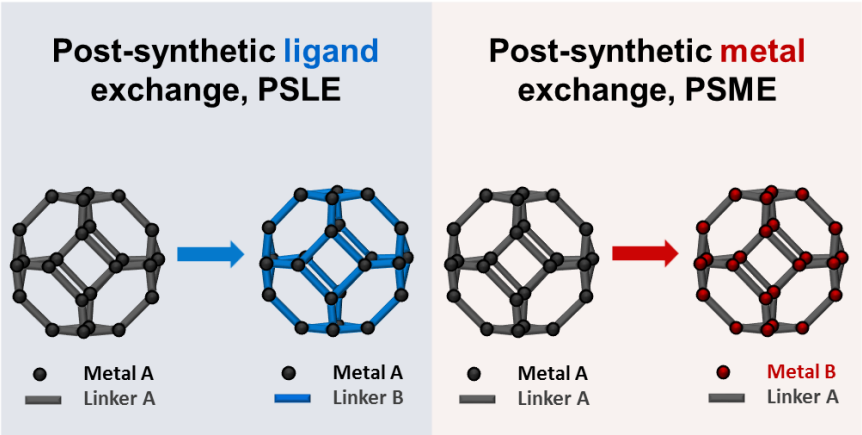

Figure 2-14 Schematics on post-synthetic linker exchange (PSLE) and post-synthetic metal exchange (PSME).

2.3.1. PSLE

Post-synthetic linker exchange (hereafter, PSLE) is also called solvent-assisted linker exchange, stepwise synthesis, and stepwise ligand exchange. Based on previously reported literature, the PSLE takes place as single-crystal-to-single-crystal transformation rather than complete dissolution and reassembly of the framework. PSLE technique conducted in MOFs is predominant, yet, some successfully utilized the technique in ZIFs. Figure 2-15 is shown imidazole derivatives as organic linkers of ZIFs. Fine-tuning framework structures in pore volume, pore environment, and aperture size is accessible by SALE technique; however, the tuning pore volume is out of the scope in membrane gas-separation. Likewise, imparting catalytic sites and hydrophobicity is accessible by SALE technique, but we do not discuss the catalytic activity. In this chapter, we will focus on examples of PSLE of ZIFs and critical synthetic parameters of PSLE in thermodynamic and kinetic aspects including those reported in MOFs.

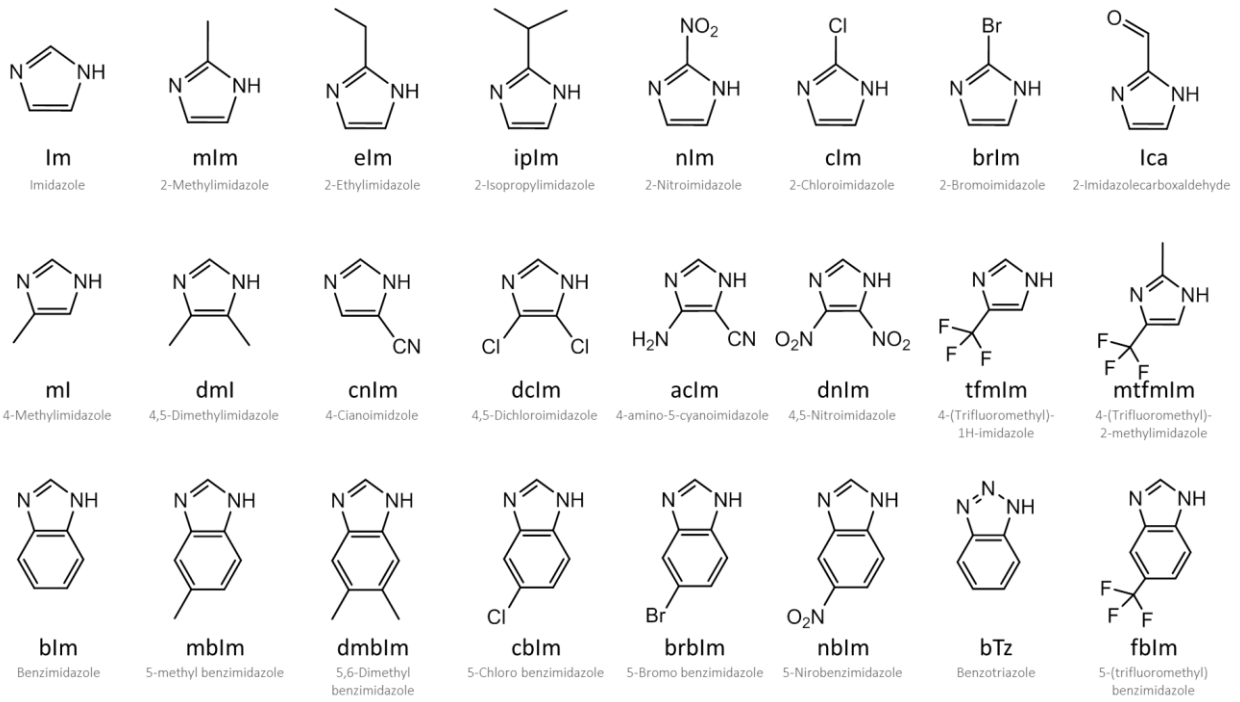

Figure 2-15 Chemical structures of imidazole derivatives. Hydrogen atoms are omitted for simplicity.

2.3.1.1. Examples

PSLE on ZIFs will be discussed in this section are summarized in Table 2-1.

Table 2-2 Summary of post-synthetic linker exchanges on ZIFs discussed in this chapter

Start		PSLE					End				Ref
ZIF-n	Composition	New linker	Solvent	Temp (°C)	Time (h)	%	ZIF-n	Composition	Topology	Back. rxn.	
ZIF-8	$Zn(mIm)_2$	Im	n-BuOH	100	168	~ 85	SALEM-2	$Zn(mIm)_{0.3}(Im)_{1.7}$	SOD	○	[95]
Pt@ZIF-8	$Zn(mIm)_2$	Im	n-BuOH	100	96	~ 90	Pt@SALEM-2	$Pt@Zn(mIm)_{0.2}(Im)_{1.8}$	SOD	N/A	[96]
ZIF-8	$Zn(mIm)_2$	mIca	n-BuOH	RT	24	~90	SIM-1	$Zn(mIm)_{2-x}(mIca)_x$	SOD	△	[97]
SIM-1	$Zn(mIm)_{2-x}(mIca)_x$	mIm	n-BuOH	RT	75	0	SIM-1	$Zn(mIm)_{2-x}(mIca)_x$	SOD		
SIM-1	$Zn(mIm)_{2-x}(mIca)_x$	mIm	DMF	100	48	~100	ZIF-8	Zn(mIm)	SOD		
ZIF-8	$Zn(mIm)_2$	Ica	MeOH	60	48	~ 26	ZIF-90	$Zn(mIm)_x(Ica)_{2-x}$	SOD	N/A	[98]
ZIF-8	$Zn(mIm)_2$	Ica	MeOH	60	196	~ 65	ZIF-90	$Zn(mIm)_x(Ica)_{2-x}$	SOD	N/A	[99]
ZIF-8	$Zn(mIm)_2$	Ica	MeOH	90	81	~ 90	ZIF-90	$Zn(mIm)_x(Ica)_{2-x}$	SOD	N/A	[99]
ZIF-8	$Zn(mIm)_2$	dmbIm	MeOH	60	24	~ 4.5	NA	$Zn(mIm)_{1.91}(dmbIm)_{0.09}$	SOD	N/A	[100]
ZIF-8	$Zn(mIm)_2$	dmbIm	MeOH	60	15	~ 9.1	NA	$Zn(dmbIm)_2$	SOD	N/A	[101]
ZIF-8	$Zn(mIm)_2$	bIm	MeOH	60	15	NA	ZIF-7	$Zn(bIm)_2$	SOD	N/A	[101]
ZIF-8	$Zn(mIm)_2$	mftIm	MeOH	60	15	NA	NA	$Zn(mftIm)_2$	SOD	N/A	[101]
ZIF-8	$Zn(mIm)_2$	ipIm	MeOH	60	15	NA	NA	$Zn(ipIm)_2$	SOD	N/A	[101]
ZIF-8	$Zn(mIm)_2$	eIm	MeOH	60	15	NA	NA	$Zn(eIm)_2$	SOD	N/A	[101]
ZIF-8	$Zn(mIm)_2$	tfmIm	MeOH	60	15	NA	NA	$Zn(tfmIm)_2$	SOD	N/A	[101]
CdIF-4	$Cd(eIm)_2$	mIm	DMF	100	48	~ 100	SALEM-1	$Cd(mim)_2$	RHO	○	[94]
SALEM-1	$Cd(mIm)_2$	nIm	DMF	100	48	~ 100	CdIF-9	$Cd(nim)_2$	RHO	×	[94]
CdIF-4	$Cd(eIm)_2$	nIm	DMF	100			CdIF-9	$Cd(nim)_2$	RHO	×	[94]

Table 2-2 Continued

Start		PSLE					End				Ref
ZIF-n	Composition	New linker	Solvent	Temp (°C)	Time (h)	%	ZIF-n	Composition	Topology	Back. rxn.	
ZIF-69	Zn(nIm)(cbIm)	fbIm	n-BuOH	120	72	~ 95	SALEM-10	Zn(nIm)(fbIm)	GME	N/A	[102]
ZIF-78	Zn(nIm)(nbIm)	fbIm	n-BuOH	120	72	~ 90	SALEM-10b	Zn(nIm)(fbIm)	GME	N/A	[102]
ZIF-76	Zn(Im)(cbIm)	fbIm	n-BuOH	120	72	~ 90	SALEM-11	Zn(Im)(fbIm)	ITA	N/A	[102]
ZIF-71	$Zn(dcIm)_2$	brIm	MeOH	55	72	~ 35	ZIF-71(Br/Cl)	$Zn(dcIm)_{2-x}(brIm)_x$	RHO	N/A	[103]
ZIF-71	$Zn(dcIm)_2$	Mn	MeOH	55	24	~ 14	ZIF-71(Zn/Mn)	$Zn_xMn_{1-x}(dcIm)_2$	RHO	○	[103]
ZIF-71(Zn/Mn)	$Zn_xMn_{1-x}(dcIm)_2$	Zn	MeOH	55	24	~ 99	ZIF-71(Zn/Mn)	$Zn_xMn_{1-x}(dcIm)_2$	RHO	○	[103]
ZIF-8	$Zn(mIm)_2$	Mn	MeOH	55	24	~ 10	ZIF-8(Zn/Mn)	$Zn_xMn_{1-x}(mIm)_2$	SOD	N/A	[103]
ZIF-7	$Zn(bIm)_2$	bTz	DMF	30	10	~16	ZIF-7-M	$Zn(mIm)_{2-x}(bTz)_x$	SOD	N/A	[104]
ZIF-7	$Zn(bIm)_2$	bTz	MeOH	30	10	~48	ZIF-7-M	$Zn(mIm)_{2-x}(bTz)_x$	SOD	N/A	[104]
ZIF-7	$Zn(bIm)_2$	bTz	DMF	50	10	~18	ZIF-7-M	$Zn(mIm)_{2-x}(bTz)_x$	SOD	N/A	[104]
ZIF-7	$Zn(bIm)_2$	bTz	MeOH	50	10	~50	ZIF-7-M	$Zn(mIm)_{2-x}(bTz)_x$	SOD	N/A	[104]

*Ending materials are given by assuming a complete exchange of ligands/metals in the framework. However, the composition of real ending materials is a combination of both ligands/metals in the framework and extra-framework ligands/metals since complete replacement cannot be achieved.

2.3.1.1.1. Tuning apertures

Synthesis of isostructural series of ZIFs is challenging in some cases due to the linker-topology relationship revealed in early studies.[69, 105] Functional groups of imidazolate linkers, especially alkyls, can serve as a structure-directing agent, studied empirically[69] and supported by DFT calculations[105]. The challenge of unattainable ZIFs by *de novo* is because the synthesis route is thermodynamical favors one topology than the desired one. For example, ZIF-8 (sodalite topology, Zn $(mIm)_2$) can be synthesized in various synthesis conditions. However, isostructural ZIF-8 with unsubstituted imidazole linkers (imidazole, hereafter Im) were not obtained de novo by far, though, other topologies (BCT, DFT, GIS, zni, cag, etc.) are available (see Figure 2-16). Karagiaridi and Hupp et al. reported ZIF-8 isostructural $Zn(Im)_2$ (what they called SALEM-2) synthesized by PSLE[95-96]. As shown in Figure 2-16, though there are many $Zn(Im)_2$ crystals reported. However, no $Zn(Im)_2$ crystals exhibits SOD topology was synthesized. ZIF-8 crystals were immersed in excess imidazole solution dissolved in n-butanol and treated at 100 °C for 7 days to obtain ~ 85 % replacement of original linker, mIm. The resulting crystal maintained its original SOD topology as evidenced by XRD. It is noteworthy the crystals lost their SOD topology during SALE procedure when using more basic solvents, *i.e.*, *N*,*N*-dimethylformamide (DMF) and dimethylacetamide (DMAc). Hypothetically, SALEM-2 would exhibit larger aperture than ZIF-8 due to its missing methyl groups on C2 of the imidazole ring. The authors conducted uptake and guest release test of activated ZIF-8 and SALEM-2 by TGA-MS. Though ZIF-8 accommodates n-hexane (kinetic diameter ~ 4.3 Å) only, SALEM-2 was capable of accommodating cyclohexane (kinetic diameter ~ 6.0 Å) and toluene (kinetic diameter ~ 6.1 Å). Later, Hupp group reported platinum nanoparticle-encapsulated ZIF-8 (Pt@ZIF-8) and their

SALE with imidazole linker (Pt@SALEM-2) to expand the aperture size. The authors conducted hydrogenation of substrates with different kinetic diameters by Pt catalysts encapsulated in ZIF-8 and SALEM-2. Conversion of substrates showed cut-off behavior in ZIF-8 and SALEM-2, 1-octene (20 vs. 30 %), cyclohexene (0 vs. 7 %), and β-pinene (0 vs. 15 %), indicating enlarged aperture of the six-membered ring after linker exchange.

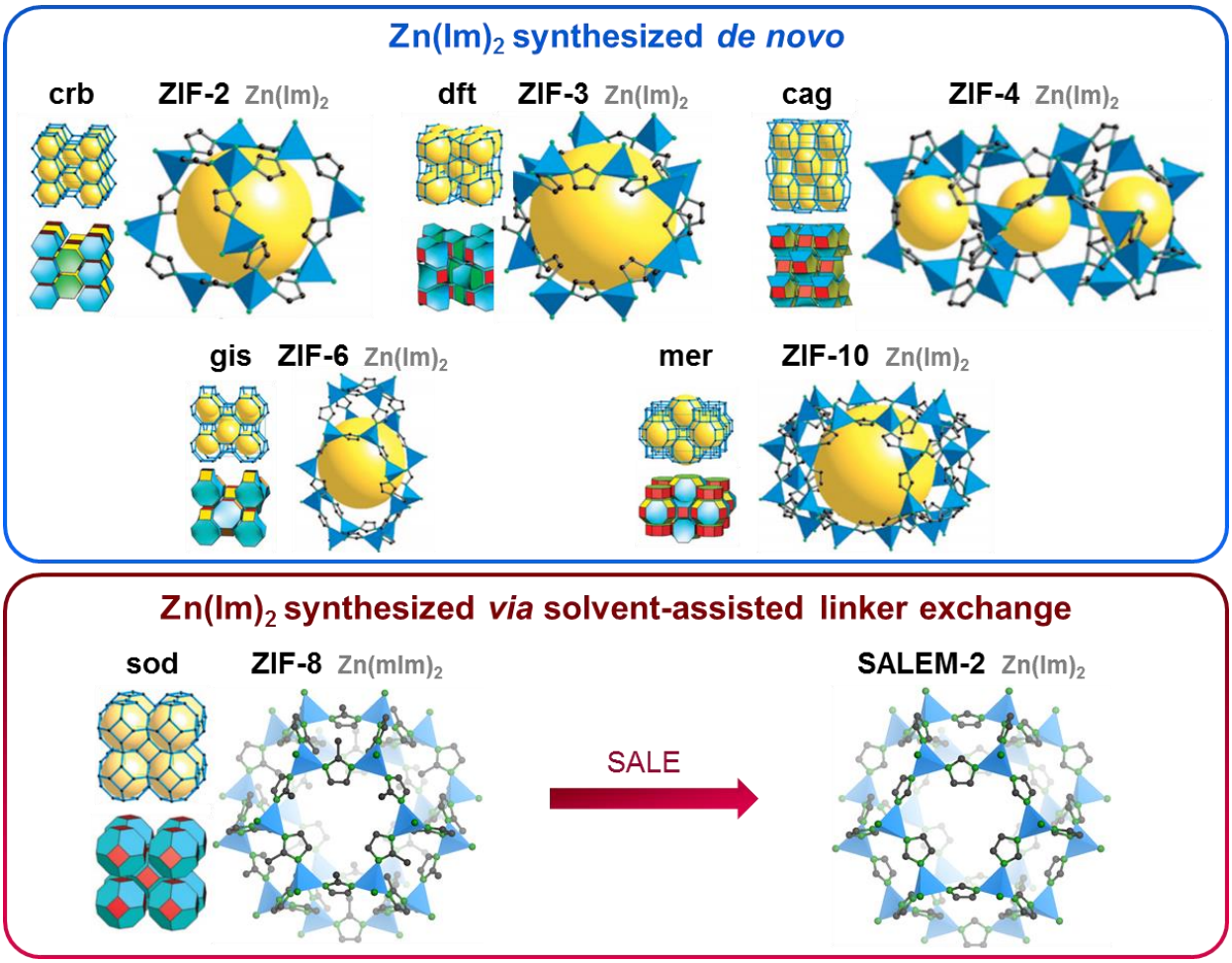

Figure 2-16 $Zn(Im)_2$ ZIFs synthesized de novo with various topologies, and sod-ZIFs synthesized de novo, ZIF-8 ($Zn(mIm)_2$), and via solvent-assisted linker exchange, SALEM-2 ($Zn(Im)_2$) from mother ZIF-8 crystal. Images of zeolitic topologies and ZIF-2, -3, -4, -6, -10 are reprinted with permission[11] Copyright 2006 by National Academy of Sciences USA. Images of ZIF-8 and SALEM-2 are generated by the material studio from the reported cif file on SALEM-2[95].

As shown in Figure 2-8, tuning apertures of SOD ZIFs (e.g., ZIF-7, -8, -67, -90) by hybrid-linker approach is attractive since it can offer sieving selective windows tuned for specific gas separations. ZIF-90, which is composed of $Zn(Ica)_2$ (imidazolecarboxaldehyde, Ica). ZIF-90 has shown greater effective aperture size (~ 5.0 Å) than that of ZIF-8 (~ 4.0 Å)[77] (see Figure 2-8). Apart from the *de novo* hybrid ZIF-8-90[77], apertures can be tuned post-synthetically by incorporating Ica onto ZIF-8 crystals[98-99] and membranes[50]. Park et al.[98] reported ZIF-8 mixed matrix membranes (MMMs) for N_2/NF_3 separation, along with MMMs containing Ica exchanged ZIF-8 crystals. 26 % of Ica incorporation was achieved after immersion of ZIF-8 crystals in Ica/methanol solution at 60 °C as evidenced by ^{1}H NMR. Krishna et al.[99] reported extensive study and comparison of the hybrid ZIF-8-90 crystals synthesized *de novo* mixed-linker and via SALE approach. Regardless of crystals size, nano- and micro-crystals, 90 % of mIm was replaced by Ica at 90 °C reaction as evidenced by ^{1}H NMR. The Ica was incorporated from the outer surface of the crystals as evidenced by confocal microscope. Lee et al. [50] reported enhanced propylene-throughput of ZIF-8 membranes via PSLE approach. The preformed ZIF-8 membrane was immersed in Ica/methanol solution at 60 °C for different duration of time. As the Ica linker incorporated to the upper layers of the ZIF-8 membranes, the propylene permeance was enhanced significantly, due to the enlarged aperture size of the upper layers.

2.3.1.1.2. Hydrophobicity

Liu et al.[101] reported hydrothermal stability of ZIF-8 and their improved hydrothermal stability *via* post-synthetic shell-ligand-exchange-reaction (SLER) with dmbIm (5,6-dimethylbenzimidazole), as shown in Figure 2-17. ZIF-8 crystals hydrolyzed under hydrothermal condition (80 °C, 24 h, ZIF-8 0.060 wt. % in distilled water), despite the size (nano- vs. micro-

crystals) and synthesis method (synthesized in water vs. methanol). Notably, ZIF-8 was protected from the hydrolysis under the condition where excess ZIF-8 (6.0 wt. %) or excess 2-methylimidazole (ZIF-8 0.060 wt. % with mIm 0.45 wt. %). Upon optimized SLER condition, with dmbIm/TEA/methanol solution at 60 °C for 15 h, the bulky and hydrophobic dmbIm linkers were introduced onto the ZIF-8 crystals' shell. The shell-ligand exchanged hybrid ZIF-8-dmbIm structure was shown by FTIR-ATR and UV-vis Raman spectroscopy. UV-vis Raman spectroscopy, equipped with lasers with a different wavelength, resulted in different spectra showing the bulky dmbIm relative to the aperture size of ZIF-8 was incorporated onto the surface of the crystals. The water contact angle measurements showed surface hydrophobicity of ZIF-8 was significantly improved after SLER (121° vs. 60°) due to the steric hindrance of dmbIm. Furthermore, the hydrothermal test in water with a very small amount of crystals (0.060 wt. %), the ZIF-8-dmbIm crystals maintained both crystallinity and morphology whereas ZIF-8 lost structural characteristics. Authors have shown the SLER was applied to other ZIFs, such as ZIF-7 and ZIF-93. Recently, Zhang et al.[100] reported ZIF-8 membrane with enhanced hydrostability via post-synthetic linker exchange. The ZIF-8 membrane was solvothermally synthesized followed by dmbIm exchange under dmbIm/TEA/methanol solution at 60 °C for 24 h. The ZIF-8 powders were also post-synthetically modified by dmbIm under the same condition. The BET surface area and pore volume change of ZIF-8 crystals were negligible. The crystallinity and morphology of the crystals as well as membranes were maintained. The water contact angle was improved dramatically in the case of ZIF-8 membranes (105° vs. 70°). 1H solution NMR on powder samples exhibited 4.5 % molar ratio of dmbIm was incorporated into the framework. Notably, Yang and coworkers[101] reported 9.1 % dmbIm incorporated with SLER performed at 60 °C for 15 h under the same dmbIm solution composition with the same ZIF-8

weight ratio. Lin and coworkers[100] explained that since dmbIm was incorporated on the outermost surface of crystals, the larger the crystal sizes, the lesser the dmbIm incorporation may occur. Note that the crystal size of Lin et al.(4 μm) is much larger than Yang et al.(60 nm). Moreover, only 1.8 % dmbIm was incorporated onto the membrane due to the compact grain boundary structure and thereby limited surface area that dmbIm can diffuse through.

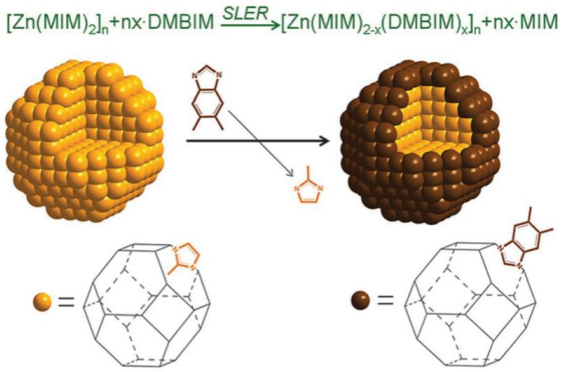

Figure 2-17 Schematic illustration of the shell-ligand exchange of ZIF-8 with dmbIm. Reprinted with permission[101]. Copyright 2013, Royal Society of Chemistry.

2.3.1.1.3. Guest encapsulations

Tsung group reported[106] guest encapsulation beyond the aperture size ZIF-8 under PSLE condition. Rhodamine 6G (R6G) (molecular diameter of 11.3 – 13.7 Å), which is 3 – 4 times larger than the aperture size of ZIF-8 (3.4 Å), was successfully encapsulated in preformed ZIF-8 crystals. ZIF-8 crystals were immersed in the R6G and mIm mixture in butanol at elevated temperature (100 °C). The proposed mechanism of guest encapsulation is described in Figure 2-18. The dissociation of linkers under PSLE condition creates open parts of framework which allows diffusion of guest molecules into the framework. The association of linkers after the guest encapsulation closes the frameworks, which traps the guest molecules in the MOFs. The guest loading was inversely proportional to the concentration of mIm. In fact, the highest guest loading

was observed when without mIm. It means that free mIm linkers in the reaction mixture can readily close the expanded apertures which are diffusion pathway of guest molecules to the frameworks.

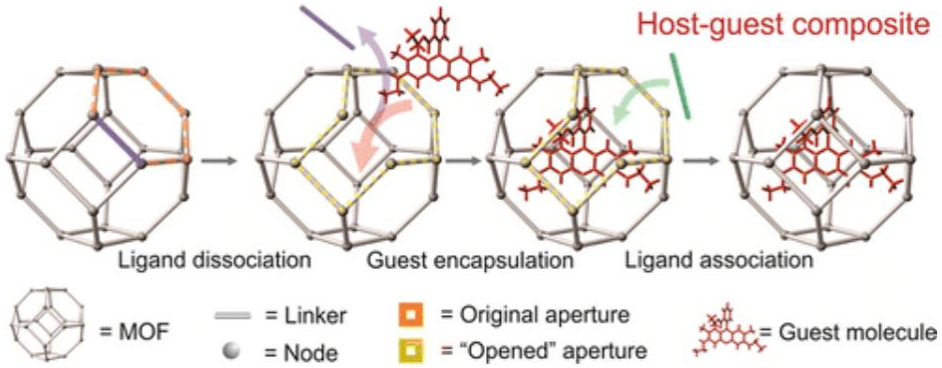

Figure 2-18 Schematic illustration of guest encapsulation of ZIF-8 via post-synthetic linker exchange approach. Reprinted with permission.[107] Copyright 2014 by American Chemical Society.

2.3.1.1.4. Size control

Crystallite size is determined by crystallization processes; nucleation and growth. The condition where nucleation is favored, the more number of nuclei is available; therefore, the large number of small crystals is prepared. On contrary, when growth is favored, the less number of nuclei is available; the small number of large crystals is prepared. As seen in Figure 2-6, the nucleation is favored with faster deprotonation. The different heating sources, such as conventional solvothermal vs. microwave heating, can produce different sized crystals. According to Marti et al. [97], fabrication of SIM-1 crystals of controlled size with uniform size distribution by conventional solvothermal methods was a lot more challenging than that of ZIF-8. SIM-1 is an isostructural ZIF-8 and composed of Zn and 4-methyl-5-imidazole carboxaldehyde (mIca). Alternative synthesis methods of SIM-1 via PSLE were investigated for gas separation

applications. Uniformly sized SIM-1 crystals were prepared by PSLE of ZIF-8 crystals in mIca/1-butanol mixture at room temperature with 90 % of mIca incorporation. Conversion of ZIF-8 to SIM-1 by PSLE and their reversible reaction was possible and confirmed by FT-IR, TGA and BET analysis.

2.3.1.1.5. Strategic PSLEs

2.3.1.1.5.1. Selective PSLEs

Hupp group reported selective PSLEs in a series of ZIFs[102]. Based on the observation and hypothesis on the CdIF-4[94], which was dissolved under SALE condition, Hupp group designed and reported the first example of selective-SALE within MOFs (see Figure 2-19).[102] Three mixed linker ZIFs, ZIF-69, ZIF-78, and ZIF-76, containing nIm were chosen for the SALE with the secondary 5-(trifluoromethyl)benzimidazole (hereafter, fbIm) linker. Under the SALE condition by immersing 30 mg of ZIF-69, the prototype of this study, in 10 mL of a 2M solution of fbIm in n-butanol at 120 °C for 3 days, 95% of cbIm was replaced by fbIm, analyzed by ^{1}H NMR. The ^{1}H NMR proved indeed it is the selective SALE occurred by that the total ratio of benzimidazole (both cbIm and fbIm) and imidazole (nIm) remains constants. The topology and porosity of the parent and the daughter crystals remained the same as GME as proved by PXRD and N2 adsorption. They proved that the selective SALE also occurred in the ZIF-78 and ZIF-76, regardless of the parent topology. Note that the de novo synthesis of SALEM-10 and -11 were not successful. The authors claimed that the selective SALE is due to the different of the pKa values for the nitrogen atoms of imidazole and imidazolium versions of the molecules deployed as linkers.

(a)

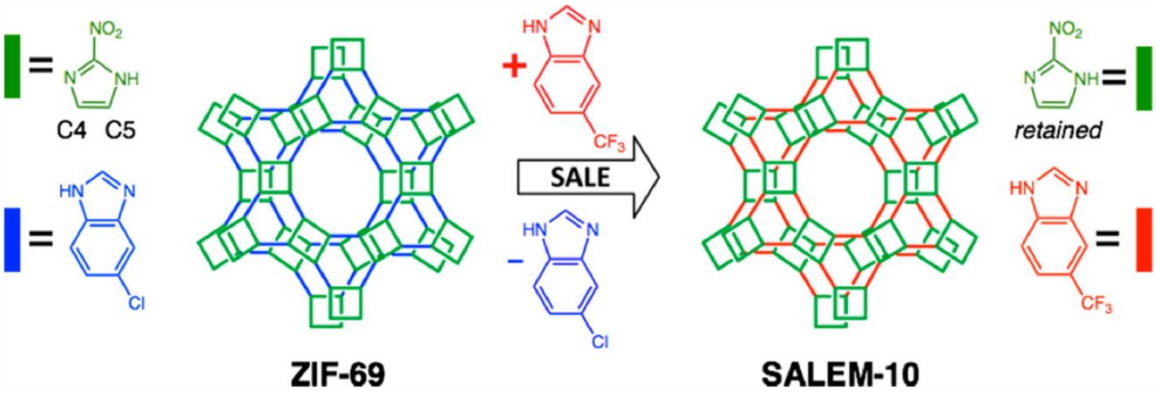

(b)

MOF	linkers	pK_a values[a]	% linker exchange[b]
ZIF-69	nIm and cbIm	–1.73 and 5.74	
SALEM-10	nIm and fbIm	–1.73 and 5.74	95
ZIF-78	nIm and nbIm	–1.73 and 5.03	
SALEM-10b	nIm and fbIm	–1.73 and 5.74	90
ZIF-76	Im and cbIm	6.97 and 5.74	
SALEM-11	Im and fbIm	6.97 and 5.74	90

[a]For the protonated N3. [b]Determined by 1 H NMR

Figure 2-19 (a) Schematic illustration of selective-SALE of ZIF-69 and resulting SALEM-10 and (b) summary of pK_a values of linkers and % linker exchange. Reprinted with permission[102]. Copyright 2015, American Chemical Society.

2.3.1.1.5.2. Reversible PSLEs

Karagiaridi et al. reported The SALEM-1[94] is the post-synthetic ligand exchange of cadmium-based ZIFs, so-called CdIFs. They were able to synthesize CdIF-9 and SALEM-1 post-synthetically, by immersing CdIF-4 in concentrated extraneous linker solution, 2-nitroimidazole, and 2-methylimidazole, respectively. Both starting and resulting ZIFs retains same topology, RHO, and high porosity. SALE was fully reversible in CdIF-4 and SALEM-1, in contrary, CdIF-9 dissolved in extraneous linker solution instead of linker substitution. According to their argument, the electron-withdrawing nitro group decreases Lewis basicity of nitrogen thus leading

to weak N-Cd bond strength. From this observation, they argued that first, the SALE is single crystal-to-single crystal linker exchange and second, the starting framework with electron-donating linker would be a good template for SALE.

2.3.1.2. Reaction

2.3.1.2.1. Associative/dissociative mechanisms

The ligand exchange of MOFs involves with the linker in the framework, ingenuous linker, substituted with the other linker, exogenous linker while the overall charge of the framework is conserved. The mechanism of ligand exchange in coordinate chemistry is dissociative or associative, analogous to that of S_N1 or S_N2 respectively. In the associative mechanism, the incoming ligand approach to the metal center while the leaving group is remaining in the framework, which is intermediate rate-determining step, then the ingenuous linker is leaving the framework. The dissociative mechanism undergoes first, the rate-determining step that outcoming of the ingenuous linker and then, the extraneous linker substitutes the open metal center. Knowing that the two mechanisms involve in different reaction kinetics, linker exchange mechanisms can be empirically distinguished. To explain, the dissociative reaction follows the first order reaction, and the associative follows second order reaction rate. Observed rate constant is determined from the slop of conversion vs. time plots for different concentration of exogenous linker solution.

Morabito et al.,[106] examined the kinetics of PSLE reaction to test the reaction mechanism under pseudo-first-order conditions by changing the initial concentration of incoming linker. And calculated observed rate constants (k_{obs}). The relationship of concentration and k_{obs} suggest that associative and dissociatvie reactions are competing reactions. Also, under the condition where

the maximum guest loading was observed, *i.e.*, without linker, which is because the associative reaction was shut down and the dissociative reaction was only involved. Under the condition where the lower guest loading was observed, *i.e.*, higher incoming linker concentration, the dissociative and associative reaction was competing.

2.3.1.2.2. Fundamental aspects of PSLE

The Linker exchange reaction of MOFs takes in place as single-crystal-to-single-crystal transformation rather than complete dissolution and reassembly of the framework. Deria et al.[108] reviewed fundamentals of linker exchange of MOFs. In light of the previous review, thermodynamics (e.g., pKa of linkers) and kinetics (e.g., size of crystals and concentration of linker solution) aspects are discussed.

2.3.1.2.2.1. Reaction conditions: temperature, time, concentration and solvents

Linker exchange reactions can take place with enough thermal energy to overcome energy barrier. Jiang et al.[104] performed PSLE of ZIF-7 with benzotriazole (btz) by varying temperatures (30 vs. 50 °C), concentration of btz (0.5 vs. 1.0 mg L^{-1}), solvents (DMF vs. methanol), and reaction time (1 vs. 3 vs. 10 days). Under the reaction condition, temperature effect was not obvious and the higher btz concentration favored the btz incorporation. The effect of reaction time was significant; the longer the reaction time, the more the btz was incorporated. This slow reaction may be due to the stability of mother crystal, ZIF-7. However, the above results are not universal. According to Krishna et al.,[99] PSLE reaction of ZIF-8 with Ica exhibited higher % Ica incorporation at 90 °C (~90 %, both nano- and microcrystals of ZIF-8) than at 60 °C (~45 %, nanocrystals and ~20 %, microcrystals) after $t^{1/2}$ ~ 8 hours.

2.3.1.2.2.2. Relative pKa of linkers

The feasibility of the reaction con be considered in light of the relative strength of existing metal-ligand bond and new metal-ligand bond. The coordinate covalent bonds of metal-ligand are sharing electron pair donated from a Lewis acid (*i.e.*, organic linkers) to a Lewis acid (i.e., metal nodes). The relative stability of metal-ligand coordination bond can be determined by (1) Irving-Williams series[109], (2) the hard soft acid base (HSAB) theory,[12, 110] and (3) the pK_a values of the conjugate acid (i.e., the monoprotonated linkers)[108]. Briefly, the Irving-Williams series descries the relative stability of metal-ligand complexes, in terms of metal ions, regardless of ligands.

$$Ba^{2+} < Sr^{2+} < Ca^{2+} < Mg^{2+} < Mn^{2+} < Fe^{2+} < Co^{2+} < Ni^{2+} < Cu^{2+} > Zn^{2+}$$

ZIFs are chemically more stable than other MOFs. This stability can be explained in light of the HSAB theory. For example, ZIF-8 is stable because both metal (Zn^{2+}) and organic linker (2-methylimidazole) is borderline acid and borderline base, respectively. The relative stability of metal-ligand bond strength can be determined by pK_a of linkers. The higher the pK_a of the monoprotonated linker, the stronger Lewis base the linker is, therefore, the stronger the metal-ligand bond strength is.

Previously, the exchange of eIm with mIm linkers of CdIF-4 and SALEM-1 are possible, however, CdIF-9 (*i.e.*, $Cd(nIm)_2$) are completely dissolved in the attempt to incorporate eIm or mIm. The lower basicity of nIm compared to eIm and mIm resulted in weaker Cd-N coordinate covalent bonds of CdIF-9 than that of CdIF-4 and SALEM-1, thus leading to complete dissolution of weaker bonds in the presence of incoming linkers. In addition to it, instability of

Cd-N itself (HSAB theory).might accelerated the dissolution of crystals. As shown in Figure 2-19, Lalonde et al.[102] hypothesized that it is possible to replace cbIm of ZIF-69 but not nIm with fbIm, due to the pK_a differences. Since nIm has low pK_a (-1.73) than fbIm (5.74), whereas cbIm (5.74) and fbIm has similar pK_a values. In this study, Zn-nIm bonds were remained after SALE, even though the Zn-nIm bond is weaker than the Zn-fbIm, where CdIF-9 was completed dissolved. This is because the Cd-N is weaker than Zn-N bond according to HSAB theory. Therefore, pKa values can imply feasibility of the PSLE reaction, however, should be carefully considered under the complex circumstances.

2.3.1.2.2.3. Size of crystals

Size of MOF crystals subject to PSLE is affecting on the % incorporation of new linkers, due to the surface area to volume ratio. The smaller the crystals become, the higher the surface area to volume ratio, thereby the higher accessibility of incoming linker to the Zn-N reaction sites. When ZIF-8 SALE with Ica was carried out with different crystal sizes (nanocrystals vs. microcrystals, the smaller the crystal size is, the SALE reaction was favored, meaning that the faster Ica incorporation to the ZIF-8 at given amount of time.

2.3.1.2.2.4. Relative size of aperture size and incoming linker

Relative size of incoming linker and aperture size affects the kinetics of PSLE. The larger the incoming linker relative to the aperture size of frameworks, higher energy would be required to overcome the energy barrier for the new linker to propagate through the frameworks. The bulky dmbIm linkers were incorporated mainly on the surface of the crystals as evidenced by Raman spectra using different light sources (325 and 514 nm).[101]

CHAPTER III

DEFECT-DEPENDENT STABILITY OF HIGHLY PROPYLENE-SELECTIVE ZEOLITIC-IMIDAZOLATE FRAMEWORK ZIF-8 MEMBRANES*

3.1. Introduction

Membrane-based gas separation[4-5] is of great interest as an alternative to conventional energy-intensive processes such as distillation because it is more energy-efficient, eco-friendly and cost-effective. In particular, membrane-based separation of propylene/propane mixture has been extensively studied by using polymer membranes[3, 6], carbon molecular sieve membranes[7-8], and zeolite membranes[9]. There are, however, no propylene/propane separation membranes commercially available due to the limitations of current membrane materials and processing techniques with respect to the performance requirements such as separation factors and propylene permeances and/or the operational requirements such as chemical/mechanical stabilities and long-term performance stabilities.

Zeolitic-imidazolate frameworks (ZIFs) are a subclass of metal-organic frameworks (MOFs), possessing zeolite topologies originated from the metal-ligand-metal bond angle of 145° similar to the T-O-T bond angle in zeolites[11]. ZIFs have well-defined micro pores with relatively good chemical and thermal stabilities as compared to other MOFs[10]. A prototypical ZIF-8, composed of zinc ions interconnected with 2-methylimidazoles, is a particularly

* Reprinted with permission from "Defect-dependent stability of highly propylene-selective zeolitic-imidazolate framework ZIF-8 membranes" by Moon Joo Lee, Hyuk Taek Kwon, and Hae-Kwon Jeong, 2017. *Journal of Membrane Science*, 529, 105–113, Copyright 2017 by Elsevier.

promising material for the kinetic separation of propylene/propane[20-21] due to its effective pore size of ~ 4 Å[22], which is in between the sizes of propylene and propane.

Several synthesis methods[45-47, 111] have been developed for polycrystalline ZIF-8 membranes. However, only a handful of those resulted in highly propylene-selective membranes. Lai and co-workers were the first to report high-quality ZIF-8 membranes prepared using seeded growth in an aqueous precursor solution for light hydrocarbon separation[112] and for propylene/propane separation[42]. Hara et al. reported ZIF-8 membranes synthesized by the counter-diffusion method showing good propylene/propane separation[76, 113-114]. Nair and co-workers demonstrated ZIF-8 membrane grown on polymeric hollow fiber by interfacial microfluidic membrane processing (IMMP) for propylene/propane separation[23, 111]. Our group has reported several synthesis methods including counter-diffusion-based *in situ* growth[45, 47] (hereafter CD method), microwave-seeding and secondary growth[46] (hereafter, MW method), and most recent heteroepitaxial secondary growth[25] to prepare high-quality ZIF-8 and ZIF-67 (Co-substitute ZIF-8) membranes with unprecedented propylene/propane separation performances.

Defects in crystalline porous materials such as zeolites and MOFs are inevitable and studied widely[115-117]. Although limited, there are a few studies on the defects in ZIF-8. Tian et al.[118] reported surface compositions of ZIF-8 thin films by using X-ray photoelectron spectroscopy (XPS) and discovered various surface terminal groups including carbonates, water/hydroxides, and secondary amines in addition to 2-methylimidazoles. Cheng et al.[119] studied water-treated ZIF-8 for H_2 adsorption and found that water treatment led to water-terminated defects, thereby inducing enhanced H_2 uptake by 77% at ambient temperature. By drawing an analogy with zeolites, Zhang et al.[120] computationally characterized and categorized

various possible point defects in ZIF-8 into linker vacancy, metal vacancy, and dangling linker. Based on the activation energies of defect formation, they concluded that those defects can be formed even in ambient conditions (in particular dangling linkers can form even at room temperature for ~ 1 hr).

The long-term stability of ZIF-8 membranes is crucial for their potential commercial applications. To the best of our best knowledge, however, there are only a few such studies reported so far [23, 40]. Liu et al.[40] studied the long-term stability of ZIF-8 membranes synthesized using the aqueous secondary growth recipe[112]. Their ZIF-8 membranes exhibited stable propylene/propane separation performances over 40 days at 35 ºC. Recently, Eum et al.[23] reported the long-term stability of ZIF-8 membranes on polymeric hollow fiber membrane fabricated by IMMP with an equimolar binary propylene/propane at 25 °C at 1 bar. During the 30 days of continuous operation, both selectivity and gas permeances were maintained.

Herein, we report the time-dependent selectivity and permeation behaviors of high-quality ZIF-8 membranes prepared by the CD and MW methods. The time-dependent separation performances of ZIF-8 membranes depend upon synthesis recipes. Upon a battery of characterizations, we attribute the recipe-dependent long-term stability of ZIF-8 membranes to defects including surface defects resulting from different synthesis conditions. In addition, the effect of atmospheric water on membrane gas transport and separation performance is discussed. Finally, we show a post-synthetic ligand treatment as an effective means to stabilize ZIF-8 membranes.

3.2. Experimental

3.2.1. Chemicals

Alpha-Al_2O_3 powder (CR6, Baikowski) was used to prepare alumina disks and polyvinyl alcohol (PVA 500, Duksan) was used as a binder for alumina disk preparation. Zinc nitrate hexahydrate ($Zn(NO_3)_2 \cdot 6H_2O$, 98%, Sigma-Aldrich) and zinc chloride ($ZnCl_2$, 99.99%, anhydrous, Alfa Aesar) were used as metal sources. 2-methylimidazole ($C_4H_6N_2$, 99%, Sigma-Aldrich) was used as an organic ligand and sodium formate (HCO_2Na, 99%, Sigma-Aldrich) was utilized as a deprotonating agent. Methanol (CH_3OH, >99%, Alfa Aesar) and deionized water were used as solvents.

3.2.2 Preparation of porous α-Al_2O_3 supports, ZIF-8 powders, and ZIF-8 membranes

Porous α-Al_2O_3 disks (diameter ~ 22 mm and thickness ~ 2 mm) were used as supports and prepared by following a previously reported procedure [45-46]. Briefly, 10 g of α-Al_2O_3 powders was mixed with 1ml of an aqueous PVA binder solution. The binder solution was prepared by dissolving 3 g of polyvinyl alcohol in a mixture of 95 ml of D.I. water and 5 ml of 1 M HNO_3. 2.1 g of the alumina and binder mixture was then pressed at 10 t for 1 min. The supports were sintered at 1100 °C for 2 hrs and one side of the sintered supports was polished with a sand paper (grit# 800). Before usage, a support was immersed in methanol and sonicated for 1 min followed by drying at 120 °C for 1 hr.

ZIF-8 membranes were synthesized using both the CD method and the MW method as reported previously from our group[45-47]. For CD-ZIF-8 membranes, a metal precursor solution and a ligand precursor solution were prepared by dissolving 0.98 g of zinc chloride in 40 mL of methanol and by dissolving 5.19 g of 2-methylimidazole (hereafter mIm) and 0.5 g of sodium

formate in 40 mL of methanol, respectively. Sodium formate was dried in an oven at 100 °C for 6 hrs under vacuum prior to usage. An alumina support was soaked in the metal precursor solution for 1 hr. The support saturated with the metal solution was inserted into a Teflon holder and then placed vertically into a Teflon-lined autoclave filled with 40 ml of the ligand solution followed by solvothermal treatment at 120 °C for 4 hrs. After cooled down to room temperature, the sample was rinsed several times with methanol and immersed in 35 ml of fresh methanol for 12 hrs. The back side of the sample was polished with sand papers (grit # 350) to remove crystals formed on the back side. Finally, the membranes were washed in 35 ml of fresh methanol for 5 days and dried at room temperature for 5 hrs and 60 °C for 1 hr. Homogeneously-formed ZIF-8 crystals were collected from the residual solution after membrane synthesis. The crystals (hereafter CD-ZIF-8 crystals) were washed and centrifuged for 4 times with fresh methanol followed by drying at 70 °C under vacuum for 12 hrs.

MW-ZIF-8 membranes were synthesized using our previously reported microwave method [46]. For microwave-assisted seeding, 2.43 g of zinc nitrate hexahydrate was dissolved in 40 ml of methanol and 2.59 g of mIm and 0.125 g of sodium formate were dissolved in 30 ml of methanol. A dried alumina support was placed vertically with the polished side facing down using a Teflon holder and soaked in the metal precursor solution for 1 hr. Afterwards the metal-soaked support was inserted in a microwave-resistant glass tube filled with the ligand precursor solution. Microwave irradiation was immediately applied with the power of 100 W for 1.5 min. After cooled down to room temperature, the seeded support was thoroughly rinsed with methanol and kept in 35 ml of fresh methanol for 1 day followed by drying at 60 °C for 4 hrs. The secondary growth of the ZIF-8 seed layer was carried out based on the aqueous recipe reported elsewhere [42]. For secondary growth, aqueous metal and ligand precursor solutions were prepared

by dissolving 0.11 g of zinc nitrate hexahydrate and 2.27 g of m-Im in 20 ml of DI water, respectively. The seeded alumina disk was placed vertically using a Teflon holder in a beaker. Meanwhile, the metal precursor solution was added into the 20 ml of the ligand precursor solution and stirred for 2 min. Then the aqueous solution mixture was poured into the beaker containing the seeded support. The beaker is then placed in a static oven at 30 °C for 6 hrs. The resulting membrane was then washed in 35 ml of fresh methanol for 5 days and dried at 60 °C for 6 hrs. Similar to CD-ZIF-8 powers, homogeneously-formed ZIF-8 crystals after the secondary growth (hereafter MW-ZIF-8 crystals) were collected, washed and dried.

3.2.3. Propylene/propane gas permeation test

Propylene/propane binary gas permeation measurements were carried out at room temperature under atmospheric pressure using the Wicke−Kallenbach technique (see Fig. S1a). An equimolar propylene/propane mixture was used as a feed. The feed and argon sweeping gases were supplied to the feed and permeate sides at a flow rate of 100 cc/ min, respectively. The composition of the permeate side stream was analyzed using a gas chromatography (Agilent GC 7890A equipped with a column of HP-PLOT/Q). For thermal activation studies, as-dried ZIF-8 membranes were subjected to further drying at 100 °C for 12 hrs under vacuum and gas drying units were installed to dehumidifying feed gases. During off-stream measurements, two different arrangements were devised depending on whether the permeation cell containing a ZIF-8 membrane inside is opened to ambient condition (open cell) or isolated from ambient condition (closed cell) after each measurement (see Figure S1b). All permeation cells were kept in a fume hood (RH: 30 ~ 80 %) regardless of open or closed cell arrangements.

3.2.4. Characterizations

X-ray diffraction (XRD) patterns were collected using a Rigaku Miniflex II powder X-ray diffractometer with Cu-Kα radiation (λ = 1.5406 Å). Electron micrographs were taken using a JEOL JSM-7500F operating at 5 keV acceleration voltage and 15 mm working distance. Solid state nuclear magnetic resonance (NMR) spectroscopy of ZIF-8 powders were taken by using a Varian INOVA 400 MHz solid-state NMR spectrometer equipped with a 7.5 mm CP/MAS probe for ^{15}N NMR (40.52 MHz) spectra. It is operated at 10 kHz of constant spinning frequency with 4 s of a pulse delay time and 1 ms of a contact time. ZIF-8 powders were packed into 7.5 mm zirconia rotors and sealed with Kel-F short caps. Infra-red spectra were collected using a NICOLET IR100 FT-IR spectrometer. Pulverized ZIF-8 particles were homogeneously mixed with KBr and pelletized for IR measurements. Note that it is repeated at least three times for each sample. Thermal gravimetric analysis (TGA) of ZIF-8 powders were conducted using a TGA system (Q50, TA instrument) from room temperature to 800 °C with a ramp rate of 5 °C/min under nitrogen environment. N_2 adsorption measurements were conducted using an ASAP 2000 (Micrometrics). X-ray photoelectron spectra were collected on an Omicron XPS instrument with a DAR 400 dual Mg/Al X-ray source. The survey spectra were collected over an energy range of -10 − 1100 at 1 eV/step with 100 eV pass energy. High resolution spectra for individual element (C 1s, N 1s, O 1s, and Zn 2p) were collected over the energy range of 20 eV at 0.05 eV/step and pass energy of 50 eV. Data analysis was performed using CasaXPS software (Casa Software, Ltd.) and peaks were fitted with a range of 1.5 – 2.5 fwhm.

3.3. Results and discussions

3.3.1. Comparison of CD-ZIF-8 and MW-ZIF-8 membranes

ZIF-8 membranes were synthesized using two different synthesis protocols, the CD method (denoted CD-ZIF-8 membranes) and the MW method (denoted MW-ZIF-8 membranes). It should be noted that there are several differences in the two methods: solvent (methanol vs. water), deprotonating agent (with vs. without), zinc source (zinc chloride anhydrous vs. zinc nitrate hexahydrate), reaction time (30 min vs. 6 hrs), and reaction temperature (120 ºC vs. 30 ºC) as summarized in detail in Table 3-1.

Table 3-1 Synthesis conditions of CD-ZIF-8 and MW-ZIF-8 power samples

	CD-ZIF-8	**MW-ZIF-8**
Zinc source	Zinc chloride (anhydrous)	Zinc nitrate hexahydrate
Solvent	Methanol	D.I. water
Deprotonator	Sodium formate	None
Reaction temperature	120 ºC	30 ºC
Reaction time	30 min*	6 hrs
Drying condition	R.T. for 5 hrs 60 ºC for 1 hr	60 ºC for 6 hrs

* Although the overall reaction time of CD-ZIF-8 powder and membrane synthesis is 4 hrs, the majority of crystals formed in 30 mins as evidenced by XRD in previously reported by Kwon et al.[45]

Figure 3-1 shows electron micrographs of CD-ZIF-8 and MW-ZIF-8 membranes before and after 60 days of off-stream measurements. As can be seen in Figures 3-1 and A-2, as-synthesized membranes possess different microstructures in grain size and thickness: the MW-ZIF-8 membrane is ~ 1.6 μm thick with grains of ~ 1 μm in size (Figures 3-1 a and A-2 a) while

the CD-ZIF-8 membrane is ~ 1 μm thick with grains of ~ 0.5 μm in size (Figures 3-1 c and A-2 c). Even after 60 days of off-stream measurements, no significant changes in the membrane microstructures were observed under SEM (see Figures A-2 b and A-2 d). Figure 3-2 presents the XRD patterns of the membranes before and after the off-stream measurements. The (110) peak intensity of the MW-ZIF-8 membrane is slightly greater than that of the CD-ZIF-8 membrane likely due to the fact that the former is thicker than the latter. Furthermore, there is little change in the XRD patterns even after 60 days of off-stream measurements, indicating that the crystallinities of both membranes were not compromised.

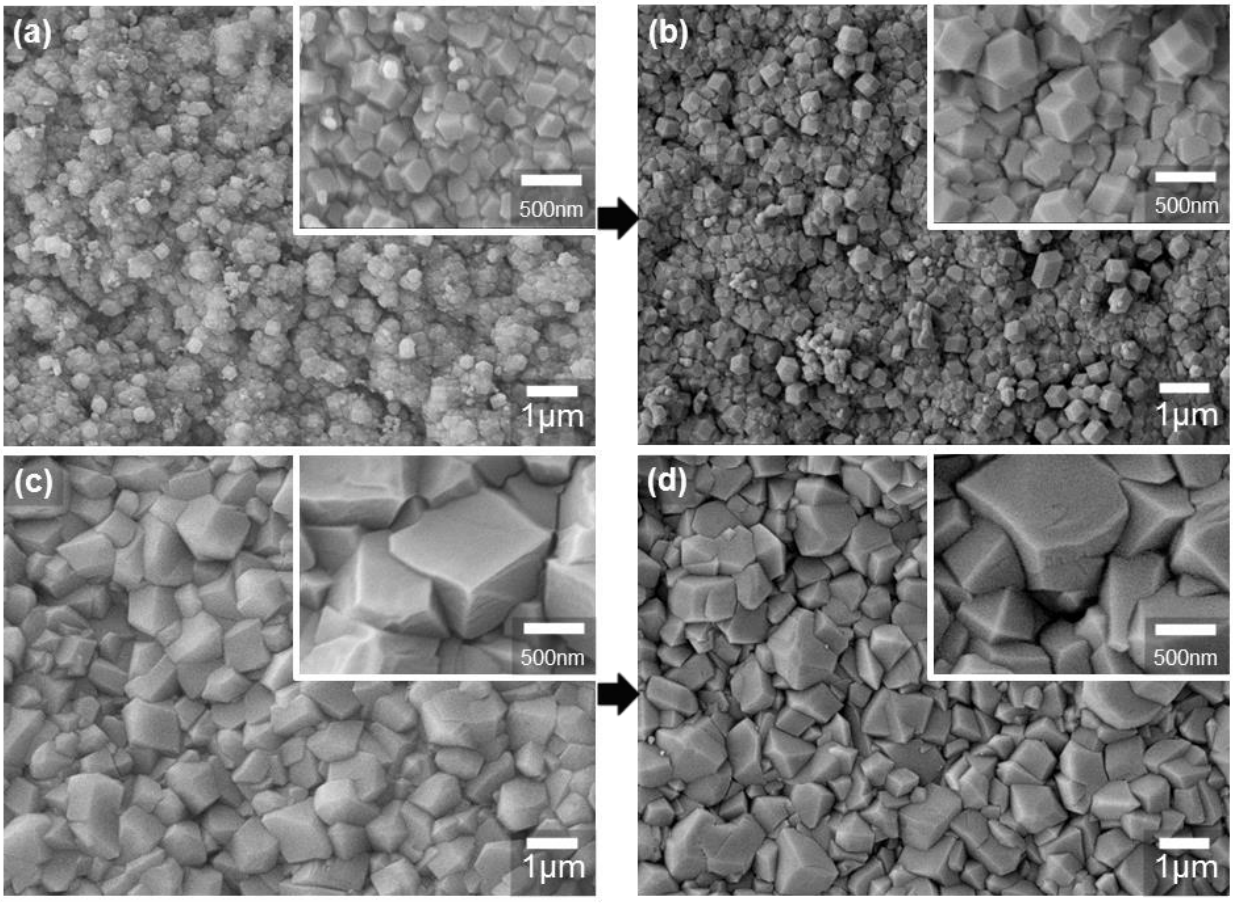

Figure 3-1 SEM images of as-synthesized CD-ZIF-8 and MW-ZIF-8 membranes (a, c) and after 60 days of off-stream measurement (b, d).

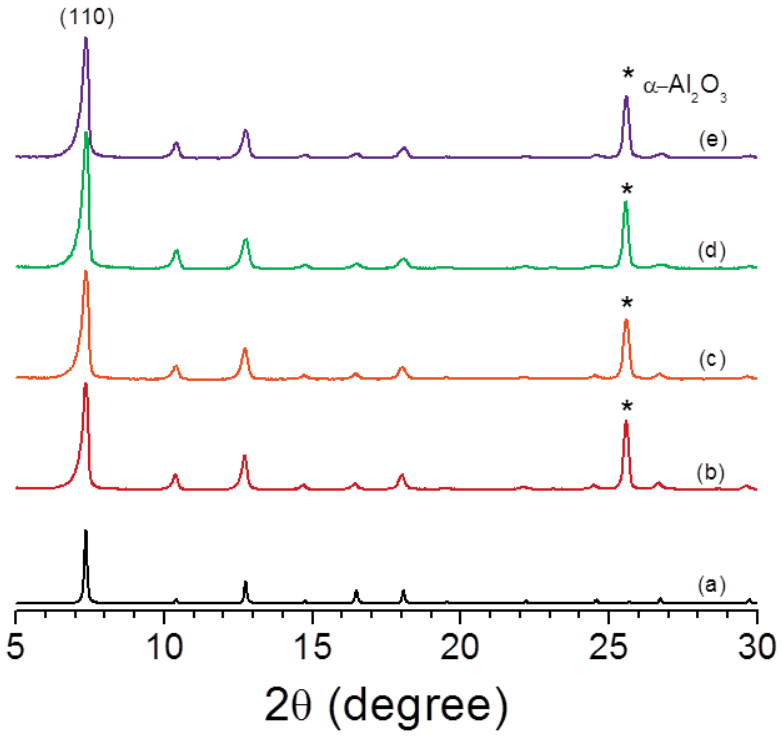

Figure 3-2 XRD patterns of (a) ZIF-8 simulated pattern, CD-ZIF-8 membrane (b) before and (c) after 60 days of off-stream measurements, and MW-ZIF-8 membrane (d) before and (e) after 60 days of off-stream measurements.

Figure 3-3 compares the time-dependent off-stream propylene/propane binary gas separation performances of ZIF-8 membranes (see Table A-1 in Appendix A for the absolute performances of the membranes). The propylene permeance of the CD-ZIF-8 membrane dropped by ~75% of its initial value while the selectivity increased 6 times of its initial value after 60 days of measurement. In contrast, the MW-ZIF-8 membrane showed much stable separation performance: although the propylene permeance decreased by ~ 25%, the selectivity remained constant even after 60 days of measurement. This drastic contrast in the long-term permeation behaviors of the CD-ZIF-8 and MW-ZIF-8 membranes is likely due to the difference in their defects including surface defects (*i.e.*, the CD-ZIF-8 membrane is more defective, thereby more

prone to change). It should be noted that the MW-ZIF-8 membranes are not as stable as previously reported ZIF-8 membranes by Lin and coworkers[40] even though the MW-ZIF-8 membranes were prepared under the similar aqueous secondary growth conditions as for the membranes by Lin and coworkers[40].

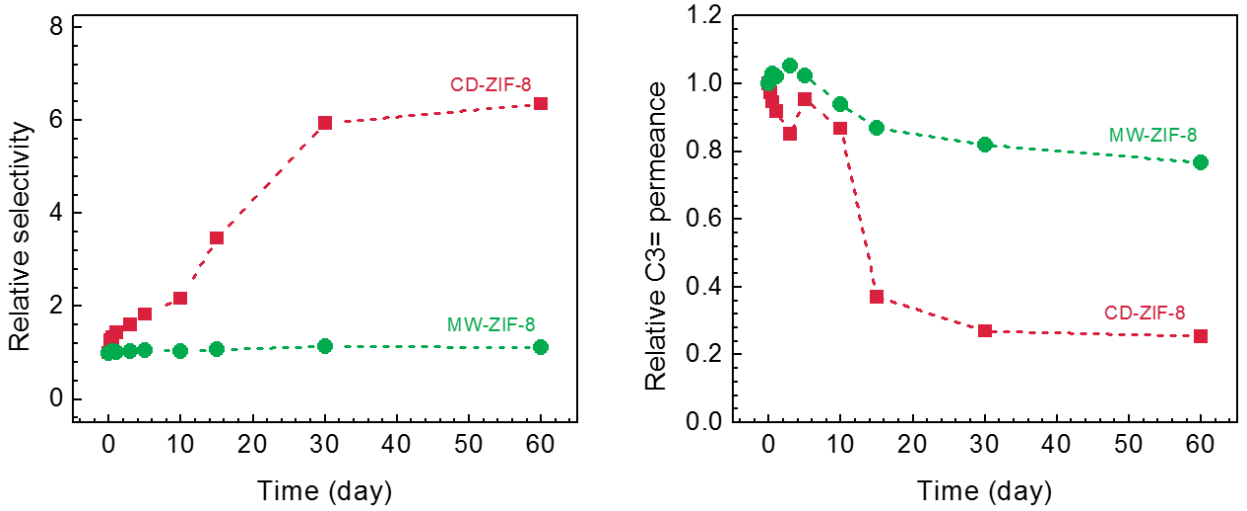

Figure 3-3 Time-dependent performances of (–■–) CD-ZIF-8 and (–●–) MW-ZIF-8 membranes. Note that separation factors and propylene permeances are normalized with respect to the initial values.

3.3.2. Defects of ZIF-8 membranes

Formation of defects in crystalline materials depends on kinetic variables such as temperature, chemical compositions, etc. In general, given similar conditions, the faster the crystals form, the more defective the crystals become due to the kinetic trapping of structures at local energy minima. The CD membranes were more rapidly synthesized as compared to the MW membranes due in part to the presence of a deprotonating agent (*i.e.*, sodium formate). It is our hypothesis that the faster CD method produces more defective ZIF-8 membranes (both in

grains and grain boundaries), thereby more reactive and less stable than the slower MW method. Moreover, Zhang et al.[120] reported in their recent work on computational characterization of point defects in ZIF-8 that when formate ions are present in an aqueous solution, linker vacancy formation is favorable under both synthesis and post-synthesis steps. It was hypothesized that formates may play an important role in the formation of defects (both bulk and surface) in ZIF-8 (CD-ZIF-8 crystals) during the synthesis step by increasing the reaction rate as a deprotonator as well as by competing with mIm as a modulating agent[83].

To prove the above-mentioned hypothesis, homogeneously-grown ZIF-8 crystals were collected from the mother solution of the CD-ZIF-8 membrane synthesis as well as from the mother solution after the secondary growth of the MW-ZIF-8 membranes (denoted CD-ZIF-8 and MW-ZIF-8, respectively). As summarized in Table 3-1, CD-ZIF-8 powders were prepared in methanol using zinc chloride in the presence of sodium formate while MW-ZIF-8 crystals were prepared in water using zinc nitrate without sodium formate. Though both ZIF-8 powder samples show well-faceted crystals (Figure 3-4), the CD-ZIF-8 crystals are much bigger than the MW-ZIF-8 crystals, indicating that the crystallization of the CD-ZIF-8 is faster than that of the MW-ZIF-8 likely due to the higher synthesis temperature and the presence of sodium formate.

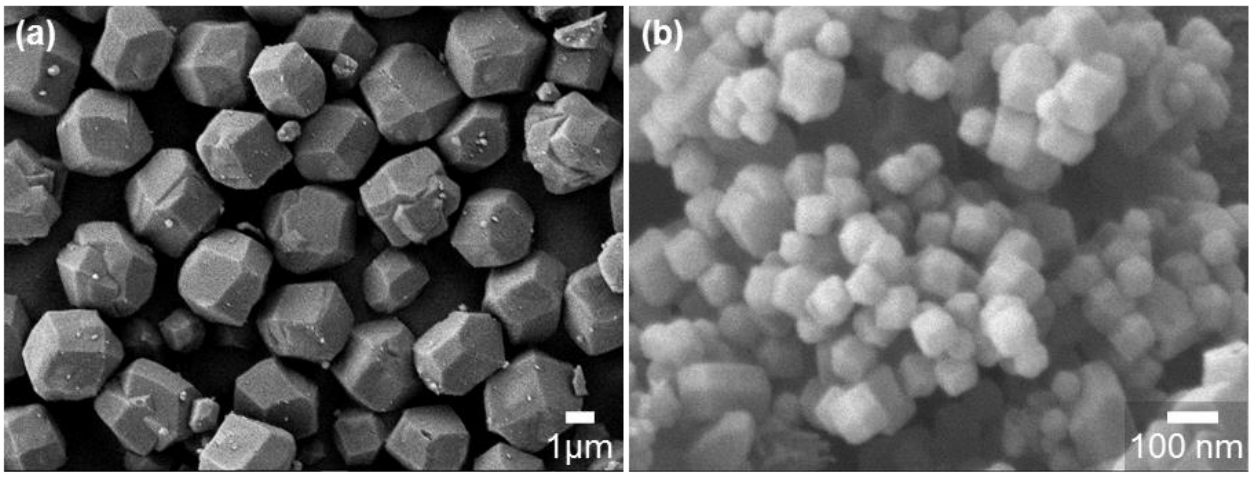

Figure 3-4 SEM images of (a) CD-ZIF-8 and (b) MW-ZIF-8 powders.

Figure 3-5 presents the normalized ^{15}N solid state NMR spectra for CD-ZIF-8 and MW-ZIF-8 powders. As shown in the figure, the CD-ZIF-8 peak is noticeably broader than that of MW-ZIF-8, clearly implying that the CD-ZIF-8 is more defective than MW-ZIF-8. N_2 adsorption analyses were conducted for both ZIF-8 particles and their BET surface areas are summarized in Table 3-2. Cheng et al.[119] related the reduction in the surface area of ZIF-8 crystals to the defects: the more defective the crystals, the smaller the surface area. As can be seen in the table, the CD-ZIF-8 exhibits substantially reduced surface area (~ 21% less) compared to the MW-ZIF-8, suggesting that the CD-ZIF-8 crystals are likely more defective than the MW-ZIF-8 crystals. Furthermore, the FT-IR spectra of the selected vibrations (see Figure 3-6) were compared. As shown in the figure, given the similar sample amounts, the CD-ZIF-8 sample displayed notably less absorbances than the MW-ZIF-8 samples, indicating that the CD-ZIF-8 sample is possibly more defective as observed by Cheng et al.[119]. This observation is further corroborated by TGA results (see Figure 3-7**)**, showing that the weight loss started at ~ 400 °C for the CD-ZIF-8 power sample which is substantially lower than ~ 560 °C for the MW-ZIF-8 sample. Initial weight loss

of MW-ZIF-8 at 100 °C is likely due to the removal of water trapped in framework during synthesis (note that water was used as a solvent). Besides, when both CD-ZIF-8 and MW-ZIF-8 membranes were exposed to steam and ligand vapor at 145 °C, as shown in Figure A-3, the CD-ZIF-8 membrane underwent a rather dramatic change while the MW-ZIF-8 membrane remained intact, consistent with the above observation that the CD-ZIF-8 membrane is more defective, thereby less stable[48].

Table 3-2 Surface areas of ZIF-8 powder samples. The reference values of ZIF-8* were taken from Park et al.[11]

	Langmuir surface area (m^2/g)	**BET surface area (m^2/g)**
CD-ZIF-8	1882.4	1160.1
MW-ZIF-8	2387.5	1474.8
ZIF-8*	1810	1630

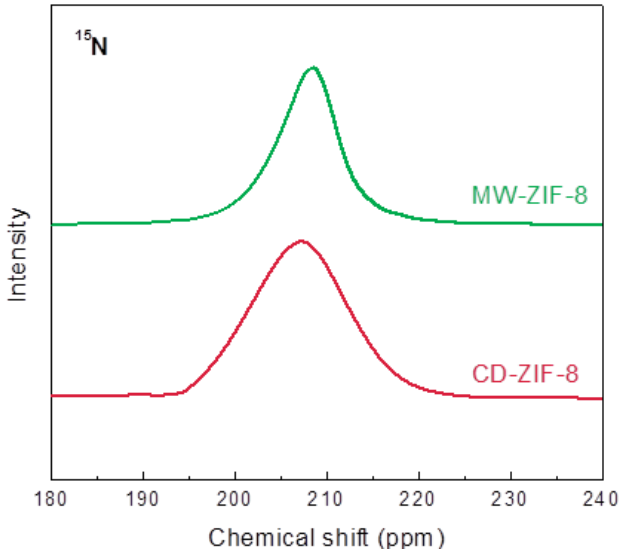

Figure 3-5 ^{15}N solid state NMR spectra of CD-ZIF-8 (—) and MW-ZIF-8 (—) powders.

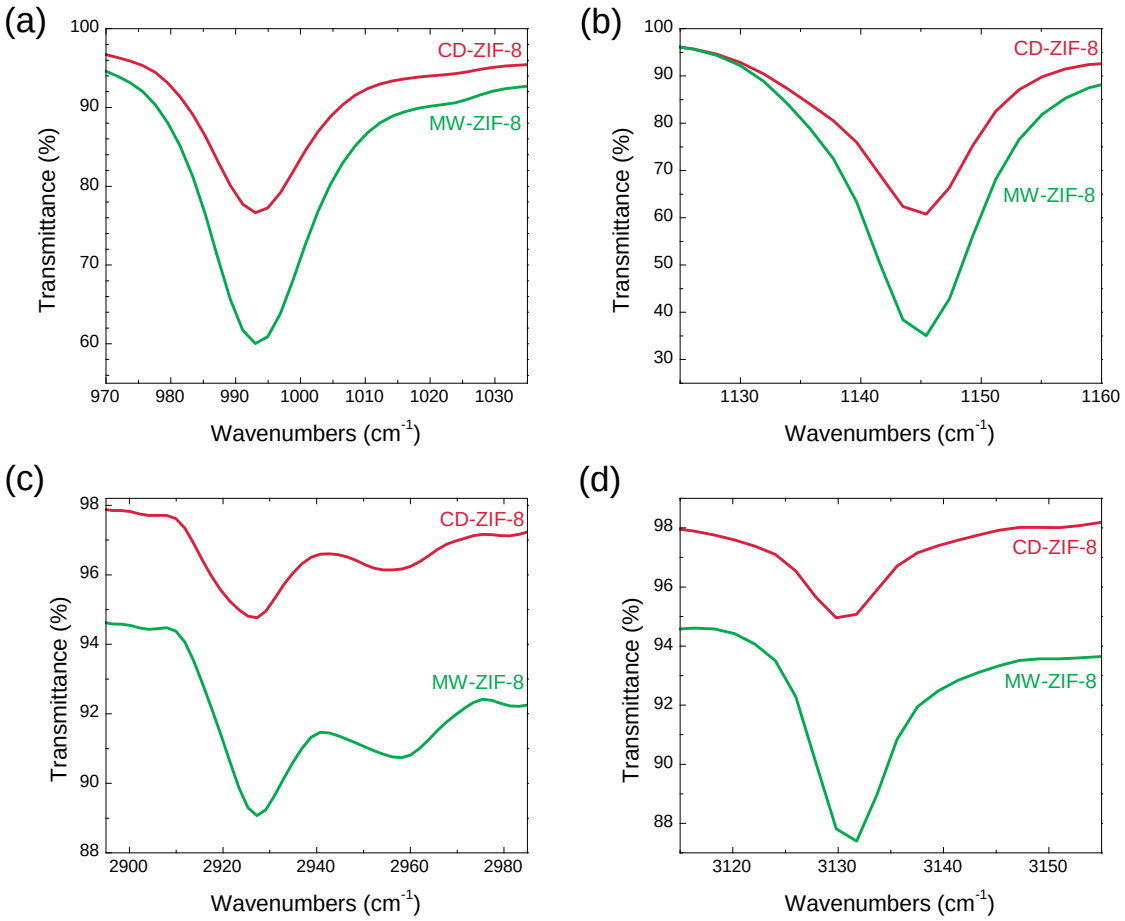

Figure 3-6 FT-IR spectra of CD-ZIF-8 (—) and MW-ZIF-8 (—) powders: (a) C=C−N twisting (out-of-plane bending, 995cm^{-1}), (b) =C−H bending and C−N bending (1146 cm^{-1}), (c) C−H symmetric and asymmetric stretching of CH_3 (2932 and 2957cm^{-1}, respectively), and (d) =C−H asymmetric stretching (3134 cm^{-1}).

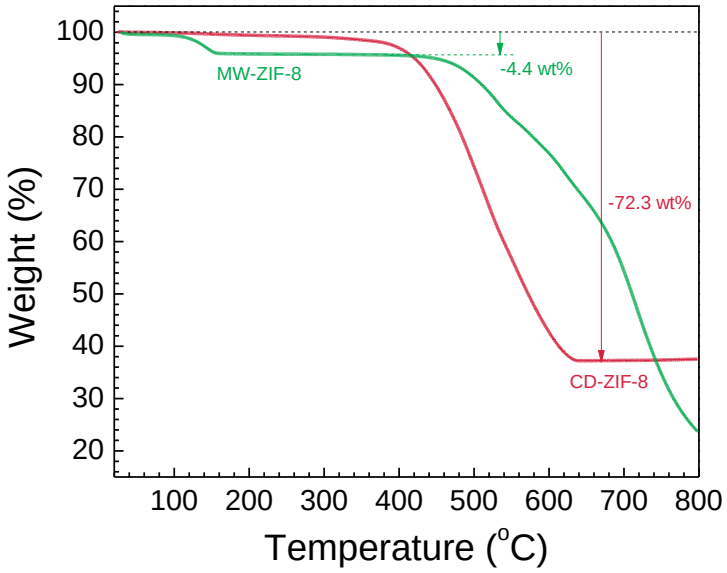

Figure 3-7 Thermal Gravimetric Analysis (TGA) results of CD-ZIF-8 (—) and MW-ZIF-8 (—) powders.

Surface termination of ZIF-8 membranes may vary depending on synthesis methods. Specifically, ZIF-8 membranes are likely to be terminated with zinc rich surfaces[121] and under coordinated zinc sites are saturated by negatively charged components available in synthetic and/or post synthetic conditions[118]. Surface terminations of as-synthesized CD- and MW-ZIF-8 membranes were investigated by XPS (see Figure 3-8). Both membranes exhibited a negligible difference in the N spectra, whereas the clear presence of formate moieties was observed in the CD-ZIF-8 membrane in the C spectra. The O spectra showed the relatively strong peaks of carbonate and hydroxide terminal groups in the MW-ZIF-8 membrane as compared to the CD-ZIF-8 membrane. This XPS observation strongly suggests that MW-ZIF-8 membranes are mostly terminated with carbonates and hydroxides due to the water in the synthesis solution while CD-ZIF-8 membranes are likely terminated with formates along with the water-associated terminal groups. It is our hypothesis that the formate terminal groups are less stable in the

presence of residual and/or ambient water than the water-originated surface terminal groups such as hydroxides and carbonates.

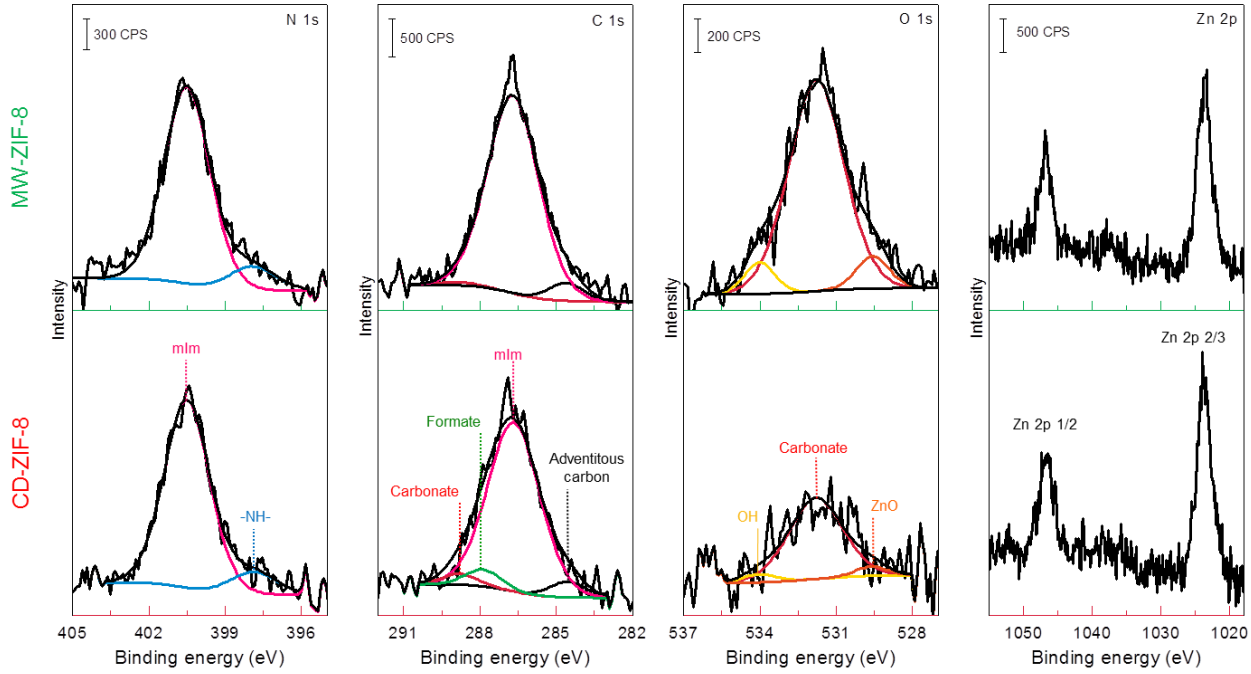

Figure 3-8 Comparison of high resolution XPS spectra of CD-ZIF-8 (bottom) and MW-ZIF-8 (top) membranes. N, C, O and Zn from the left.

Preceding results suggest that as compared to MW-ZIF-8 membranes, CD-ZIF-8 membranes possess more bulk defects (*i.e.*, more defective grains) and more reactive surfaces (*i.e.*, more reactive grain boundaries and external surfaces). As a result, CD-ZIF-8 membranes are more prone to undergoing changes not only in their local structures but also their surface structures in the presence of water. These structural changes might result in the improved grain boundary structures, thereby reducing the propylene permeance while enhancing the propylene/propane separation factor.

3.3.3. Thermal activation of CD-ZIF-8 membranes prior to off-stream measurement

As mentioned above, we hypothesized that the ambient water molecules as well as the residual water molecules in the framework might lead to changes in both bulk and surface structures of more defective CD-ZIF-8 membranes, consequently affecting their performance during the off-stream measurements. It is worthy of mentioning here that relative humidity in Texas (RH: 30 ~ 80 % in a fume hood) is significantly higher than that in Arizona (RH: 20.9 ~ 23.6 %) [40]. It is reminded that the long-term stability measurements were conducted in an open cell arrangement where the membranes were exposed to ambient conditions between permeation measurements (Figure A-1 b in Appendix A). To test this above-mentioned hypothesis, first, we dried the CD-ZIF-8 membranes at 100 °C for 12 hrs under vacuum to remove any solvent molecules trapped in the framework. Second, to prevent ambient water molecules from contacting ZIF-8 membranes in-between permeation measurements, we isolated the permeation cell between the permeation measurements (*i.e.*, closed cell arrangement) by capping the four union fittings connected to the cell (Figure A1 b). The CD-ZIF-8 membrane dried at 100 °C before the off-stream measurement and kept in a closed cell is denoted CD-ZIF-8-100-C while maintained in an opened cell is named CD-ZIF-8-100-O.

After membranes were additionally activated at 100 °C under vacuum, as presented in Figure A6, the selectivities remained the same while the propylene permeances dropped significantly. It is surmised that the additional activation at 100 °C for 12 hrs under vacuum might have decreased the sticking coefficients of gases on the membrane surface due to the rearrangement of surface terminal groups, thereby reducing gas adsorption which in turn resulted in decreased permeances but similar selectivities. The time-dependent off-stream measurement results are plotted in Figure 9. Several observations can be made. First, the propylene

permeances of CD-ZIF-8 membranes regardless of open vs closed cell arrangement, when further activated at 100 °C for 12 hrs under vacuum, decreased less than that of the as-activated membranes. The time-dependent selectivity of the CD-ZIF-8 membranes after further activation, however, shows a stark contrast depending on whether the cell is open or closed between the measurements: when open, the selectivity increases while when closed, the selectivity is relatively stable, though slightly decreased. This relatively stable selectivity and propylene permeance of the CD-ZIF-8-100-C membranes can be explained by the fact that the membranes are completely isolated from ambient water before and during the measurements. With no water interacting with defects (both bulk and surface defects), the membranes show more stable long-term performances.

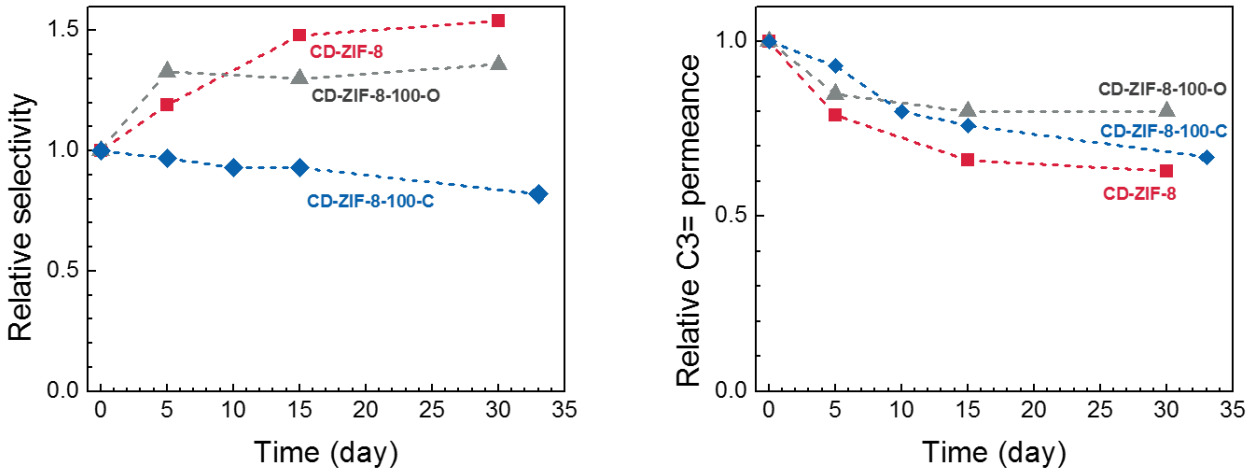

Figure 3-9 Time-dependent separation performances of (−■−) CD-ZIF-8 and (−▲−) CD-ZIF-8-100-O, (−◆−) CD-ZIF-8-100-C. Note that separation factors and propylene permeances are normalized with respect to the initial values.

3.3.4. Post-synthetic ligand treatment to stabilize the performance of CD-ZIF-8 membranes

Based on the observations made above, in order to stabilize the performance of CD-ZIF-8 membranes, we reasoned it critical to reduce their defects (in particular, surface defects). We reckoned that post-synthetic ligand treatment (PL) might reduce more reactive defects such as formate terminal groups, thereby stabilizing CD-ZIF-8 membranes. It is noted that post-synthetic ligand treatment was used to stabilize defective ZIF-67 membranes in our recent report [25]. CD-ZIF-8 membranes were post-synthetically treated at 60 and 120 °C in aqueous ligand (mIm) solutions with two different ligand concentrations (15 and 25 wt. %) and named according to treatment conditions (denoted CD-PL-120-15, CD-PL-120-25, and CD-PL-60-25, respectively), as described in the Supplementary Information. After the post-synthetic ligand treatment, as seen in the electron micrographs (Figure 3-10), ZIF-8 membranes treated at 120 °C regardless of ligand concentrations underwent more drastic morphological change than CD-PL-60-25. The XRD patterns of the treated membranes (see Figure 3-11) suggest that while all membranes retained crystal structures, when treated in 25 wt. % ligand solutions, the crystallinities of the membranes were somewhat compromised as evidenced by the reduction in the (110) peak intensity. The membranes treated at 120 °C did not show any gas separation regardless of the ligand concentrations. On the contrary, as shown in Figure 3-12, the membranes treated at 60 °C with 25 wt. % ligand concentration exhibited much enhanced long-term stability as compared with untreated CD-ZIF-8 membranes: the separation factor initially increased two folds then remained unchanged while the permeance value dropped initially and then stabilized. Table S2 shows the absolute values of binary gas performance data. After post-synthetic ligand treatment, the propylene permeance of the CD-ZIF-8 membrane was decreased while its selectivity was increased. The enhanced selectivity with decreased permeance is most likely due to the healing

of the grain boundary defects by the post-synthetic ligand treatment, leading to the reduction in the non-selective diffusion pathways. This explanation is supported by the XPS analysis after the hydrothermal ligand treatment as presented in Figure A-6 in Appendix A. As shown in the figure, the more reactive secondary amine and formate moieties were notably decreased while the less reactive hydroxide and carbonate moieties increased. This strongly suggests that the hydrothermal ligand treatment saturates under coordinated surface zinc sites with more stable surface terminal groups such as hydroxide moieties, thereby making the membranes more stable.

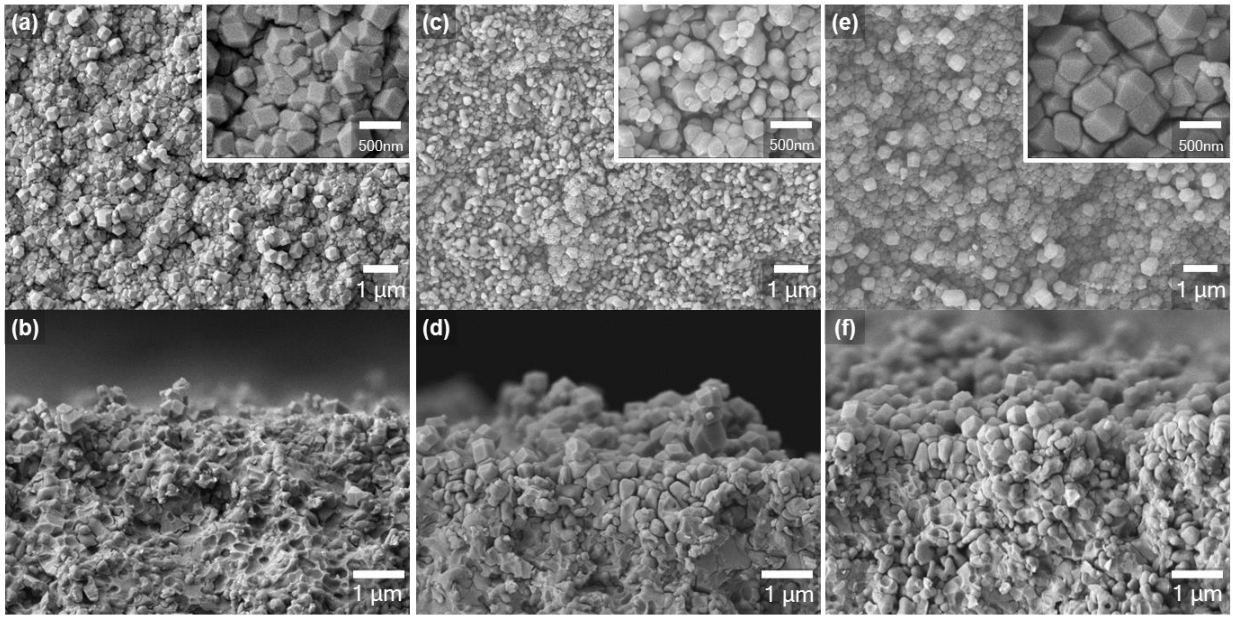

Figure 3-10 SEM images of top (upper) and cross-sectional (lower) views of (a, b) CD-PL-60-25, (c, d) CD-PL-120-15, and (e, f) CD-PL-120-25, respectively.

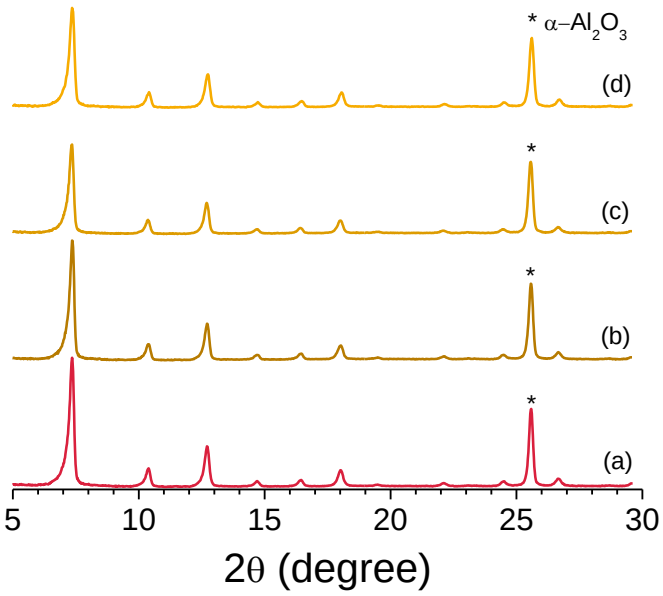

Figure 3-11 XRD patterns of (a) CD-ZIF-8, (b) CD-PL-120-15, (c) CD-PL-120-25, and (d) CD-PL-60-25 membranes.

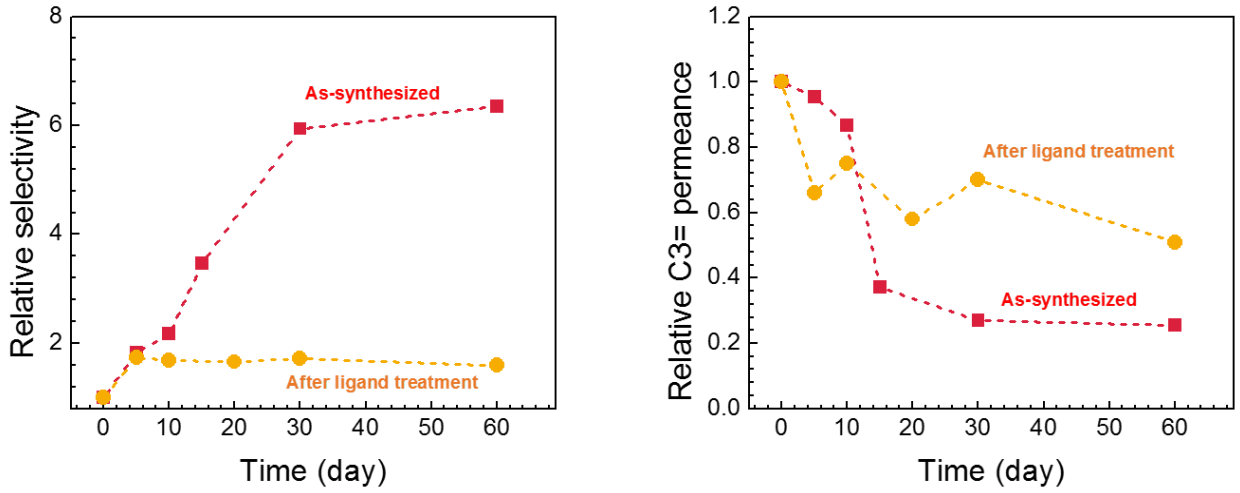

Figure 3-12 Time-dependent propylene/propane separation performances of CD-ZIF-8 membranes (ZIF-8-PL-60-25) (–●–) before and (–■–) after ligand treatment. Note that separation factors and propylene permeances are normalized with respect to the initial values.

3.4. Conclusion

In conclusion, we report the time-dependent propylene/propane separation performances of highly propylene-selective ZIF-8 membranes prepared by two different synthesis methods, counter-diffusion-based *in situ* (CD method) and microwave-assisted seeding and secondary growth (MW method). ZIF-8 membranes prepared by the CD method (CD-ZIF-8 membranes) were found to be less stable than those by the MW method (MW-ZIF-8 membranes). The propylene permeance of CD-ZIF-8 membranes was reduced by ~ 75% after 60 days while their propylene/propane selectivity increased more than 6 times. The relative instability of CD-ZIF-8 membranes was attributed to the more defective nature (both bulk and surface) of the CD-ZIF-8 membranes resulting from the faster crystallization in combination with other synthesis parameters such as the presence of sodium formate. It was shown that the high energy defect sites on the CD-ZIF-8 membranes likely underwent local structural changes, especially on the grain boundaries in the presence of ambient water, resulting in the dynamic permeation behaviors of the membranes. Lastly, the long-term stability of the CD-ZIF-8 membranes was improved by post-synthetically treating the membranes in an aqueous ligand solution possibly resulting from the reduction of defects upon the treatment. The current study is a significant step forward in the practical applications of these promising ZIF-8 membranes by not only providing understanding on the long-term stability of the membranes but also offering ways to improve their stability.

CHAPTER IV

HIGH-FLUX ZEOLITIC IMIDAZOLATE FRAMEWORK MEMBRANES FOR PROPYLENE/PROPANE SEPARATION BY POSTSYNTHETIC LINKER EXCHANGE*

4.1. Introduction

Separation of light olefins from paraffins (for example, ethylene and propylene from ethane and propane, respectively) is one of the most significant separations in the chemical and petrochemical industries; however, this task remains challenging because of similarities in the physicochemical properties of these olefins.[1-3] A traditional olefin/ paraffin separation method is cryodistillation, resulting in significant energy consumption and capital cost.[2-3] Hence, energy-efficient membrane-based separations have attracted tremendous research interest as an alternative. There are, however, no commercially available membranes for the separation of light olefin/paraffin molecules.[2] This is mainly because of the limitation of current polymeric materials, [1c] thereby making the development of new membrane materials highly desirable.

Zeolitic imidazolate frameworks (ZIFs),[10-11, 56] a subclass of metal–organic frameworks (MOFs),[12, 122]] are composed of metal ions (usually Zn^{2+} or Co^{2+}) and imidazole-derived organic linkers. ZIFs are considered promising new membrane materials since they display ultramicroporosities (pores less than 5 c) and relatively robust thermal/chemical stabilities compared to other MOFs.[19, 22-23, 42, 45-46, 112, 123-125] In particular, membranes of a prototypical ZIF-8 made of zinc and 2-methylimidazole (forming a sodalite (SOD) topology) have shown impressive kinetic propylene/propane separation capabilities[20, 126] because of an effective

* Reprinted with permission from "High-flux zeolitic imidazolate framework membranes for propylene/propane separation by postsynthetic linker exchange" by Moon Joo Lee, Dr. Hyuk Taek Kwon, and Prof. Dr. Hae-Kwon Jeong, 2018. *Angewandte Chemie International Ed.*, 57, 156-161, Copyright 2017 by John Wiley and Sons.

aperture size in the range of 4.0–4.2 Å[22] In fact, polycrystalline ZIF-8 membranes have recently demonstrated propylene/propane separation factors greater than 150.[23-24] However, for practical purposes a significant improvement in the productivity (that is, throughput) of polycrystalline ZIF-8 membranes is required so as to justify their relatively high cost per unit area as compared to polymer membranes[127] The membrane productivity is determined according to the following equation [Eq. (4-1)]:

$$Q_i = -P_i\,(\Delta\rho_i/l)A \qquad (4\text{-}1)$$

where P_i, $\Delta\rho_i$, l, and A are the permeability of gas A, partial pressure difference of gas i between feed and permeate sides, membrane thickness, and membrane area, respectively. Given fixed operation conditions, the membrane productivity can, therefore, be enhanced by increasing membrane area and substantially reducing membrane thickness.

To increase membrane area, ZIF-8 membranes have been prepared on tubular and hollow fiber supports, such as ceramic[17, 128-129] and carbon[130-132] tubes as well as ceramic[76, 85, 133-136] and polymer[23, 111, 137] hollow fibers. Some of these ZIF-8 membranes have shown excellent propylene/propane separation performances[23, 76, 85]. On the other hand, decreasing membrane thickness turns out to be a lot more challenging because of the increased chance of poor grain boundary structure and the surface roughness of supports. Shamsaei et al.[92] reported submicron thick ZIF-8 membranes (ca. 200 nm thick) prepared on an asymmetric polymer substrate by chemical vapor modification. Hou et al.[138] prepared ZIF-8 membranes with a thickness of about 400 nm on titania-coated porous polymeric supports using a simple immersion technique. Interestingly, Wang and his coworkers[139-140] reported the preparation of ultrathin ZIF-8/graphene-oxide nanocomposite membranes (ca. 430 nm thick) on anodized aluminum oxide supports. The resulting membranes showed an ideal propylene/propane selectivity of about 35,

with relatively low propylene permeance given their submicron membrane thickness. None of these submicron thick ZIF-8 membranes were tested for binary propylene/propane separation. Recently, Kwon et al.[48] reported thin ZIF-8 membranes (ca. 300–400 nm thick) upon merging ZIF-8 seed nanocrystals by an Ostwald-ripening-like process in the presence of a ligand vapor at elevated temperature. Unfortunately, only one of their submicron thick ZIF-8 membranes demonstrated a good propylene/propane separation factor, with unexpectedly low propylene permeance. The low propylene permeance of the membrane might be a result of the presence of extra framework linkers in the SOD cages, thereby impeding gas transport. All of the aforementioned reports attest to the challenge of reducing the thickness of ZIF-8 membranes using conventional approaches. In fact, Tsapatsis[127] argues that, with the current high costs per unit area of zeolite membranes, increasing the flux by an order of magnitude as compared to the current state of the art is the only way forward. This means that the thickness of zeolite membranes needs to be decreased to about 50 nm for certain separations,[127] which is the case for ZIF membranes as well. As described above, obtaining sub 100 nm thick ZIF-8 membranes is a formidable task, requiring unconventional strategies.

Postsynthetic modification (PSM) has been widely utilized in MOFs because of the labile nature of the coordination chemistry of MOFs.[108, 141-143] Given the complex and sensitive nature of the direct crystallization of MOFs, PSM can provide an efficient and facile means by which to prepare MOFs that are difficult to synthesize by de novo methods. The PSM of MOFs includes 1) postsynthetic ligand exchange (PSLE) or solvent-assisted ligand exchange (SALE),[95, 98-101] 2) postsynthetic metal exchange (PSME or transmetalation),[144] and 3) post-synthetic thermal/chemical modification[145-147]. Upon PSM, the chemical structure of a parent MOF is

changed while the topology of the child MOF may or may not be the same as that of the parent.[94-95]

Herein, we propose a novel approach to significantly increase the propylene permeance of ZIF-8 membranes by reducing the effective membrane thickness with PSLE. ZIF-8 membranes were prepared using a counter-diffusion-based in situ method (hereafter, CD method). The 2-methylimidazole linkers (hereafter mIm) of ZIF-8 membranes were partially exchanged with 2-imidazolecarboxaldehyde (hereafter Ica) ZIF-90 linkers. ZIF-90 is isostructural to ZIF-8, with an effective aperture size of approximately 5.0 Å[77]. A series of characterization tools was utilized to determine the crystalline structures and morphologies of linker-exchanged ZIF-8 membranes, as well as the kinetics of linker exchange. The propylene/propane separation performances of linker-exchanged ZIF-8 membranes were measured and compared with those of as-synthesized ZIF-8 membranes. ZIF-8 membranes synthesized using a different method were also subjected to the linker-exchange process to examine how synthesis methods affect this linker-exchange effect. The linker-exchanged membranes were subsequently decorated with long hydrocarbon chains to improve their water repellency.

4.2. Experimental

4.2.1. Materials

α-Al_2O_3 powder was obtained from Baikowski, and polyvinyl alcohol (PVA) was purchased from Duksan. Zinc nitrate hexahydrate ($Zn(NO_3)_2 \cdot 6H_2O$, 98%), 2-methylimidazole ($C_4H_6N_2$, 99%, hereafter mIm), sodium formate (HCO_2Na, 99%), and acetic acid-d_4 (CD_3CO_2D, ≥99.9 atom % D) were obtained from Sigma Aldrich. Zinc chloride ($ZnCl_2$, 99.99%, anhydrous),

methanol (CH_3OH, >99%), and 2-imidazolecarboxaldehyde ($C_4H_4N_2O$, 97%, hereafter Ica) were obtained from Alfa Aesar. Dodecylamine ($CH_3(CH_2)_{11}NH_2$, puriss., ≥99.5%, hereafter DDA) was purchased from Fluka.

4.2.2. Preparation of porous α-Al_2O_3 supports, ZIF-8 powders, and ZIF-8 membranes

Porous α-Al_2O_3 support disks were fabricated as previously reported.[45] In short, 10 g of alumina powder and 1 ml of a PVA binder solution were homogeneously mixed. The PVA binder solution was formulated by dissolving 3 g of PVA in 95 ml of D.I. water along with 5 ml of 1M HNO_3 at 85 ^oC for 90 min. A support disk was prepared by loading 2.1 g of the alumina/binder mixture into a die and subsequently compressing at 10 t for 1 minute followed by sintering at 1100 ° C for 2 hrs. The sintered disk was polished with a sand paper (grit# 800), ultrasonically cleaned in methanol for 1 min and subsequently dried at 120 °C for 1 hr before use.

ZIF-8 membranes were prepared by using counter-diffusion *in situ* method (CD method) previously reported from our group[45, 47] (hereafter, CD-ZIF-8 membranes). A metal precursor solution (0.98 g of zinc chloride in 40 ml methanol) and a ligand solution (5.19 g of mIm and 0.5 g of sodium formate in 40 ml methanol) were prepared at room temperature. All reagents were used as received without further purification except sodium formate vacuum-dried at 100 °C for 6 hrs before use. An alumina disk was saturated with Zn^{2+} in the metal precursor solution for 1 hr and then transferred to a Teflon-lined autoclave containing 40 ml of the ligand precursor solution. The autoclave was kept in a convection oven at 120 °C for 4 hrs and then naturally cooled to room temperature. The resulting membrane was washed in 35 ml of fresh methanol for 12 hrs. The back of the disk was rubbed with sand papers (grit # 350). The membrane was

washed in 35 ml of fresh methanol for 5 days and dried at room temperature for 5 hrs and at 60 °C for 1 hr.

ZIF-8 membranes were fabricated by using our previously reported microwave-assisted seeding and secondary growth method (MW method) [46] and, hereafter, are referred to as MW-ZIF-8 membranes. Briefly, to prepare a ZIF-8 seed crystal layer, an alumina disk was first saturated with Zn^{2+} by immersing in 2.43 g of zinc nitrate hexahydrate in 40 ml of methanol for 1 hr. Subsequently, the Zn^{2+} saturated support was placed in the microwave-resistant tube containing 30 ml of ligand solution (2.59 g of mIm and 0.125 g of sodium formate in 40 ml methanol) and then treated under microwave (100W) for 1.5 min. The seeded alumina support was washed in 35 ml of fresh methanol for 1 day under gentle rocking followed by dried at 60 °C for 4 hrs. The subsequent secondary growth was carried out based on the aqueous recipe reported elsewhere[112]. Aqueous metal and ligand precursor solutions were prepared by dissolving 0.11 g of zinc nitrate hexahydrate and 2.27 g of mIm in 20 ml of DI water, respectively. The metal solution was added rapidly to the ligand solution and continued for stirring for 2 min. The resulting growth solution was poured into a beaker with the seeded support placed vertically using a custom-made Teflon holder. The hydrothermal reaction was conducted in a vacuum oven at 30 °C for 6 hrs under ambient pressure. After the reaction, the membrane was washed in 35 ml of fresh methanol for 5 days and then dried in an oven at 60 °C for 6 hrs.

4.2.3. Post-synthetic linker exchange (PSLE)

An as-prepared ZIF-8 membrane was solvothermally treated with a new linker (2-imidazolecarboxaldehyde, Ica) solution under a modified condition based on the literature.[98] The Ica solution was prepared by dissolving 0.1 g of Ica in 40 ml of methanol at 60 °C for 4 hrs.

Three as-prepared ZIF-8 membranes, not dried, were immersed in 40 ml of the Ica solution in a sealed Teflon container. The PSLE reaction proceeded in a preheated convection oven at 60 °C for *x* days where *x* varied from 1 to 4. After the reaction, the container was taken out of the oven and cooled to room temperature. The membrane was washed with 35 ml of fresh methanol on a gentle rocking station for 2 days by replenishing every 12 hrs. The washed linker-exchanged membrane (hereafter, Ica-ZIF-8 membrane) was then dried at room temperature for 12 hrs.

4.2.4. Post-synthetic modification (PSM)

The surface of an Ica-ZIF-8 membrane was modified by an imine condensation reaction between the carbonyl group of Ica and the amine group of dodecylamine (DDA). In a typical modification, a DDA solution was prepared by dissolving 0.585 g of DDA in 20 ml of methanol. An Ica-ZIF-8 membrane exchanged for 3 days was immersed in the DDA solution at room temperature for 24 hrs. The resulting membrane was then washed with 35 ml of methanol for 2 days followed by drying at ambient temperature for 12 hrs.

4.2.5. Propylene/propane gas permeation test

The propylene/propane binary permeation performances of ZIF-8 membranes were evaluated by the Wicke-Kallenbach technique (see Figure B-1 in Appendix B) at room temperature under atmospheric pressure. An equimolar mixture of propylene/propane was provided at 100 cc/min to a feed side while an argon sweep gas was supplied at 100 cc/min to a permeate side. Steady state was declared after the feed gas was provided to the membrane for 2 hrs. The composition of permeate gas was then analyzed by a gas chromatography (Agilent GC 7280A) with a column (HP-PLOT/Q) installed.

4.2.6. Characterizations

X-ray diffraction (XRD) patterns were obtained with a desktop X-ray diffractometer (Rigaku, Miniflex II) with Cu-Kα radiation (λ = 1.5406 Å). Scanning electron microscope (SEM) images were collected with a JEOL JSM-7500F operated at 5 keV of an acceleration voltage with 15 mm of working distance by using a lower secondary electron image (LEI) detector. Energy dispersive X-ray (EDX) mapping was conducted with an Oxford EDS system operated at 20 keV of an acceleration voltage with 8 mm working distance by using secondary electron image (SEI) detector. Solution ^{1}H NMR measurements were performed using an INOVA 500 MHz spectrometer (Varian) to determine the degree of linker exchange. Prior to the measurements, Ica-exchanged ZIF-8 membranes were dissolved in d_4-acetic acid. ATR-FTIR spectra of ZIF-8 membranes were obtained by using a single reflection diamond ATR crystal (surface area = 1.8 mm^2, refractive index = 2.4) within a Quest accessory (constant load capacity of anvil = 18 kg, Specac Inc.) using an FT-IR spectrometer (Nicolet 6700 Series, Thermo Electron). Peak heights were calculated by OMNIC™ (Thermo Ficher Scientific, Inc.). Contact angle measurements were performed and analyzed by using ImageJ software[148] with a drop analysis plug-in. Raman spectra were acquired using a Thermo Scientific DXR Raman microscope (Thermo Fisher Scientific, Inc.) with 780 nm diode laser, which is connected with a high-resolution diffraction grating (~2 cm^{-1}), a Rayleigh rejection filter, and a CCD detector.

4.3. Results and discussion

Figure 4-1 illustrates how the proposed PSLE on ZIF-8 membranes might lead to enhanced propylene permeance. Notably, the ZIF-8 membranes were synthesized by a counter-diffusion-based in situ method (hereafter, CD-ZIF-8).[45, 47] The organic mIm linkers of ZIF-8 were then replaced by Ica linkers. According to the literature,[99, 101] the linker exchange of ZIF-8 is not only a single-crystal to single-crystal transformation but also a diffusion-limited process. Based on these previously observed PSLE kinetics, it was assumed that PSLE reaction occurs from the external surface to the inner layers of the ZIF-8 membranes, and the upper layers can be considered as ZIF-90 equivalent. Notably, the effective aperture size of ZIF-90 (ca. 5.0 Å)[77] is much greater than that of ZIF-8 (ca. 4.0 Å)[22] while both share the same SOD topology (that is, they are isostructures). Since the gas diffusion in ZIFs is a thermally activated process following an Arrhenius-type temperature dependence, a slight increase in the effective apertures (that is, a decrease in the diffusional activation energy) can lead to a substantial increase in the diffusion coefficients. Therefore, it is expected that the propylene permeability of these top ZIF-90 equivalent layers could be much higher than that of the ZIF-8 bottom layers, without compromising the propylene/propane selectivity of the membranes. It is our key hypothesis that the careful exchange of mIm with Ica can lead to a reduction in the effective thickness of ZIF-8 membranes, resulting in the enhancement of the membrane productivity (that is, propylene permeance).

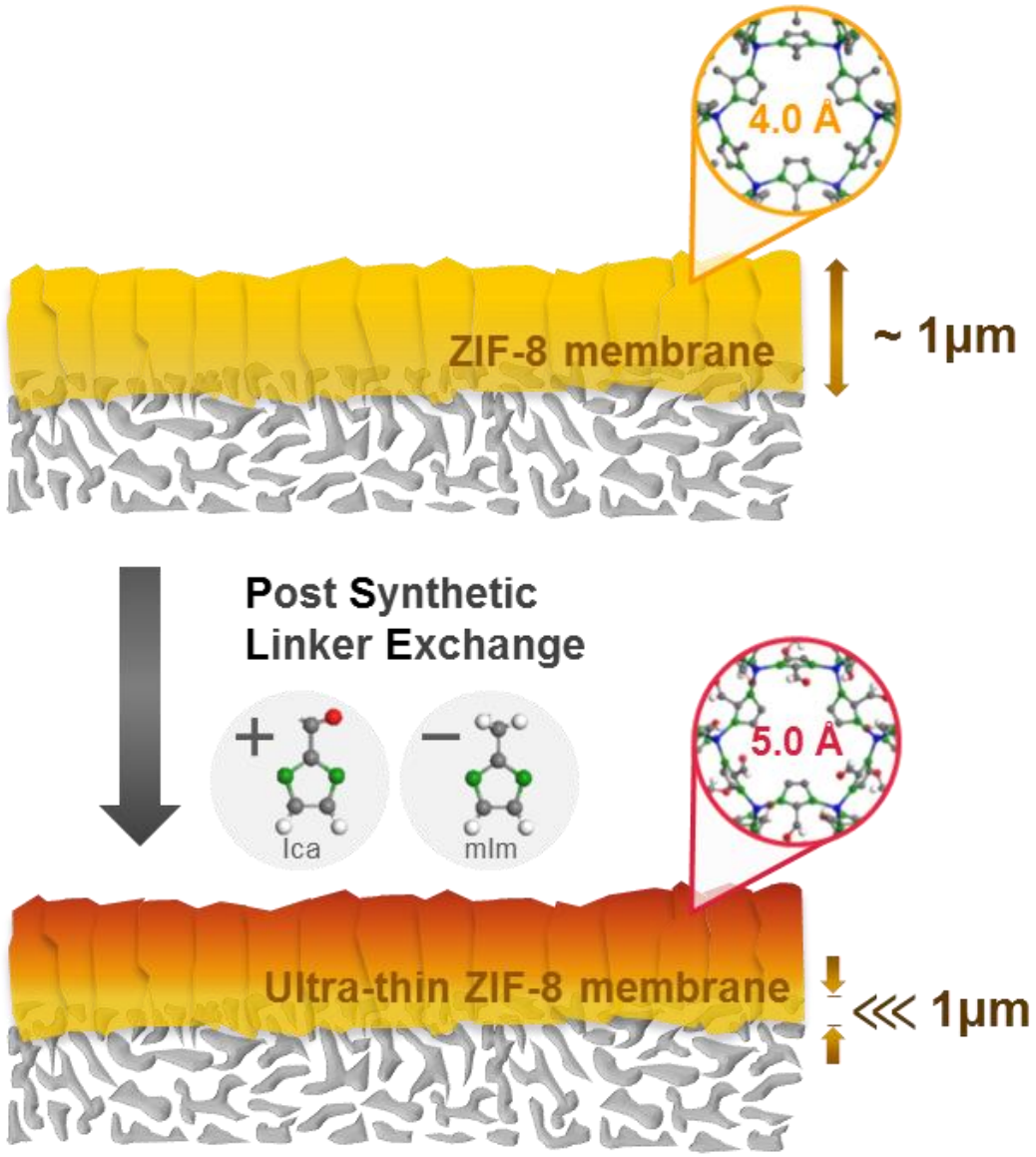

Figure 4-1 Illustration of the PSLE of mIm (ZIF-8 linker) of ZIF-8 membranes with Ica (ZIF-90 linker), resulting in a reduction of the effective membrane thickness because of an enlarged aperture upon Ica incorporation. The effective aperture sizes of ZIF-8 and ZIF-90 are ca. 4.0 and ca. 5.0 b, respectively. Key: ZIF-90 equivalent (red), ZIF-8-90 mixed linker (orange), and ZIF-8 frameworks (yellow).

4.3.1. Post-synthetic linker exchange

PSLE reactions were performed on as-synthesized ZIF-8 membranes (that is, CD-ZIF-8 membranes) by solvothermally treating them in an Ica/methanol solution at 60 8C for x days (x

varied from 1 to 4), denoted as xd-Ica-CD-ZIF-8. The membranes displayed a visible color changes upon PSLE; Ica has a yellow hue whereas mIm is white (Appendix B, Figure B-2). The systematic color change upon PSLE indicates that Ica is incorporated into the ZIF-8 framework.[99] Figure B-2 presents the attenuated total reflectance Fourier-transform infrared (ATR-FTIR) spectra of CD-ZIF-8 membranes before and after PSLE. The incorporation of Ica linkers is confirmed by the appearance of =C-H stretching bands at 2850 and 2740 cm^{-1} (Figure B-3 a - b) and the carbonyl stretching at 1700 cm^{-1} (Figure B-3 c). Figure B-3 d in the Appendix 2 presents the reaction-time-dependent absorbance of the carbonyl stretch (that is, the kinetics of Ica incorporation), showing that the amount of Ica in the framework increased as the reaction time increased and then saturated, which is confirmed by the Ica amounts normalized by the Ica amount of 4d-Ica-CD-ZIF-8 determined using ^{1}H NMR spectroscopy (Figure B-4). The total amount of Ica incorporated after 4 days of exchange was less than 7%. This relatively low extent of Ica incorporation is likely a consequence of a large number of ZIF-8 crystals formed inside the support, as shown in the scanning electron microscopy (SEM) images and energy-dispersive X-ray spectroscopy (EDX) mappings (Figure B-5).

The X-ray diffraction (XRD) patterns of the linker-exchanged membranes are shown in Figure 4-2 a, corroborating that the membranes did not show any degradation in their overall crystallinities while maintaining the SOD structures. Figures 4-2 b – f and Figure B-6 present SEM images showing the morphologies of the Ica-exchanged ZIF-8 membranes treated for different PSLE reaction periods. The top- and cross-sectional views in Figure 4-2 b – f were taken from the central regions of the membranes. The thickness of the ZIF-8 membranes was estimated to be approximately 1 mm. Upon PSLE, the size of grains did not change, while the facets of grains became more rounded, confirming single-crystal to single-crystal transformation,

as observed previously.[95, 99] Notably, this smoothening of grain facets was limited to the top layers, as evidenced by cross-sectional images (Figure 4-2 b – f). Interestingly Lee et al.[24] made similar observations when ZIF-8 membranes were solvothermally treated in an mIm/methanol solution. Furthermore, the surface of the membranes underwent nonuniform etching (Figure B-6), which appeared to be dependent upon the locations of the membrane surfaces; that is, the further away from the center, the more crystals etched. In contrast, Jayachandrabadu et al.[99] observed uniform etching of ZIF-8 microcrystal powders upon PSLE with Ica. The non-uniform etching of grains on the surface of the membranes is attributed to the concentration gradient of Ica along the radial direction of the membranes, in combination with a difference in the pKa values of monoprotonated Ica (H-Ica) and monoprotonated mIm (H-mIm). As in the case of Jayachandrabadu et al.,[99] while the diffusion of Ica to the powder samples is threedimensional, that to the membranes is two-dimensional, leading to an inhomogeneous Ica concentration profile along the radial direction (that is, the further away from the center, the higher the Ica concentration). Moreover, the pKa of H-Ica (10.2, estimated with the ACE&JChem predictor[149]) is significantly lower than that of H-mIm (14.2),[150] meaning that H-Ica can be deprotonated much more easily than H-mIm under the same conditions. The local H-Ica concentration becomes higher away from the center of the membranes, resulting in an increased proton concentration, and consequently, etching of the crystals. Notably, a similar treatment of CD-ZIF-8 membranes in H-mIm did not lead to the crystal etching,[24] likely because of the relatively higher pKa value of H-mIm.

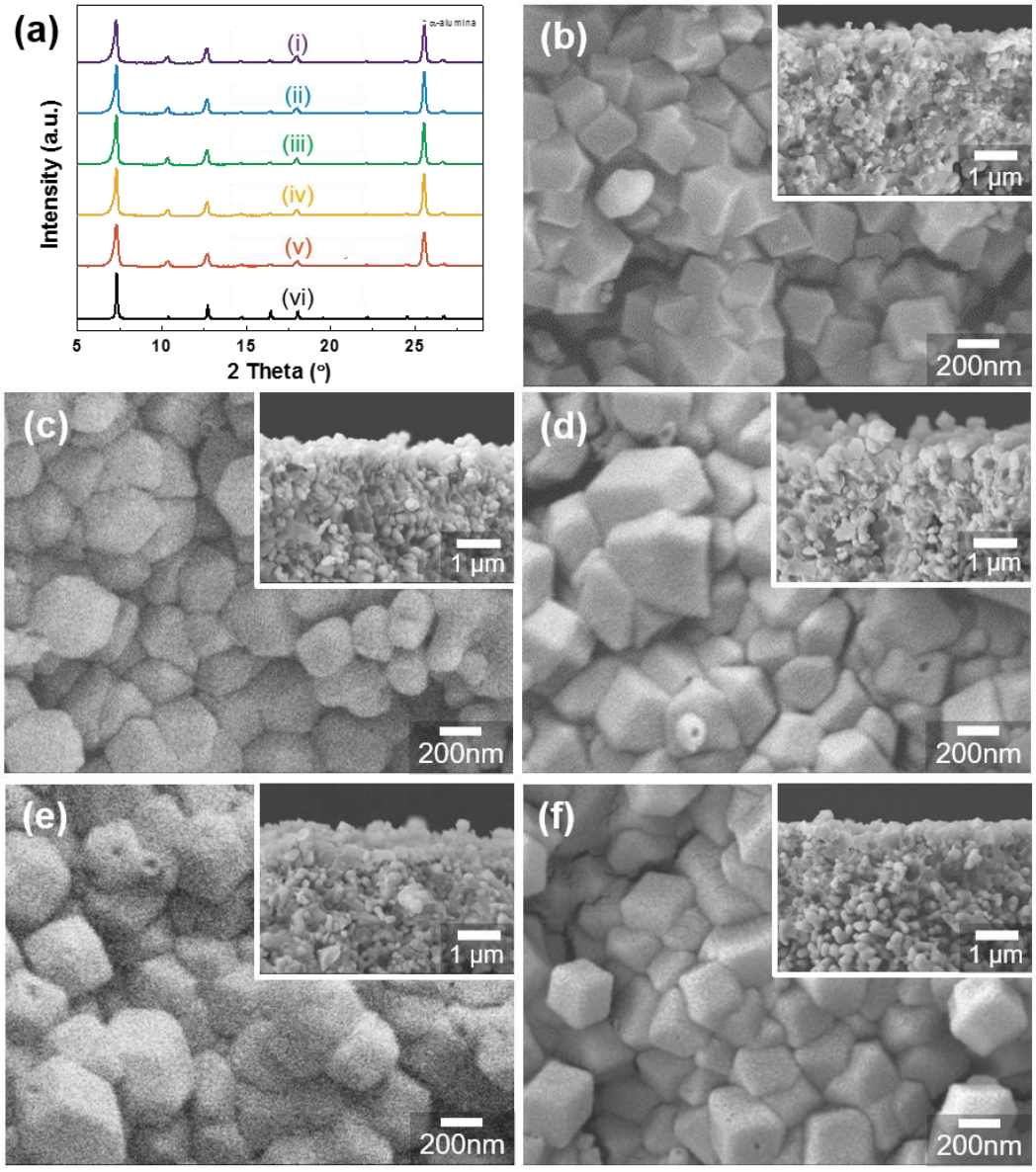

Figure 4-2 a) XRD patterns of CD-ZIF-8 membranes that have undergone Ica-exchange; i) 4d-Ica-CD-ZIF-8, ii) 3d-Ica-CD-ZIF-8, iii) 2d-IcaCD-ZIF-8, iv) 1d-Ica-CD-ZIF-8; in comparison to v) as-synthesized and vi) ZIF-8 simulated patterns. The peak at ca. 25.58 is associated with a-alumina. b–f) SEM images of top- and cross-sections of as-synthesized CD-ZIF-8 (b), 1d-Ica-CD-ZIF-8 (c), 2d-Ica-CD-ZIF-8 (d), 3d-Ica-CD-ZIF-8 (e), and 4d-Ica-CD-ZIF-8 membranes (f).

4.3.2.Propylene/propane separation performances

The binary (50/50) propylene/propane separation performances of the Ica-CD-ZIF-8 membranes were tested by the Wicke–Kallenbach method (Figure 4-3). As-synthesized ZIF-8 membranes prepared by the CD method (that is, CD-ZIF-8 membranes) displayed a propylene/propane separation factor of about 55 and a propylene permeance of 211×10^{-10} mol·m^{-2}·s^{-1}·Pa^{-1}. Upon 3 days of PSLE, the propylene permeance of the membranes (3d-Ica-CD-ZIF-8) was enhanced by 370% to 780×10^{-10} mol·m^{-2}·s^{-1}·Pa^{-1} or 260 GPU (gas permeance unit), while their separation factor was slightly compromised to about 40. To the best of our knowledge, this is the highest propylene permeance among propylene-selective membranes reported to date, including polymer[6, 30-35], carbon[8, 38-39], ZIF-8[23, 40-49, 53, 151-152] and ZIF-67 membranes (Figure 4-4). It is noted that the separation factor of ~ 40 still meets the commercially attractive separation performance for sufficient energy savings[54]. According to Colling *et al.*,[54] membranes with the propylene separation factor of 35 and the propylene permeability of 1 Barrer are required in commercially-viable three-stage membrane processes to obtain 99.6% propylene purity with 40.5 % of energy reduction. A relatively small reduction in the separation factors strongly suggests that the grain-boundary structure of the membranes remains virtually intact upon PSLE. A sharp increase in the propylene permeance of the Ica-exchanged ZIF-8 membranes (an almost fourfold enhancement) can then be attributed to a significant reduction in the effective thickness of the membranes. One plausible explanation for this decrease in the effective membrane thickness is that the effective aperture size of the upper layer of the Ica-exchanged ZIF-8 membranes was enlarged to a size similar to that of ZIF-90.

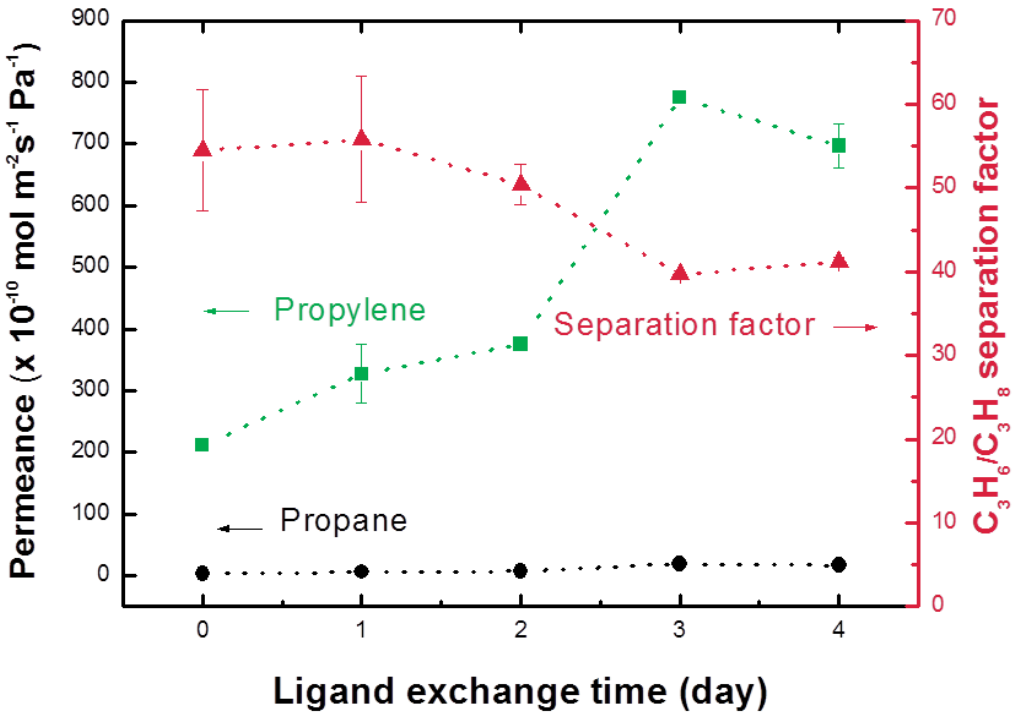

Figure 4-3 Binary propylene/propane separation performances of CD-ZIF-8 membranes postsynthetically linker exchanged with Ica for different reaction times. Permeation measurements were conducted at room temperature.

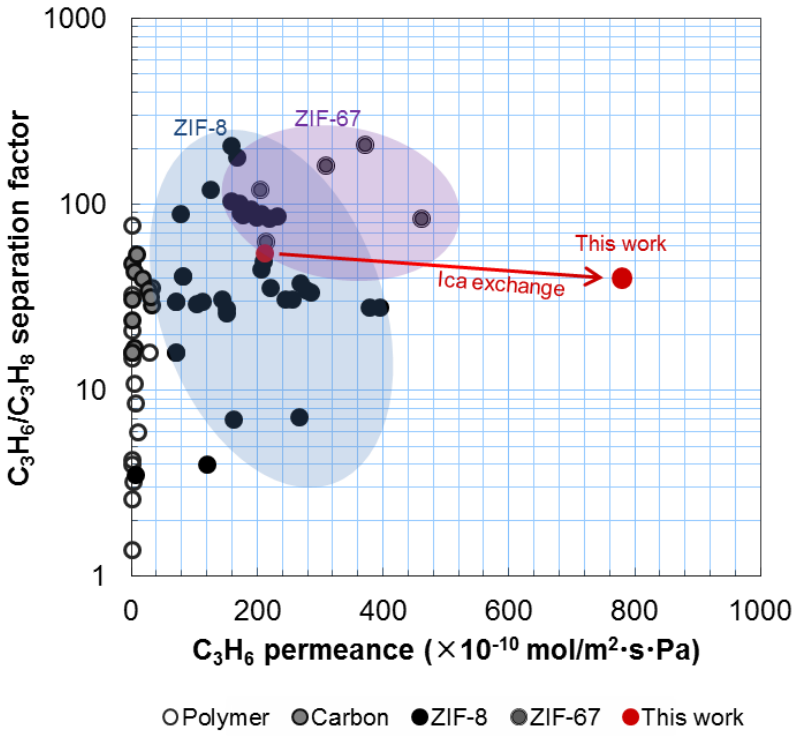

Figure 4-4 Propylene/propane separation performances of as-synthesized CD-ZIF-8 and 3d-Ica-CD-ZIF-8 membranes (●) in comparison with those of polymer, carbon, ZIF-8, and ZIF-67 membranes. Propylene permeances of polymer and carbon membranes are back-calculated based on the thickness and permeability reported in the literature. Data for some polymer and carbon membranes were based on single gas measurements.

4.3.3. Improving hydrophobicity by post-synthetic modification (PSM)

ZIF-8 is prone to hydrolysis or dissolution in water,[101, 153] although it is relatively stable in dry gas conditions.[40] Therefore, the moisture stability of ZIF-8 membranes is an important criterion for commercial applications. One way to improve the moisture stability of ZIF-8 membranes is by grafting hydrophobic functional groups onto the surface.[79, 100-101, 154] The hydrophobicity of the Ica exchanged CD-ZIF-8 membrane was improved using an imine condensation reaction between the carbonyl group of the Ica and the amine group of the dodecylamine. SEM images of the 3d-Ica-CD-ZIF-8 membrane after PSM (hereafter, 3d-Ica-CD-ZIF-8-DDA) indicate negligible microstructure deterioration and crystallinity degradation of the membrane (Figure 4-5 a; Figure B-7). Upon PSM, the formation of an amide bond was confirmed by the appearance of a C-N stretch at about 1680 cm^{-1} in the Raman spectra (Figure 4-5 b). Contact angle measurements show that the PSM improves the surface hydrophobicity of the membrane. The as-prepared CD-ZIF-8 is hydrophilic (ca. 8°) because of the defective nature of the material.[24, 155] Upon Ica exchange, the membrane became more hydrophilic (ca. 8° vs. ca. 24°) in response to the presence of carbonyl groups; while upon PSM, the membrane became hydrophobic (ca. 101°; Figure 4-5 c; Appendix B, Table B-1). The 3d-Ica-CDZIF-8-DDA membranes showed reduced average propylene permeance (ca. 250×10^{-10} mol m^{-2} s^{-1} Pa^{-1}) and their average propylene/propane separation factor was unchanged. This observation strongly suggests that PSM is limited mostly to the external surface of the membranes; thereby compromising the adsorption/surface diffusion properties (that is, sticking coefficient, jumping frequency, and density of available pore mouth) of the membranes without affecting their gas transport properties.

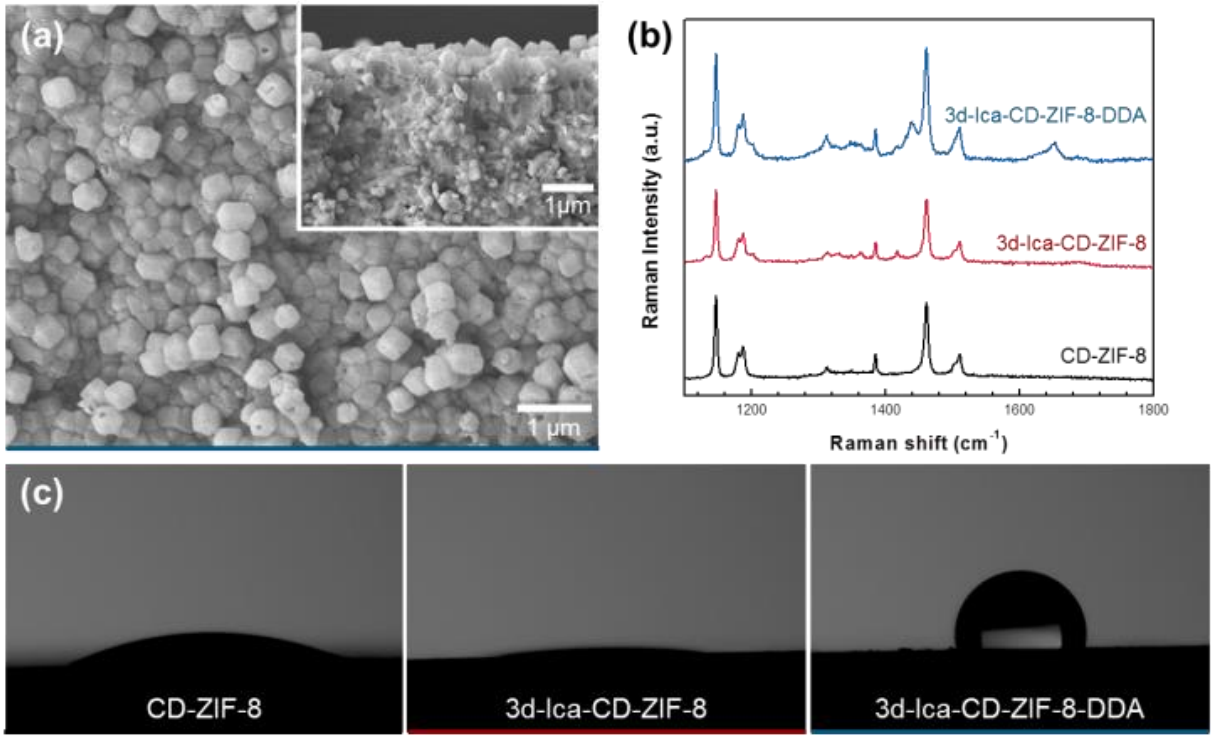

Figure 4-5 a) SEM image of the 3d-Ica-CD-ZIF-8-DDA membrane. b) Raman spectra, and c) water droplet measurement of as-synthesized CD-ZIF-8, 3d-Ica-CD-ZIF-8, and the 3d-Ica-CD-ZIF-8-DDA membrane (for a summary of the contact angle data see the Appendix B, Table B-1).

4.3.4. PSLE on differently-prepared ZIF-8 membranes

Recently, we reported that the separation performance stability of ZIF-8 membrane depends on how the membranes were prepared.[24] ZIF-8 membranes prepared by microwave-assisted seeding and secondary growth[46] (hereafter, MW-ZIF-8 membranes) were more stable than those obtained by a counter-diffusion in situ method (that is, CD-ZIF-8 membranes). This difference in long-term stability was attributed to the differences in defect densities and natures stemming from the synthesis methods. We hypothesized that the kinetics of the PSLE reaction for the CD- and MW-ZIF-8 membranes might be affected by the difference in their defect density and characteristic differences. To investigate this hypothesis, MW-ZIF-8 membranes were prepared (Appendix B) and subjected to PSLE and PSM. When PSLE was performed on MW-ZIF-8 membranes, their crystallinity and morphology remained intact (Figures B-8 and B-9). As in the case of the CD-ZIF-8 membrane, the MW-ZIF-8 membranes attained a yellow hue after PSLE (Figure B-10). Compared with the 4d-Ica-CD-ZIF-8 membrane (Figure B-2), the color of the 4d-Ica-MW-ZIF-8 membrane is lighter, indicating less Ica incorporation. The ATR-FTIR spectra confirmed the incorporation of Ica in the MW-ZIF-8 membranes (Figure B-11). The stretches at 1700 cm^{-1} (-C=O stretch) of the MW-ZIF-8 membranes were calculated using the OMNICS Software Suite (plotted in the Appendix B, Figure B-11 d. The absorbance of Ica-CD-ZIF-8 membranes (Figure B-3 d) increases much more rapidly than that of Ica-MW-ZIF-8 membranes. Furthermore, the absorbance of 4d-Ica-CD-ZIF-8 is 275% greater than that of the 4d-Ica-MW-ZIF-8 membrane, indicating that the surface Ica moiety of the 4d-Ica-CD-ZIF-8 membrane is more prevalent than that for Ica-MW-ZIF-8 membranes. This result is in accordance with the visible color changes of the membranes; that is, Ica-CD-ZIF-8 membranes are darker than Ica-MW-ZIF-8 membranes. The differences in the kinetics of the PSLE reaction

of the CD- and MW-ZIF-8 membranes is attributed to their physicochemical properties, such as defect density,[24] surface hydrophilicity, and grain size. For example, CD-ZIF-8 membranes were more defective, and therefore more reactive, than MW-ZIF-8 membranes.[24] Future studies will be conducted to understand how the physicochemical properties of ZIF-8 membranes affect the kinetics of PSLE.

The Ica-MW-ZIF-8 membranes were tested for propylene/propane permeation measurements (Figure B-12). Unlike the CD-ZIF-8 membranes, the permeances of the MW-ZIF-8 membranes exhibited negligible change. This is likely owing to the fact that the more stable MW-ZIF-8 membranes were less prone to the PSLE reaction than the less stable CD-ZIF-8 membranes.

Finally, the 3d-Ica-MW-ZIF-8 membrane was surfacemodified using the imine condensation reaction, without degradation of the surface morphology and crystallinity of the membrane (Figures B-13 a - b). According to the contact angle measurements (Figure B-13 c), as-synthesized MW-ZIF-8 membranes were initially somewhat hydrophobic (95°) and became slightly hydrophilic (74°) upon PSLE, and finally, became hydrophobic (111°) after the imine condensation reaction.

4.4. Conclusion

In summary, we have reported that the PSLE of mIm with Ica in ZIF-8 membranes is an effective means of improving the separation productivity of ZIF-8 membranes. The single-crystal to single-crystal linker exchange of CD-ZIF-8 membranes was confirmed by a series of characterization tools, including XRD, SEM, ATR-FTIR, and Raman and 1H NMR

spectroscopies. The Ica-exchanged ZIF-8 membranes showed a significant increase in their propylene permeance by about four times, approximately 780 × 10^{-10} mol·m^{-2}·s^{-1}·Pa^{-1} (ca. 260 GPU), in comparison to as-synthesized CD-ZIF-8 membranes. On the other hand, their propylene/propane separation factors were relatively stable, indicating their grain boundary structures remaining intact upon PSLE. This enhancement of propylene permeance with a relatively stable separation factor is attributed to a reduction in the effective thickness of CD-ZIF-8 membranes as a result of PSLE with Ica. The external surface of the Ica-CD-ZIF-8 membranes was then decorated with long hydrocarbon chains using the imine condensation reaction; thereby improving water resistance. Finally, the kinetics and the degree of PSLE reaction were dependent on the synthesis method. Membranes obtained by the microwave method were less prone to PSLE reaction; likely because they are less defective than those membranes prepared by the counter-diffusion method. Our novel strategy, based on PSLE, enhances the productivity of ZIF-8 membranes remarkably, and is expected to open up new opportunities for development of highly propylene-selective ZIF-8 membranes that are well-suited to specific practical applications.

CHAPTER V

ULTRATHIN ZEOLITIC-IMIDAZOLATE FRAMEWORK ZIF-8 MEMBRANES ON POLYMERIC HOLLOW FIBERS FOR PROPYLENE/PROPANE SEPARATION[*]

5.1. Introduction

Light olefin/paraffin separations, e.g., ethylene/ethane and propylene/propane, are one of the most challenging separations, currently performed by energy-intensive cryogenic distillation processes. Membrane-based separation is a promising energy-efficient alternative to conventional thermally-driven processes[4]. There are, however, no membranes commercially available for olefin/paraffin separations mainly due to the limited separation capabilities of current membrane materials and the lack of cost-effective processing methods to process advanced membrane materials with large surface area-to-volume ratio[3-4].

Zeolitic-imidazolate frameworks (ZIFs)[11, 57], a subclass of metal-organic frameworks (MOFs), are crystalline hybrid materials. ZIFs possess ultra-microporosities (< 5.0 Å) and relatively high chemical/thermal stabilities as compared to other MOFs, thereby attractive for gas separations. ZIF-8 is composed of divalent zinc ions and 2-methylimidazoles, forming sodalite (SOD) topology with a large cage (~ 11.4 Å) interconnected with six-membered rings (6MR). Due to the effective aperture size (~ 4.0 Å) of 6MR[22], ZIF-8 has shown great potential for the kinetic separation of propylene (~ 4.0 Å) from propane (~ 4.3 Å) molecules[20]. In fact, several polycrystalline ZIF-8 membranes supported on planar supports were synthesized by *in situ*[45, 47]

[*] Reprinted with permission from "Ultrathin Zeolitic-Imidazolate Framework ZIF-8 Membranes on Polymeric Hollow Fibers for Propylene/Propane Separation" by Moon Joo Lee, Mohamad Rezi Abdul Hamid, Jongmyeong Lee, Ju Sung Kim, Young Moo Lee, and Hae-Kwon Jeong, *Journal of Membrane Science*, https://doi.org/10.1016/j.memsci.2018.04.041. Copyright 2018 by Elsevier.

and secondary (seeded) growth[41-42, 44, 46] methods, showing impressive propylene/propane separation performances. It is, however, imperative to increase the propylene throughput (*i.e.*, productivity) of ZIF-8 membranes for their practical applications by reducing membrane thickness and using scalable supports with higher surface-to-volume ratio (*i.e.*, either ceramic or polymer hollow fibers). In general, the secondary growth leads to the formation of thinner membranes than *in situ* growth due to the decoupling of nucleation and growth steps[12, 15, 156-157].

Lai and his co-workers[133] reported ZIF-8 membranes (~ 2 μm thick) on the outer surface of ceramic YSZ hollow fibers (1.5 mm OD) using a secondary growth for hydrogen/propane separation. Hara et al.[76] reported ZIF-8 membranes (~ 80 μm thick) on the outer surface of α-alumina capillary tubes (3 mm OD) using a counter-diffusion *in situ* method. Their membranes showed the propylene/propane separation factor (hereafter, SF) of 59 and the propylene permeance of 7.5 GPU (gas permeation unit, 1 GPU = 3.348×10^{-10} mol m^{-2} s^{-1} Pa^{-1}). There are, however, no ceramic hollow fiber supports commercially utilized because they are expensive and difficult to handle. In contrast, polymeric hollow fibers are prevalent in commercial membrane markets since they are inexpensive, easy to handle, and simple to form high surface-to-volume modules, thereby attractive as supports for high-throughput ZIF-8 membranes.

Coronas and his co-workers[137] reported the first ZIF-8 membranes (~ 3.6 μm thick) prepared on the bore side of polysulfone hollow fiber supports (520 μm OD) by using microfluidic *in situ* growth. They tested binary gas separation performances of the membranes using H_2/CH_4 and CO_2/CH_4 pairs. The Nair group[111] reported ZIF-8 membranes (~ 8.8 μm thick) on Torlon hollow fibers (300 μm OD) by an *in situ* method (what they called, interfacial microfluidic processing technique). The technique enabled the fabrication of the membranes on either bore or shell side of the hollow fibers. With polydimethylsiloxane lumen sealing,

membranes showed hydrogen/propane separation and propylene/propane separation (SF of 12 and propylene permeance of 27 GPU) at 25 °C. Optimization of the processing conditions led to somewhat thinner ZIF-8 membranes (~ 5 μm thick), thereby higher propylene permeance (66 GPU) with SF of 66[52] and eventually to much-improved membranes (~ 8.1 μm thick, SF ~ 180 and propylene permeance ~ 45 GPU) [23]. Biswal et al. [158] reported ZIF-8 membranes (~ 10 – 25 μm thick) prepared on polybenzimidazole (PBI) hollow fibers (780 μm OD) by an interfacial microfluidic technique (using *i*-butyl alcohol/water) for hydrogen separation. Hou et al.[138] fabricated ultrathin ZIF-8 membranes (~ 1 μm thick) on the shell side of APTES-functionalized (APTES, (3-aminopropyl)triethoxysilane)) TiO_2-coated polyvinylidene fluoride (PVDF) hollow fibers by direct immersion of the hollow fiber in a ZIF-8 synthesis solution for hydrogen separation. Recently, Venna and his coworkers[159] reported ZIF-8 membranes (~ 8.5 μm thick) grown on the shell side of Torlon hollow fibers (400 μm OD) by a continuous flow processing for CO_2/N_2 separation. Most recently, Li et al. [51] reported ultrathin ZIF-8 membranes (~ 87 nm thick) on the shell side of ammoniated PVDF hollow fiber membranes (1.5 mm OD) via gel-vapor deposition. The membranes showed the propylene/propane SF of 73 and the propylene permeance of 840 GPU. Among ZIF-8 membranes prepared on polymeric hollow fiber substrates, only a few by Nair et al. [23, 52] and most recently Li et al. [51] showed propylene/propane separation performances. This rarity of propylene-selective ZIF-8 membranes on polymeric hollow fibers attests to the challenges of preparing high-quality polycrystalline ZIF-8 membranes on polymer hollow fibers. Furthermore, all of the ZIF-8 membranes supported on polymer hollow fibers were prepared by *in situ* methods, exhibiting their thickness of several microns, too thick for commercial applications, with only two exceptions by Hou et al.[138] and Li et al.[51]. For practical applications, it is vital to be able to package polycrystalline ZIF-8 membranes into

scalable modules and therefore essential to maintain the mechanical robustness of the relatively fragile polycrystalline membranes during packaging processes. Consequently, it is highly desirable to form ZIF-8 membranes on the bore side of hollow fibers, particularly when the membranes are ultrathin (*i.e.*, 1 μm or less). Unfortunately, both ultrathin ZIF membranes by Hou et al.[138] and Li et al.[51] were prepared on the shell side of hollow fibers owing to the limitations of their preparation methods.

Here we report, for the first time, the synthesis of well-intergrown ultrathin ZIF-8 membranes on bore side of polymeric hollow fibers by a secondary (or seeded) growth. High-quality seed layers were rapidly prepared on polymeric hollow fibers (hereafter, pHFs) in a few minutes under microwave irradiation[46] after systematic optimization. Subsequent microfluidic hydrothermal secondary growth enabled the growth of the seed crystals into well-intergrown ultrathin ZIF-8 films. Crystallinities and microstructures of the seed layers and membranes were characterized using X-ray diffraction and electron microscopy. The propylene/propane separation performances of ZIF-8 membranes supported on pHFs were tested using a Wicke-Kallenbach method.

5.2. Experimental

5.2.1. Materials

Matrimid® 5218 (Figure C-1 in Appendix C, Alfa Aesar) and N-methyl-2-pyrrolidinone (NMP, 99.8%, Daejung Chemicals & Metals, Siheung, Republic of Korea) were used to prepare Matrimid® hollow fibers. Zinc nitrate hexahydrate ($Zn(NO_3)_2 \cdot 6H_2O$, 98%, Sigma-Aldrich) and 2-methylimidazole ($C_4H_6N_2$, 99%, Sigma-Aldrich) were used as metal and linker sources,

respectively. Sodium formate (HCOONa, 99%, Sigma-Aldrich) was used as a deprotonating agent. Methanol (CH_3OH, > 99%, Alfa-Aesar) and deionized (DI) water were used as solvents. All chemicals were used as received without further purification.

5.2.2. Methods

5.2.2.1. Fabrication of porous polymeric hollow fiber

Porous Matrimid® polymeric hollow fibers (hereafter, pHFs) were fabricated by a dry-wet jet spinning technique as conditions previously optimized and reported[160]. The fabrication parameters are summarized in Table C-1. The bore solution composition and the coagulation bath temperature were appropriately manipulated to obtain hollow fibers having porous morphology on bore and shell sides, respectively.

5.2.2.2. Preparation of hollow fiber setup for ZIF-8 seeding and secondary growth

A 30 cm long porous Matrimid® pHF was housed into a Teflon PTFE tubing (0.3175 cm OD), similar in length to the pHF (see Figure C-2). To seal the pHF housed in the tubing, epoxy resin (Devcon® epoxy adhesive, ITW polymer adhesives) was applied to the shell side of the pHF ends and allowed to cure at room temperature for 24 hrs. Excess pHF ends were removed carefully using a sharp razor blade.

5.2.2.3. Preparation of ZIF-8 seed layers

High-quality ZIF-8 seed layers were synthesized based on our previously reported recipe[46] with a minor modification. Briefly, a metal precursor solution was prepared by dissolving 2.43 g of zinc nitrate hexahydrate in 40 ml of methanol (hereafter, metal solution)

while a ligand precursor solution was prepared by dissolving 2.59 g of 2-methylimidazole and 0.125 g of sodium formate in 30 ml of methanol (hereafter, ligand solution). The above-mentioned concentration is noted as C1. Concentration of the ligand precursor solution was further optimized (denoted as C2) by dissolving 3.89 g of 2-methylimidazole and 0.125 g of sodium formate in 30 ml of methanol. Continuous flow processing technique was implemented for both pHF substrates saturation and ZIF-8 seeding process. Using a syringe pump (Havard apparatus, USA), the metal solution was flowed through the bore side of the pHF at a flow rate of 0.33 ml/min for a total of 1 hr, followed by the ligand solution with a flow rate of 0.11 ml/min. While the ligand solution was still flowing, the pHF was placed into a microwave transparent tube containing 30 ml of methanol and immediately subjected to microwave radiation in a microwave oven (Discover, CEM) at 100 W for 1.5 min. The resulting sample (seeded pHF) was then allowed to cool down naturally to room temperature for 30 mins. After that, the seeded pHF was washed by flowing fresh methanol through the bore side of the pHF at a flow rate of 0.11 ml/min. Finally, the seeded pHF was dried in a convective oven for 60 °C for 4 hrs. To prepare ZIF-8/pHF seed layer on the shell side, additional tube connection was added to the original setup to allow metal and ligand solution to flow in the shell side (see Figure C-2 b). Seeding was performed following aforementioned procedures with the C2 concentration.

5.2.2.4. Preparation of ZIF-8 membranes

ZIF-8 membranes on pHFs were prepared via secondary growth method reported by Pan et al.[112] with a slight adjustment. In brief, a metal precursor solution was prepared by dissolving 0.11 g of zinc nitrate hexahydrate in 20 ml of DI water. Simultaneously, a ligand precursor solution was prepared by dissolving 2.27 g of 2-methylimidazole in 20 ml of DI water. The metal

precursor solution was then poured into the ligand precursor solution (hereafter, growth solution) followed by continuous mixing for 2 mins. Then, using a syringe pump, the growth solution was flowed through the bore side of a seeded pHF at a flow rate of 0.05 ml/min for 6 hrs. The resulting sample (ZIF-8/pHF membrane) was washed with fresh methanol at a flow rate of 0.11 ml/min for 1 hr. The membrane was finally dried at room temperature for 36 hrs. To prepare ZIF-8/pHF membrane on the shell side, the growth solution and methanol was injected through the additional tube connection (see Figure C-2 b). Synthesis of the membrane was performed following aforementioned procedures.

5.2.3. Characterization

X-ray diffraction (XRD) patterns were recorded using a Rigaku Miniflex II powder X-ray diffractometer with Cu-Kα radiation (λ = 1.5406 Å). Scanning electron micrographs were collected using a JEOL JSM-7500F operating at 5 keV acceleration voltage and 15 mm working distance. Binary propylene/propane gas separation measurements were carried out at room temperature (ca. 20 °C) under atmospheric pressure using the Wicke-Kallenbach technique (see Figure C-3). An equimolar propylene/propane mixture was supplied to the feed side while argon sweeping gas was supplied to permeate side. The flow rate for feed and sweep gases were set at 50 cc/min. The composition of the permeate stream was analyzed using gas chromatography (Agilent GC 7890A equipped with a column of HP-PLOT/Q).

5.3. Results and discussion

Matrimid® was selected as a pHF substrate due to its high chemical, thermal, and mechanical resistances. Matrimid® pHFs were spun by a dry-wet jet spinning under a condition modified from the one previously reported[160] and the fabrication parameters are summarized in Table C-1. The resulting pHFs are macroporous (N_2 permeance of ~ 12,100 GPU, see Table C-2) with the outer and inner diameters of ~ 545 μm and ~ 344 μm, respectively (Figure C-4).

Figure 5-1 illustrates the overall ZIF-8/pHF membrane synthesis procedure based on the microwave-assisted seeding and secondary growth[46]. First, a bare pHF was assembled in a microwave-transparent PTFE tube and sealed with epoxy (see Figure C-2). Second, ZIF-8 seed crystals were rapidly formed on the pHF under microwave irradiation while flowing ligand precursor solution through the Zn^{2+} saturated pHF. Finally, continuous well-intergrown defect-free ZIF-8/pHF membranes were formed by flowing growth solution through the seeded pHF (*i.e.*, microfluidic secondary growth). ZIF-8 seed layers can be formed on either bore or shell side of pHFs. Consequently, ZIF-8 membranes can be prepared on either side (see Figure C-5). Due to its advantage of handling and mechanical stability, ZIF-8 membranes on the bore side of hollow fibers were chosen for current studies.

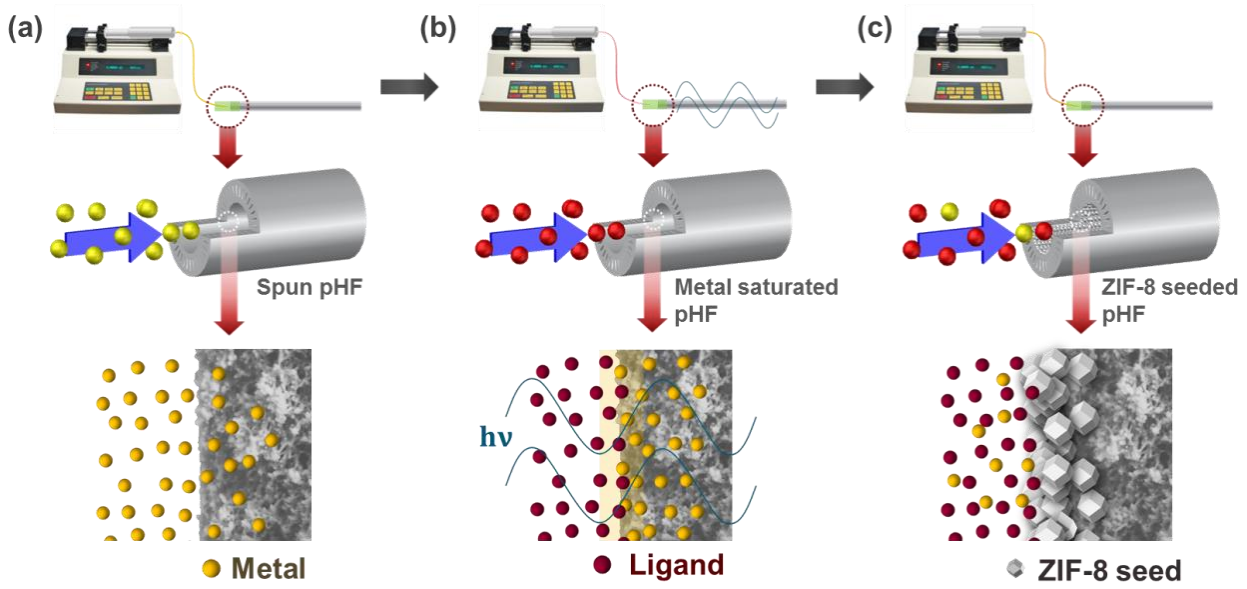

Figure 5-1 Schematic illustration of the synthesis of ZIF-8 membranes on the bore side of Matrimid® spun polymer hollow fibers (pHFs): (a) an as-spun pHF was subjected to metal saturation, (b) followed by an injection of ligand precursor solution and microwave irradiation to form densely-packed ZIF-8/pHF seed layers and then, (c) the seeded pHF was subjected to the microfluidic secondary growth by flowing growth solution to prepare an ultrathin well-intergrown ZIF-8 membrane on the hollow fiber.

5.3.1. Microwave-assisted ZIF-8 seeding on polymer hollow fibers

Regardless of supports, polycrystalline ZIFs membrane synthesis methods can be classified into two categories: *in situ* growth and secondary (seeded) growth. The *in situ* method is economical and straightforward while the secondary growth technique is advantageous in the controlled synthesis of thinner polycrystalline membranes with better grain boundary structures. As such, polycrystalline membranes prepared by the secondary growth typically resulted in better gas separation performances. A challenge is, however, to obtain high-quality seed layers strongly attached to polymeric hollow fibers, especially on the bore side. High-quality seed layers consist of densely-packed nanocrystals firmly adhered to polymer supports with uniform surface coverage. Conventional seeding techniques such as dip- and slip-coating fail due to the

lack of solid binding between seed crystals and polymers. It is hypothesized that the unique nature of microwave heating and the microfluidic processing enables not only the rapid formation of high-quality ZIF-8 seed layers but also the simple control of seed layer location (*i.e.*, either bore or shell side).

High-quality ZIF-8/pHF seed layers were obtained by systematic optimization based on our previously reported recipe[46]. As a starting point, the metal and ligand solutions previously reported[46] were used without modification (denoted as C1). The resulting ZIF-8 seed layers presented in Figure 5-2 a exhibited relatively large crystals (~ 180 nm) sparsely packed on the support. As such, the seeding condition was further optimized to promote the nucleation by 1) increasing the concentration of the ligand precursor solution by 1.5 times with a fixed metal concentration (denoted as C2) and 2) increasing the concentration of both metal and ligand precursor solutions by 1.5 times (denoted as C3). As shown in Figure 5-2 b, with the increased ligand concentration (C2), the seed crystals became much smaller (~ 60 nm) and greater in numbers, completely covering the bore side of the pHF. Increasing ligand-to-metal ratio from C1 to C2 accelerates the deprotonation step, consequently favoring the nucleation as previously reported in the literature[68, 150]. As pointed out by Cravillon et al.[150], the protonated ligand (HmIm) is more basic (pKa ~ 14.2) than the $[Zn(HmIm)]^{2+}$ complex (pKa ~ 10.3), meaning that HmIm can deprotonate the complex, thereby initiating polymerization (*i.e.*, nucleation). In contrast, when both metal and ligand concentrations were increased (from C2 to C3), larger crystals (~ 120 nm) were formed, barely covering the pHF surface (Figure 5-2 c). The ligand-to-metal ratio of C3 is the same as that of C1 led to larger crystal size, similar to the C1 case. Besides, as compared to the C2 case, the local temperature in the pHF in the case of C3 is expected higher due to the increased number of strongly microwave-absorbing zinc ions, thereby

favoring crystal growth than nucleation. Öztürk et al.[68] made similar observations that the crystal growth was favored at elevated temperature. It is, therefore, surmised that increased ligand-to-metal ratio in the C2 condition promoted nucleation, leading to the formation of nano-sized seed crystals in a substantial number.

The strong adhesion of ZIF-8 crystals onto polymeric substrates is crucial to synthesize well-intergrown ZIF-8 films[12, 15]. Surface modifications are, therefore, often employed on polymeric substrates so as to achieve strong adhesion of seed crystals[51, 138]. In our previous report[46], we found the microwave-assisted seeding resulted in strongly attached seed crystals on α-alumina discs compared to a conventional dip-coating seeding method. The strong attachment was attributed to both physical anchoring and possibly chemical bonding resulting from high local temperature under microwaves[161]. It was, therefore, surmised that microwave seeding led to strongly attached seed crystals on pHFs as compared to conventional seeding. As a control, ZIF-8/pHF seed layers were prepared by flowing a ZIF-8 nanocrystal suspension through pHFs (hereafter, microfluidic seeding), resembling conventional seeding methods (see Appendix C-4 and Figure C-6 a - b). ZIF-8 films resulting from the secondary grown of the seed layers exhibited delamination (see Figure C-6 c - d), confirming poor adhesion between seed crystals and polymer surface. It is noted that a pHF subjected to *in situ* growth without a seed layer led to a poorly-intergrown ZIF-8 layer (see Figure C-7). These observations confirm the critical role of seed crystal layers strongly bound to pHF substrates to obtain well-intergrown ZIF-8/pHF membranes under the current synthesis condition without surface modifications of pHFs.

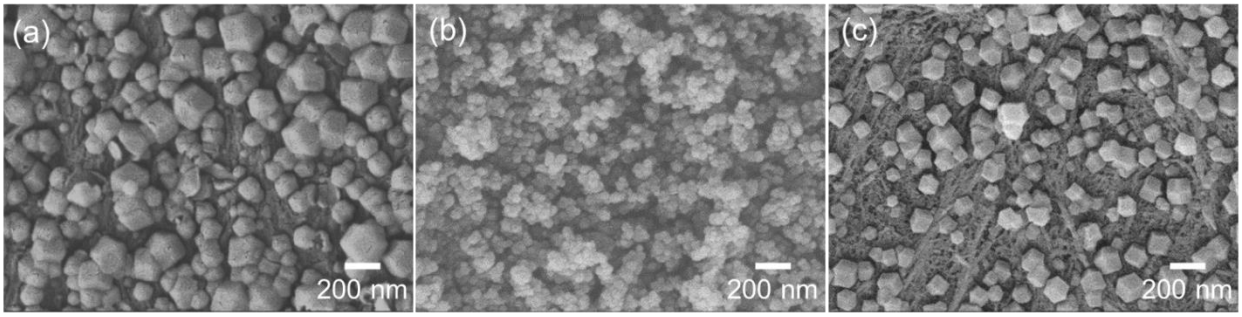

Figure 5-2 SEM images of ZIF-8 seed layers on the bore side of pHFs prepared under microwave using (a) standard concentration (C1), (b) increased ligand concentration (C2), and (c) increased both metal and ligand concentration (C3). With the increased ligand concentration (C2), ZIF-8 nanocrystals (~ 60 nm) were densely-packed on the pHF support.

5.3.2. Membrane formation

The high-quality ZIF-8/pHF seed layers (C2) were secondarily grown into ultrathin well-intergrown ZIF-8/pHF membranes under a scalable and environmentally friendly microfluidic condition. Briefly, an aqueous secondary growth solution was continuously injected on the bore side of a seeded pHF at room temperature (ca. 20 °C) for 6 hours at a flow rate of 0.05 ml/min. Powder XRD patterns of the seed layers and the resulting ZIF-8 membranes are presented in Figure 5-3 a. The (110) peak intensity of the seed layers increased after the secondary growth, indicating crystal growth from the seed crystals. Figure 5-3 b – d displays the SEM images of the ZIF-8 membrane. The ZIF-8 membrane is well-intergrown with no macroscopic defects. The thickness of the membrane is estimated ~ 800 nm, which is one of the thinnest ZIF-8 membranes supported on polymeric hollow fibers (see Table C-3).

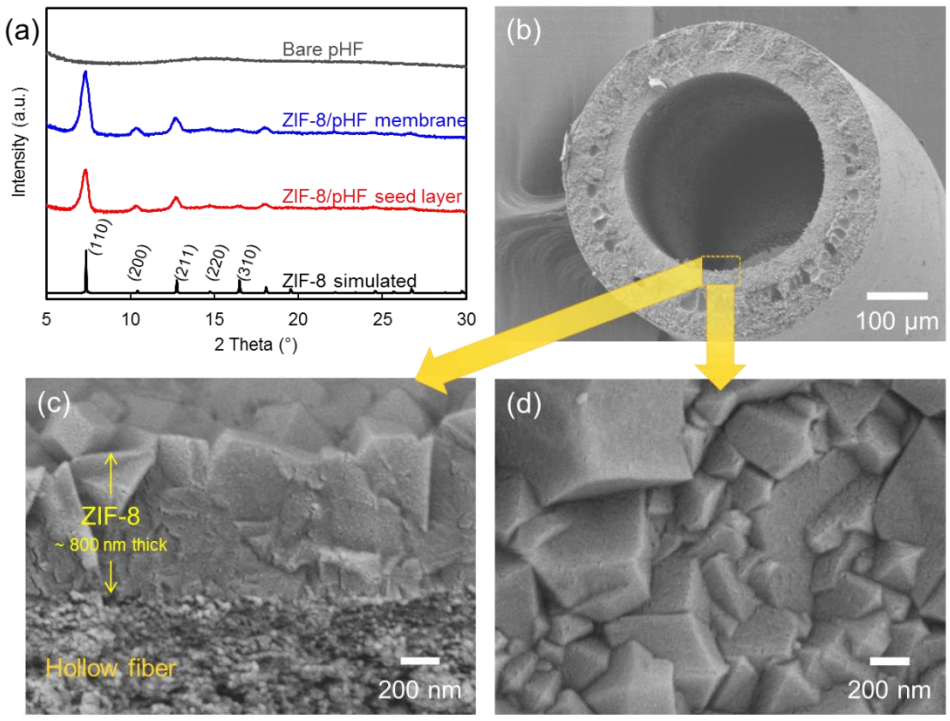

Figure 5-3 (a) Powder XRD patterns of ZIF-8 simulated, ZIF-8/pHF seed layer (C2), ZIF-8/pHF membrane, and bare pHF and SEM images of ZIF-8 /pHF membrane: (b) cross-sectional view in lower magnification, (c) cross-sectional view in higher magnification, and (d) top view.

5.3.3. Separation performance

A well-intergrown ultrathin ZIF-8/pHF membrane was assembled in a custom-made stainless-steel permeation cell and sealed with epoxy on each end. The binary propylene/propane (50:50) permeation measurements were performed at a total volumetric flow rate of 50 cc/min at room temperature using the Wicke-Kallenbach technique (see Fig C-3). The separation performance of four membranes is presented in Table 5-1 and Fig 5-4. The membranes exhibited the average propylene/propane separation factor (hereafter, SF) of ~ 46 and the average propylene permeance of ~ 183 × 10^{-10} mol m^{-2} s^{-1} Pa^{-1} or 55 GPU (permeability ~ 49.4 Barrer). The result in this study is consistent with the separation performance of ZIF-8 membranes

supported on α-alumina discs synthesized from the same method[46] (SF of ~ 40 and propylene permeance of 62 GPU with a thickness of ~ 1.5 μm). Our most recent alumina-supported ZIF-8 membranes (~ 1.6 μm thick)[24] exhibited a much higher SF of ~ 208 with the propylene permeance of ~ 47 GPU (see Table C-3). This variation in the separation factors attests to the sensitive nature of the secondary growth of polycrystalline ZIF-8 membranes. It is likely that the current continuous flow processing led to the formation of ZIF-8 membranes with grain boundary structures that are not as good as those synthesized under the static condition[24]. Furthermore, ZIF-8/pHF membranes were extensively washed in methanol immediately after the secondary growth. Unfortunately, Matrimid® hollow fibers were swollen in methanol, potentially compromising the grain boundary structures of the membranes. Further studies are currently underway to resolve this swelling issue.

Table 5-1 Binary propylene/propane separation performance of ZIF-8/pHF membranes conducted at ambient temperature (~ 20 °C) under ambient pressure.

Sample	Separation factor	Propylene permeance ($\times 10^{-10}$ mol m^{-2} s^{-1} Pa^{-1})
M1	51	200.2
M2	42	179.9
M3	42	164.3
M4	47	188.4
Average ± stdev.	45.5 ± 3.8	183.2 ± 13.1

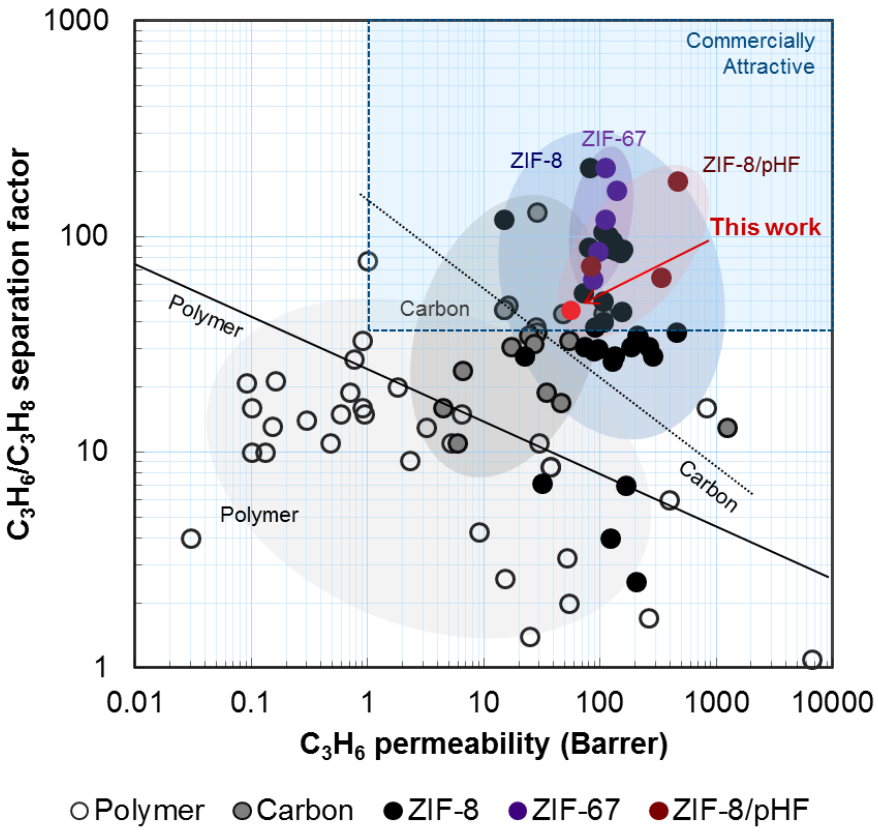

Figure 5-4 Propylene/propane separation performances of polymer[3, 6, 30-37], carbon[8, 37-39], ZIF-8[24, 40-50], ZIF-67[25, 53], and ZIF-8/pHF membranes[23, 51-52] from the literature. An average separation performance of ZIF-8/pHF membranes in this work is presented in filled red circle (●). Data for some polymer and carbon membranes were based on single gas measurements. The upper bounds for polymer[3] (solid line) and carbon[8] (dotted line) are shown as well as the commercially attractive performances[54]. 1 Barrer = 3.348×10^{-16} mol·m·m^{-2}·s^{-1}·Pa^{-1}.

Table C-3 presents a summary of ZIF-8 (or isostructural ZIF-67) membranes prepared on various substrates using several different methods, showing diverse membrane thicknesses and propylene/propane separation performances. Only a few ZIF-8 membranes on pHFs have shown promising propylene/propane separation performances depending on the processing techniques. The ZIF-8/pHF membranes reported here are one of the thinnest membranes with a relatively simple and scalable processing technique with reasonable propylene/propane separation performance.

5.4. Conclusion

In conclusion, well-intergrown ultrathin ZIF-8 membranes supported on Matrimid® hollow fibers were prepared, for the first time, via rapid-seeding under microwaves followed by microfluidic secondary growth. High-quality ZIF-8/pHF seed layers were fabricated in few minutes under microwaves and their location (either on bore or shell) was readily controlled. Subsequent microfluidic secondary growth led to the formation of well-intergrown ultrathin ZIF-8 membranes on the bore side of pHFs with a thickness of ~ 800 nm, one of the thinnest ZIF-8 membranes supported on polymer hollow fibers. The resulting ultrathin membranes were made possible by the unique microwave-seeding and microfluidic secondary growth. Finally, the ZIF-8/pHF membranes exhibited an average propylene/propane separation factor of ~ 46 and average propylene permeance of ~ 183×10^{-10} mol m^{-2} s^{-1} pa^{-1} or 55 GPU (permeability ~ 49.4 Barrer). The facile synthesis of high-quality ultrathin ZIF-8/pHF membranes with sub-micron thickness is a significant step forward to the industrial application of ZIF-8 membranes for propylene/propane separation.

CHAPTER VI CONCLUSION AND FUTURE DIRECTIONS

6.1. Conclusion

In this dissertation, we discussed the practical challenges of ZIF-8 membrane for their industrial propylene/propane separation application. The long-term stability of the membrane in propylene/propane separation performance, dependent on processing conditions was explored and on purpose processing condition for targeting application can be chosen. Drastic reduction of membrane thickness was effectively mitigated via post-synthetic linker exchange method by reducing their effective thicknesses while their physical thickness is remained intact. Scalable processing technique for highly propylene-selective ZIF-8 membranes on polymeric hollow fiber substrates is studied.

Our first objective was to study the defect-dependent stability of highly propylene-selective ZIF-8 membranes dependent on their fabrication conditions and to stabilize kinetically-unstable ZIF-8 membranes effectively. This study was discussed in Chapter III. Highly propylene-selective ZIF-8 membranes were fabricated on α-alumina discs by two different processing methods, counter-diffusion-based *in situ* (CD method) and microwave-assisted seeding and secondary growth (MW method), which were previously established by our group. A range of characterizations indicated that CD-ZIF-8 membranes were less stable than MW-ZIF-8 membranes. The defective nature of CD- and MW-ZIF-8 on surface and bulk defects were characterized by XPS and ^{14}N solid-state NMR. The as-prepared CD-ZIF-8 membranes showed the propylene permeances reduced by ~ 75% after 60 days while propylene/propane separation factors increased more than 6 times. The kinetic changes of CD-ZIF-8 membranes were most

likely because of their defective nature as the CD method employed facile crystallization that involved with other synthesis parameters. The kinetically unstable defect sites are prone to change; therefore, on-purpose synthesis condition can be designed for the application. Post-synthetic hydrothermal ligand treatment healed defective sites thereby CD-ZIF-8 membranes showed stabilized time-dependent propylene/propane separation performances.

The second objective of our study was to drastically reduce effective thickness of ZIF-8 membranes for the binary propylene/propane separation, as discussed in Chapter IV. The PSLE of mIm with Ica in ZIF-8 membranes resulted in hybrid layers of ZIF-8-90 with larger aperture size on top of the membranes and propylene-selective ZIF-8 bottom layers. The PSLE was effectively utilized to enhance propylene permeance of ZIF-8 membranes. The systematic linker exchange was employed, and their kinetic changed were confirmed by characterizations, including spectroscopies, XRD and SEM. The Ica-exchanged CD-ZIF-8 membranes shown propylene permeance increased up to four times, approximately 780×10^{-10} $mol \cdot m^{-2} \cdot s^{-1} \cdot Pa^{-1}$ (ca. 260 GPU), compared to as-prepared ones. The further surface modification was conducted to improve water repellency of the membrane surface by utilizing newly-introduced aldehyde functional groups after PSLE. The PSLE technique was effectively utilized in the case of CD-ZIF-8 membranes than MW-ZIF-8 membranes. Their defective nature affected different kinetic energy states, resulting in CD-ZIF-8 membranes favorable for post-synthetic modifications.

The final objective was to improve propylene throughput by increasing surface area-to-volume of ZIF-8 membranes prepared on polymeric hollow fiber substrates, in Chapter V. Ultrathin ZIF-8 membranes were successfully prepared by our unique MW method, modified as scalable microfluidic processing technique. Microwave-seeding conditions were systematically

optimized to favor nucleation conditions. High-quality ZIF-8/pHF seed layers were fabricated in few minutes under microwaves regardless of their location either on bore or shell. Microfluidic hydrothermal growth led to one of the thinnest ZIF-8 membranes supported on polymer hollow fibers. The binary propylene/propane separation performances of resulting ZIF-8/pHF membranes were conducted.

6.2. Future directions

6.2.1. Ultra-thin ZIF-8 membrane synthesis

6.2.1.1. Post-synthetic linker exchange of ZIF-90 membrane with mIm

In Chapter IV, the effective thickness of ZIF-8 membrane was effectively reduced via PSLE technique. The PSLE can be employed on ZIF-90 membranes to incorporate ultrathin ZIF-8 layers on top of ZIF-90 membranes. Since the effective aperture size of ZIF-90 is greater than that of ZIF-8, the ZIF-90 bottom-layers remained intact from PSLE, would neither impede propylene transport significantly nor separate propylene/propane molecules. Therefore, we propose a few layers of the ultra-thin propylene-selective ZIF-8 membrane prepared on top of the ZIF-90 membrane via systematic linker exchange of ZIF-90 membrane with a ZIF-8 linker (*i.e.*, 2-methylimidazole). Careful linker-exchange would make possible of propylene-selective ZIF-8 layers below 50 nm thick, which in turn, can increase propylene permeance by 20 times. We have been working on 1) preparation of thin and well-intergrown defect-free ZIF-90 membranes and 2) mIm linkers exchange on ZIF-90 powders. The results of the latter project showed that mIm linkers were incorporated into ZIF-90 frameworks.

6.2.1.2. Mass-transport-limited hydrothermal ZIF-8 growth

We are proposing de novo ultrathin ZIF-8 membrane synthesis by limiting mass transport of growth species, based on our MW method. Current MW method has two-step synthesis; MW-assisted seeding and secondary growth. The high-quality ZIF-8 seed layers prepared under microwave have thickness of ca. 150 nm, consist of densely packed ZIF-8 seed crystals (size ~ 50 nm). The ultrathin ZIF-8 membrane can then be prepared by simply filling the gaps of the seed crystals with defect-free grainboundary structures. Current growth system has excess amounts of growth species so that membranes (ca. 1 μm) can be continuously grow during the growth period. The preliminary results indicate that the membrane growth was limited under limited-mass-transport condition resulting in sub-micron membrane thickness. However, the propylene/propane separation factor is not as impressive as our MW method and current project is ongoing to prepare ultrathin ZIF-8 membranes with improved grainboundary structure.

6.2.2. ZIF/pHF membrane processing techniques

6.2.2.1. Performance optimization

In Chapter V, the ZIF-8/pHF membranes were synthesized by our MW method (hereafter, microfluidic MW method). However, the separation performance was not as exciting as out MW-ZIF-8 membranes prepared on α-alumina disc. We hypothesized this is because of 1) the sensitive nature of crystal growth and 2) the swelling of the Matrimid hollow fibers during washing steps performed after the secondary growth. The MW method is a batch processing that doesn't allows any dynamic flow of growth species during the six hours of growth period, however, the microfluidic MW method is a flow processing that delivers growth species to the seed crystals under continuous flow. Our previous research indicated improved separation

performance of MW-ZIF-8 membranes synthesized in a non-vibrational oven than the one prepared in a vibrational oven. It is our hypothesis that current microfluidic MW method could possibly generate unwanted turbulence that impedes formation of perfect grainboundary structure. Therefore, optimized flow and static processing is necessary for improved separation processing. Also, find right solvent could possibly enhance separation factors by not only prevent pHFs from swelling but also activate the membranes effectively.

6.2.2.2. Other ZIFs/pHFs seed layers

Successful preparation of high-quality seed layers is relatively difficult than finding the secondary growth condition. By use our microwave technique, high-quality ZIF-8 seed layers were prepared both on α-alumina discs and polymeric hollow fiber substrates. However, preparation of other high-quality ZIFs seed layers, such as ZIF-67 and ZIF-90, were not straightforward due to the complexity of different nucleation and growth environment with different metal and linkers. The complex nature of nucleation and growth requires optimizations when applying the same processing technique to synthesize other types of crystals (*i.e.*, other MOFs and ZIFs). In general, in ZIFs synthesis, the nucleation is favored on higher linker-to-metal ratio, under rapid deprotonating conditions. On the other hand, the growth is generally favored at higher temperature, at higher metal-to-linker ratio. In the case of ZIF-90, solubility of Ica is much lower than that of mIm, leading to lower linker-to-metal ratio and growth-preferred condition. Addition of deprotonating agents would accelerate deprotonation steps which can lead to the nucleation-favored condition.

6.2.3. Tuning apertures of ZIFs via PSLE techniques

There are a handful of ZIFs exhibits SOD topologies (Chapter II, Figure 2-6), and therefore, limited aperture sizes are available. As the effective aperture sizes are depended on the combination of metals and linkers, *de novo* mixed linker and/or mixed metal approaches are exciting method to tune the effective aperture sizes.[53, 77, 162] Likewise, post-synthetic linker and/or metal exchange is effective method to systematically incorporate new linkers and prepare hybrid-ZIFs membranes, as discussed in Chapter II. Our ongoing study on the bIm-exchanged ZIF-8 membranes showed shifts of aperture as shown in Figure 6-1. Thorough study of the kinetics of linker exchange and resulting separation performance change is undergoing. By this method, CO2 separation performance can then be effectively performed with linker-exchanged ZIF8 membranes. Likewise, the aperture size can be enlarged by incorporating different linkers, such as Ica and Im.

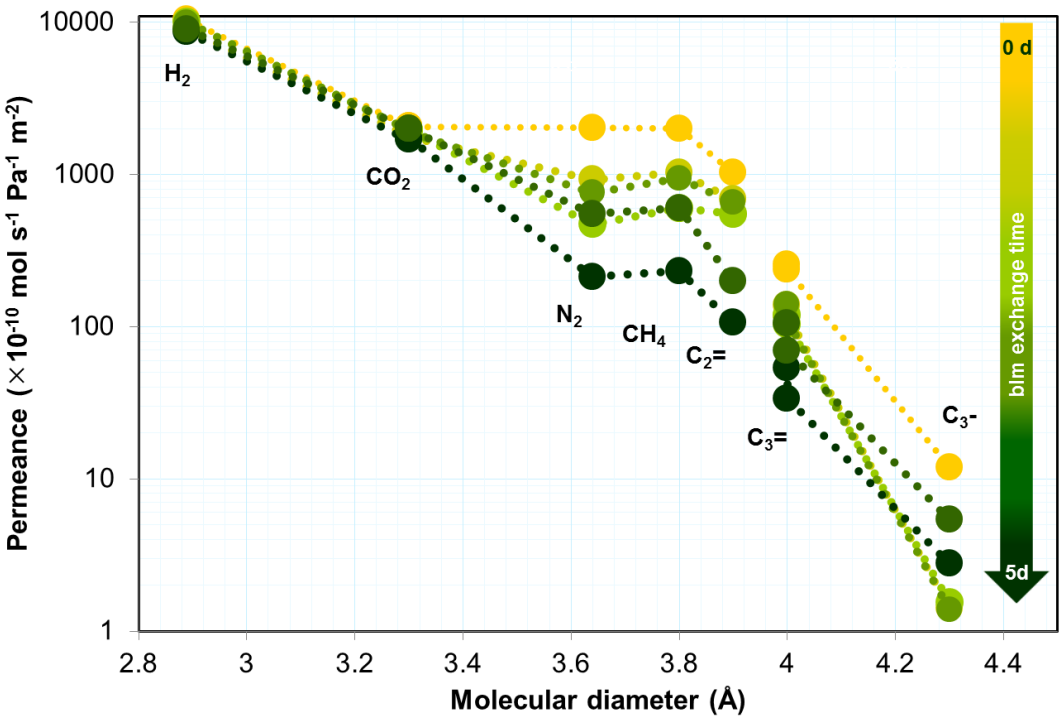

Figure 6-1 Gas permeances of different gas molecules of ZIF-8 membranes as-synthesized and after post-synthetic bIm exchange at different reaction time.

REFERENCES

(1) Eldridge, R. B. Olefin/paraffin separation technology: a review. *Industrial & Engineering Chemistry Research* **1993,** *32* (10), 2208-2212

(2) Baker, R. W. Future Directions of Membrane Gas Separation Technology. *Industrial & Engineering Chemistry Research* **2002,** *41* (6), 1393-1411

(3) Burns, R. L.; Koros, W. J. Defining the challenges for C3H6/C3H8 separation using polymeric membranes. *Journal of Membrane Science* **2003,** *211* (2), 299-309

(4) Koros, W. J.; Fleming, G. K. Membrane-based gas separation. *Journal of Membrane Science* **1993,** *83* (1), 1-80

(5) Koros, W. J.; Mahajan, R. Pushing the limits on possibilities for large scale gas separation: which strategies? *Journal of Membrane Science* **2000,** *175* (2), 181-196

(6) Staudt-Bickel, C.; Koros, W. J. Olefin/paraffin gas separations with 6FDA-based polyimide membranes. *Journal of Membrane Science* **2000,** *170* (2), 205-214

(7) Ma, X.; Williams, S.; Wei, X.; Kniep, J.; Lin, Y. S. Propylene/Propane Mixture Separation Characteristics and Stability of Carbon Molecular Sieve Membranes. *Industrial & Engineering Chemistry Research* **2015,** *54* (40), 9824-9831

(8) Hayashi, J.-i.; Mizuta, H.; Yamamoto, M.; Kusakabe, K.; Morooka, S.; Suh, S.-H. Separation of Ethane/Ethylene and Propane/Propylene Systems with a Carbonized BPDA−pp‘ODA Polyimide Membrane. *Industrial & Engineering Chemistry Research* **1996,** *35* (11), 4176-4181

(9) Giannakopoulos, I. G.; Nikolakis, V. Separation of Propylene/Propane Mixtures Using Faujasite-Type Zeolite Membranes. *Industrial & Engineering Chemistry Research* **2005,** *44* (1), 226-230

(10) Banerjee, R.; Phan, A.; Wang, B.; Knobler, C.; Furukawa, H.; Keeffe, M.; Yaghi, O. M. High-Throughput Synthesis of Zeolitic Imidazolate Frameworks and Application to CO_2 Capture. *Science* **2008,** *319* (5865), 939

(11) Park, K. S.; Ni, Z.; Côté, A. P.; Choi, J. Y.; Huang, R.; Uribe-Romo, F. J.; Chae, H. K.; O’Keeffe, M.; Yaghi, O. M. Exceptional chemical and thermal stability of zeolitic imidazolate frameworks. *Proceedings of the National Academy of Sciences* **2006,** *103* (27), 10186-10191

(12) Shah, M.; McCarthy, M. C.; Sachdeva, S.; Lee, A. K.; Jeong, H.-K. Current Status of Metal–Organic Framework Membranes for Gas Separations: Promises and Challenges. *Industrial & Engineering Chemistry Research* **2012,** *51* (5), 2179-2199

(13) Aceituno Melgar, V. M.; Kim, J.; Othman, M. R. Zeolitic imidazolate framework membranes for gas separation: A review of synthesis methods and gas separation performance. *Journal of Industrial and Engineering Chemistry* **2015,** *28* (Supplement C), 1-15

(14) Pimentel, B. R.; Parulkar, A.; Zhou, E.-k.; Brunelli, N. A.; Lively, R. P. Zeolitic Imidazolate Frameworks: Next-Generation Materials for Energy-Efficient Gas Separations. *ChemSusChem* **2014,** *7* (12), 3202-3240

(15) Yao, J.; Wang, H. Zeolitic imidazolate framework composite membranes and thin films: synthesis and applications. *Chemical Society Reviews* **2014,** *43* (13), 4470-4493

(16) Bux, H.; Liang, F.; Li, Y.; Cravillon, J.; Wiebcke, M.; Caro, J. Zeolitic Imidazolate Framework Membrane with Molecular Sieving Properties by Microwave-Assisted Solvothermal Synthesis. *Journal of the American Chemical Society* **2009,** *131* (44), 16000-16001

(17) Venna, S. R.; Carreon, M. A. Highly Permeable Zeolite Imidazolate Framework-8 Membranes for CO2/CH4 Separation. *Journal of the American Chemical Society* **2010,** *132* (1), 76-78

(18) Chmelik, C.; Voß, H.; Bux, H.; Caro, J. Adsorption and Diffusion – Basis for Molecular Understanding of Permeation through Molecular Sieve Membranes. *Chemie Ingenieur Technik* **2011,** *83* (1-2), 104-112

(19) Bux, H.; Feldhoff, A.; Cravillon, J.; Wiebcke, M.; Li, Y.-S.; Caro, J. Oriented Zeolitic Imidazolate Framework-8 Membrane with Sharp H2/C3H8Molecular Sieve Separation. *Chemistry of Materials* **2011,** *23* (8), 2262-2269

(20) Li, K.; Olson, D. H.; Seidel, J.; Emge, T. J.; Gong, H.; Zeng, H.; Li, J. Zeolitic Imidazolate Frameworks for Kinetic Separation of Propane and Propene. *Journal of the American Chemical Society* **2009,** *131* (30), 10368-10369

(21) Chmelik, C. Characteristic features of molecular transport in MOF ZIF-8 as revealed by IR microimaging. *Microporous and Mesoporous Materials* **2015,** *216* (Supplement C), 138-145

(22) Zhang, C.; Lively, R. P.; Zhang, K.; Johnson, J. R.; Karvan, O.; Koros, W. J. Unexpected Molecular Sieving Properties of Zeolitic Imidazolate Framework-8. *Journal of Physical Chemistry Letters* **2012,** *3* (16), 2130-4

(23) Eum, K.; Ma, C.; Rownaghi, A.; Jones, C. W.; Nair, S. ZIF-8 Membranes via Interfacial Microfluidic Processing in Polymeric Hollow Fibers: Efficient Propylene Separation at Elevated Pressures. *ACS Applied Materials & Interfaces* **2016,** *8* (38), 25337-25342

(24) Lee, M. J.; Kwon, H. T.; Jeong, H.-K. Defect-dependent stability of highly propylene-selective zeolitic-imidazolate framework ZIF-8 membranes. *Journal of Membrane Science* **2017,** *529*, 105-113

(25) Kwon, H. T.; Jeong, H.-K.; Lee, A. S.; An, H. S.; Lee, J. S. Heteroepitaxially Grown Zeolitic Imidazolate Framework Membranes with Unprecedented Propylene/Propane Separation Performances. *Journal of the American Chemical Society* **2015,** *137* (38), 12304-12311

(26) U.S. Energy Information Administration, e. *Hydrocarbon Gas Liquids (HGL): Recent Market Trends and Issues*; 2014.

(27) Bricker, J. In *History and State of the Art of Ethane/Propane Dehydrogenation Catalysis*, The Board on Chemical Sciences and Technology Workshop on The Changing Landscape of Hydrocarbon Feedstocks for Chemical Production: Implications for Catalysis, Washington, DC, March 7–9, 2016; Washington, DC, 2016.

(28) National Academies of Sciences, E.; Medicine. *The Changing Landscape of Hydrocarbon Feedstocks for Chemical Production: Implications for Catalysis: Proceedings of a Workshop*, The National Academies Press: Washington, DC, 2016.

(29) Sholl, D. S.; Lively, R. P. Seven chemical separations: to change the world. *Nature* **2016,** *532* (7600), 435-438

(30) Krol, J. J.; Boerrigter, M.; Koops, G. H. Polyimide hollow fiber gas separation membranes: preparation and the suppression of plasticization in propane/propylene environments. *Journal of Membrane Science* **2001,** *184* (2), 275-286

(31) Bai, S.; Sridhar, S.; Khan, A. A. Metal-ion mediated separation of propylene from propane using PPO membranes. *Journal of Membrane Science* **1998,** *147* (1), 131-139

(32) Sridhar, S.; Khan, A. A. Simulation studies for the separation of propylene and propane by ethylcellulose membrane1IICT communication no: 4101.1. *Journal of Membrane Science* **1999,** *159* (1), 209-219

(33) Shimazu, A.; Ikeda, K.; Hachisuka, H. Method of selectively separating unsaturated hydrocarbon. US5749943 A, 12 May 1998, 1998.

(34) Tanaka, K.; Taguchi, A.; Hao, J.; Kita, H.; Okamoto, K. Permeation and separation properties of polyimide membranes to olefins and paraffins. *Journal of Membrane Science* **1996,** *121* (2), 197-207

(35) Swaidan, R. J.; Ghanem, B.; Swaidan, R.; Litwiller, E.; Pinnau, I. Pure- and mixed-gas propylene/propane permeation properties of spiro- and triptycene-based microporous polyimides. *Journal of Membrane Science* **2015,** *492*, 116-122

(36) Okamoto, K.; Noborio, K.; Jianqiang, H.; Tanaka, K.; Kita, H. Permeation and separation properties of polyimide membranes to 1,3-butadiene and n-butane. *Journal of Membrane Science* **1997,** *134* (2), 171-179

(37) Okamoto, K.-i.; Kawamura, S.; Yoshino, M.; Kita, H.; Hirayama, Y.; Tanihara, N.; Kusuki, Y. Olefin/Paraffin Separation through Carbonized Membranes Derived from an Asymmetric

Polyimide Hollow Fiber Membrane. *Industrial & Engineering Chemistry Research* **1999,** *38* (11), 4424-4432

(38) Chng, M. L.; Xiao, Y.; Chung, T.-S.; Toriida, M.; Tamai, S. Enhanced propylene/propane separation by carbonaceous membrane derived from poly (aryl ether ketone)/2,6-bis(4-azidobenzylidene)-4-methyl-cyclohexanone interpenetrating network. *Carbon* **2009,** *47* (7), 1857-1866

(39) Ma, X.; Lin, B. K.; Wei, X.; Kniep, J.; Lin, Y. S. Gamma-Alumina Supported Carbon Molecular Sieve Membrane for Propylene/Propane Separation. *Industrial & Engineering Chemistry Research* **2013,** *52* (11), 4297-4305

(40) Liu, D.; Ma, X.; Xi, H.; Lin, Y. S. Gas transport properties and propylene/propane separation characteristics of ZIF-8 membranes. *Journal of Membrane Science* **2014,** *451*, 85-93

(41) James, J. B.; Wang, J.; Meng, L.; Lin, Y. S. ZIF-8 Membrane Ethylene/Ethane Transport Characteristics in Single and Binary Gas Mixtures. *Industrial & Engineering Chemistry Research* **2017,** *56* (26), 7567-7575

(42) Pan, Y.; Li, T.; Lestari, G.; Lai, Z. Effective separation of propylene/propane binary mixtures by ZIF-8 membranes. *Journal of Membrane Science* **2012,** *390*, 93-98

(43) Pan, Y.; Liu, W.; Zhao, Y.; Wang, C.; Lai, Z. Improved ZIF-8 membrane: Effect of activation procedure and determination of diffusivities of light hydrocarbons. *Journal of Membrane Science* **2015,** *493*, 88-96

(44) Sheng, L.; Wang, C.; Yang, F.; Xiang, L.; Huang, X.; Yu, J.; Zhang, L.; Pan, Y.; Li, Y. Enhanced C3H6/C3H8 separation performance on MOF membranes through blocking defects and hindering framework flexibility by silicone rubber coating. *Chemical Communications* **2017,** *53* (55), 7760-7763

(45) Kwon, H. T.; Jeong, H.-K. In Situ Synthesis of Thin Zeolitic–Imidazolate Framework ZIF-8 Membranes Exhibiting Exceptionally High Propylene/Propane Separation. *Journal of the American Chemical Society* **2013,** *135* (29), 10763-10768

(46) Kwon, H. T.; Jeong, H.-K. Highly propylene-selective supported zeolite-imidazolate framework (ZIF-8) membranes synthesized by rapid microwave-assisted seeding and secondary growth. *Chemical Communications* **2013,** *49* (37), 3854-3856

(47) Kwon, H. T.; Jeong, H.-K. Improving propylene/propane separation performance of Zeolitic-Imidazolate framework ZIF-8 Membranes. *Chemical Engineering Science* **2015,** *124*, 20-26

(48) Kwon, H. T.; Jeong, H.-K.; Lee, A. S.; An, H. S.; Lee, T.; Jang, E.; Lee, J. S.; Choi, J. Defect-induced ripening of zeolitic-imidazolate framework ZIF-8 and its implication to vapor-phase membrane synthesis. *Chemical Communications* **2016,** *52* (78), 11669-11672

(49) Shamsaei, E.; Lin, X.; Low, Z.-X.; Abbasi, Z.; Hu, Y.; Liu, J. Z.; Wang, H. Aqueous Phase Synthesis of ZIF-8 Membrane with Controllable Location on an Asymmetrically Porous Polymer Substrate. *ACS Applied Materials & Interfaces* **2016,** *8* (9), 6236-6244

(50) Lee, M. J.; Kwon, H. T.; Jeong, H.-K. High-Flux Zeolitic Imidazolate Framework Membranes for Propylene/Propane Separation by Postsynthetic Linker Exchange. *Angewandte Chemie International Edition* **2018,** *57* (1), 156-161

(51) Li, W.; Su, P.; Li, Z.; Xu, Z.; Wang, F.; Ou, H.; Zhang, J.; Zhang, G.; Zeng, E. Ultrathin metal–organic framework membrane production by gel–vapour deposition. *Nature Communications* **2017,** *8* (1), 406

(52) Eum, K.; Rownaghi, A.; Choi, D.; Bhave, R. R.; Jones, C. W.; Nair, S. Fluidic Processing of High-Performance ZIF-8 Membranes on Polymeric Hollow Fibers: Mechanistic Insights and Microstructure Control. *Advanced Functional Materials* **2016,** *26* (28), 5011-5018

(53) Hillman, F.; Zimmerman, J. M.; Paek, S.-M.; Hamid, M. R. A.; Lim, W. T.; Jeong, H.-K. Rapid microwave-assisted synthesis of hybrid zeolitic-imidazolate frameworks with mixed metals and mixed linkers. *Journal of Materials Chemistry A* **2017,** *5* (13), 6090-6099

(54) Colling, C. H., G. Bartels, J. Processes using solid perm-selective membranes in multiple groups for simultaneous recovery of specified products from a fluid mixture. US 20040004040 A1, 2004.

(55) Hayashi, H.; Cote, A. P.; Furukawa, H.; O'Keeffe, M.; Yaghi, O. M. Zeolite A imidazolate frameworks. *Nature Material* **2007,** *6* (7), 501-506

(56) Morris, W.; Doonan, C. J.; Furukawa, H.; Banerjee, R.; Yaghi, O. M. Crystals as Molecules: Postsynthesis Covalent Functionalization of Zeolitic Imidazolate Frameworks. *Journal of the American Chemical Society* **2008,** *130* (38), 12626-12627

(57) Wang, B.; Cote, A. P.; Furukawa, H.; O/'Keeffe, M.; Yaghi, O. M. Colossal cages in zeolitic imidazolate frameworks as selective carbon dioxide reservoirs. *Nature* **2008,** *453* (7192), 207-211

(58) Rowsell, J. L. C.; Yaghi, O. M. Metal–organic frameworks: a new class of porous materials. *Microporous and Mesoporous Materials* **2004,** *73* (1-2), 3-14

(59) Zhou, H. C.; Long, J. R.; Yaghi, O. M. Introduction to metal-organic frameworks. *Chem Rev* **2012,** *112* (2), 673-4

(60) Furukawa, H.; Cordova, K. E.; O'Keeffe, M.; Yaghi, O. M. The Chemistry and Applications of Metal-Organic Frameworks. *Science* **2013,** *341* (6149),

(61) Lee, J.; Farha, O. K.; Roberts, J.; Scheidt, K. A.; Nguyen, S. T.; Hupp, J. T. Metal-organic framework materials as catalysts. *Chemical Society Reviews* **2009,** *38* (5), 1450-1459

(62) Horcajada, P.; Serre, C.; Maurin, G.; Ramsahye, N. A.; Balas, F.; Vallet-Regí, M.; Sebban, M.; Taulelle, F.; Férey, G. Flexible Porous Metal-Organic Frameworks for a Controlled Drug Delivery. *Journal of the American Chemical Society* **2008,** *130* (21), 6774-6780

(63) Sun, C. Y.; Qin, C.; Wang, X. L.; Yang, G. S.; Shao, K. Z.; Lan, Y. Q.; Su, Z. M.; Huang, P.; Wang, C. G.; Wang, E. B. Zeolitic Imidazolate framework-8 as efficient pH-sensitive drug delivery vehicle. *Dalton Trans* **2012,** *41* (23), 6906-9

(64) Dong, G.; Li, H.; Chen, V. Challenges and opportunities for mixed-matrix membranes for gas separation. *Journal of Materials Chemistry A* **2013,** *1* (15), 4610-4630

(65) Li, J.-R.; Kuppler, R. J.; Zhou, H.-C. Selective gas adsorption and separation in metal-organic frameworks. *Chemical Society Reviews* **2009,** *38* (5), 1477-1504

(66) Cravillon, J.; Schröder, C. A.; Bux, H.; Rothkirch, A.; Caro, J.; Wiebcke, M. Formate modulated solvothermal synthesis of ZIF-8 investigated using time-resolved in situ X-ray diffraction and scanning electron microscopy. *CrystEngComm* **2012,** *14* (2), 492-498

(67) Jian, M.; Liu, B.; Liu, R.; Qu, J.; Wang, H.; Zhang, X. Water-based synthesis of zeolitic imidazolate framework-8 with high morphology level at room temperature. *RSC Advances* **2015,** *5* (60), 48433-48441

(68) Öztürk, Z.; Filez, M.; Weckhuysen, B. M. Decoding Nucleation and Growth of Zeolitic Imidazolate Framework Thin Films with Atomic Force Microscopy and Vibrational Spectroscopy. *Chemistry – A European Journal* **2017,** *23* (45), 10915-10924

(69) Huang, X.-C.; Lin, Y.-Y.; Zhang, J.-P.; Chen, X.-M. Ligand-Directed Strategy for Zeolite-Type Metal–Organic Frameworks: Zinc(II) Imidazolates with Unusual Zeolitic Topologies. *Angewandte Chemie International Edition* **2006,** *45* (10), 1557-1559

(70) Kolokolov, D. I.; Stepanov, A. G.; Jobic, H. Mobility of the 2-Methylimidazolate Linkers in ZIF-8 Probed by 2H NMR: Saloon Doors for the Guests. *The Journal of Physical Chemistry C* **2015,** *119* (49), 27512-27520

(71) Casco, M. E.; Cheng, Y. Q.; Daemen, L. L.; Fairen-Jimenez, D.; Ramos-Fernandez, E. V.; Ramirez-Cuesta, A. J.; Silvestre-Albero, J. Gate-opening effect in ZIF-8: the first experimental proof using inelastic neutron scattering. *Chemical Communications* **2016,** *52* (18), 3639-3642

(72) Fairen-Jimenez, D.; Moggach, S. A.; Wharmby, M. T.; Wright, P. A.; Parsons, S.; Duren, T. Opening the gate: framework flexibility in ZIF-8 explored by experiments and simulations. *J Am Chem Soc* **2011,** *133* (23), 8900-2

(73) Fairen-Jimenez, D.; Galvelis, R.; Torrisi, A.; Gellan, A. D.; Wharmby, M. T.; Wright, P. A.; Mellot-Draznieks, C.; Duren, T. Flexibility and swing effect on the adsorption of energy-related gases on ZIF-8: combined experimental and simulation study. *Dalton Transactions* **2012,** *41* (35), 10752-10762

(74) Garberoglio, G.; Taioli, S. Modeling flexibility in metal–organic frameworks: Comparison between Density-Functional Tight-Binding and Universal Force Field approaches for bonded interactions. *Microporous and Mesoporous Materials* **2012,** *163*, 215-220

(75) Krokidas, P.; Castier, M.; Moncho, S.; Sredojevic, D. N.; Brothers, E. N.; Kwon, H. T.; Jeong, H.-K.; Lee, J. S.; Economou, I. G. ZIF-67 Framework: A Promising New Candidate for Propylene/Propane Separation. Experimental Data and Molecular Simulations. *The Journal of Physical Chemistry C* **2016,** *120* (15), 8116-8124

(76) Hara, N.; Yoshimune, M.; Negishi, H.; Haraya, K.; Hara, S.; Yamaguchi, T. Diffusive separation of propylene/propane with ZIF-8 membranes. *Journal of Membrane Science* **2014,** *450*, 215-223

(77) Eum, K.; Jayachandrababu, K. C.; Rashidi, F.; Zhang, K.; Leisen, J.; Graham, S.; Lively, R. P.; Chance, R. R.; Sholl, D. S.; Jones, C. W.; Nair, S. Highly Tunable Molecular Sieving and Adsorption Properties of Mixed-Linker Zeolitic Imidazolate Frameworks. *Journal of the American Chemical Society* **2015,** *137* (12), 4191-4197

(78) Huang, A.; Bux, H.; Steinbach, F.; Caro, J. Molecular-sieve membrane with hydrogen permselectivity: ZIF-22 in LTA topology prepared with 3-aminopropyltriethoxysilane as covalent linker. *Angew Chem Int Ed Engl* **2010,** *49* (29), 4958-61

(79) Huang, A.; Dou, W.; Caro, J. Steam-Stable Zeolitic Imidazolate Framework ZIF-90 Membrane with Hydrogen Selectivity through Covalent Functionalization. *Journal of the American Chemical Society* **2010,** *132* (44), 15562-15564

(80) Zhu, Y.; Liu, Q.; Huang, A. Microwave synthesis of tubular zeolitic imidazolate framework ZIF-8 membranes for CO2/CH4 separation. *Separation Science and Technology* **2016,** *51* (5), 883-891

(81) Liu, Q.; Wang, N.; Caro, J.; Huang, A. Bio-Inspired Polydopamine: A Versatile and Powerful Platform for Covalent Synthesis of Molecular Sieve Membranes. *Journal of the American Chemical Society* **2013,** *135* (47), 17679-17682

(82) Huang, A.; Liu, Q.; Wang, N.; Caro, J. Highly hydrogen permselective ZIF-8 membranes supported on polydopamine functionalized macroporous stainless-steel-nets. *Journal of Materials Chemistry A* **2014,** *2* (22), 8246-8251

(83) Shah, M.; Kwon, H. T.; Tran, V.; Sachdeva, S.; Jeong, H.-K. One step in situ synthesis of supported zeolitic imidazolate framework ZIF-8 membranes: Role of sodium formate. *Microporous and Mesoporous Materials* **2013,** *165* (Supplement C), 63-69

(84) Yao, J.; Dong, D.; Li, D.; He, L.; Xu, G.; Wang, H. Contra-diffusion synthesis of ZIF-8 films on a polymer substrate. *Chemical Communications* **2011,** *47* (9), 2559-2561

(85) Hara, N.; Yoshimune, M.; Negishi, H.; Haraya, K.; Hara, S.; Yamaguchi, T. ZIF-8 membranes prepared at miscible and immiscible liquid–liquid interfaces. *Microporous and Mesoporous Materials* **2015,** *206*, 75-80

(86) Arnold, M.; Kortunov, P.; Jones Deborah, J.; Nedellec, Y.; Kärger, J.; Caro, J. Oriented Crystallisation on Supports and Anisotropic Mass Transport of the Metal-Organic Framework Manganese Formate. *European Journal of Inorganic Chemistry* **2006,** *2007* (1), 60-64

(87) Yoo, Y.; Jeong, H.-K. Rapid fabrication of metal organic framework thin films using microwave-induced thermal deposition. *Chemical Communications* **2008,** (21), 2441-2443

(88) Ranjan, R.; Tsapatsis, M. Microporous Metal Organic Framework Membrane on Porous Support Using the Seeded Growth Method. *Chemistry of Materials* **2009,** *21* (20), 4920-4924

(89) Snyder Mark , A.; Tsapatsis, M. Hierarchical Nanomanufacturing: From Shaped Zeolite Nanoparticles to High-Performance Separation Membranes. *Angewandte Chemie International Edition* **2007,** *46* (40), 7560-7573

(90) Li, Y.-S.; Liang, F.-Y.; Bux, H.; Feldhoff, A.; Yang, W.-S.; Caro, J. Molecular Sieve Membrane: Supported Metal–Organic Framework with High Hydrogen Selectivity. *Angewandte Chemie International Edition* **2010,** *49* (3), 548-551

(91) Shekhah, O.; Swaidan, R.; Belmabkhout, Y.; du Plessis, M.; Jacobs, T.; Barbour, L. J.; Pinnau, I.; Eddaoudi, M. The liquid phase epitaxy approach for the successful construction of ultra-thin and defect-free ZIF-8 membranes: pure and mixed gas transport study. *Chemical Communications* **2014,** *50* (17), 2089-2092

(92) Shamsaei, E.; Low, Z.-X.; Lin, X.; Mayahi, A.; Liu, H.; Zhang, X.; Zhe Liu, J.; Wang, H. Rapid synthesis of ultrathin, defect-free ZIF-8 membranes via chemical vapour modification of a polymeric support. *Chemical Communications* **2015,** *51* (57), 11474-11477

(93) Catalan, J.; Claramunt, R. M.; Elguero, J.; Laynez, J.; Menendez, M.; Anvia, F.; Quian, J. H.; Taagepera, M.; Taft, R. W. Basicity and acidity of azoles: the annelation effect in azoles. *Journal of the American Chemical Society* **1988,** *110* (13), 4105-4111

(94) Karagiaridi, O.; Bury, W.; Sarjeant, A. A.; Stern, C. L.; Farha, O. K.; Hupp, J. T. Synthesis and characterization of isostructural cadmium zeolitic imidazolate frameworks via solvent-assisted linker exchange. *Chemical Science* **2012,** *3* (11), 3256-3260

(95) Karagiaridi, O.; Lalonde, M. B.; Bury, W.; Sarjeant, A. A.; Farha, O. K.; Hupp, J. T. Opening ZIF-8: A Catalytically Active Zeolitic Imidazolate Framework of Sodalite Topology with Unsubstituted Linkers. *Journal of the American Chemical Society* **2012,** *134* (45), 18790-18796

(96) Stephenson, C. J.; Hupp, J. T.; Farha, O. K. Postassembly Transformation of a Catalytically Active Composite Material, Pt@ZIF-8, via Solvent-Assisted Linker Exchange. *Inorganic Chemistry* **2016,** *55* (4), 1361-1363

(97) Marti, A. M.; Van, M.; Balkus, K. J. Tuning the crystal size and morphology of the substituted imidazole material, SIM-1. *Journal of Porous Materials* **2014,** *21* (6), 889-902

(98) Park, S.; Kang, W. R.; Kwon, H. T.; Kim, S.; Seo, M.; Bang, J.; Lee, S. h.; Jeong, H. K.; Lee, J. S. The polymeric upper bound for N2/NF3 separation and beyond; ZIF-8 containing mixed matrix membranes. *Journal of Membrane Science* **2015,** *486*, 29-39

(99) Jayachandrababu, K. C.; Sholl, D. S.; Nair, S. Structural and Mechanistic Differences in Mixed-Linker Zeolitic Imidazolate Framework Synthesis by Solvent Assisted Linker Exchange and de Novo Routes. *Journal of the American Chemical Society* **2017,** *139* (16), 5906-5915

(100) Zhang, H.; James, J.; Zhao, M.; Yao, Y.; Zhang, Y.; Zhang, B.; Lin, Y. S. Improving hydrostability of ZIF-8 membranes via surface ligand exchange. *Journal of Membrane Science* **2017,** *532*, 1-8

(101) Liu, X.; Li, Y.; Ban, Y.; Peng, Y.; Jin, H.; Bux, H.; Xu, L.; Caro, J.; Yang, W. Improvement of hydrothermal stability of zeolitic imidazolate frameworks. *Chemical Communications* **2013,** *49* (80), 9140-9142

(102) Lalonde, M. B.; Mondloch, J. E.; Deria, P.; Sarjeant, A. A.; Al-Juaid, S. S.; Osman, O. I.; Farha, O. K.; Hupp, J. T. Selective Solvent-Assisted Linker Exchange (SALE) in a Series of Zeolitic Imidazolate Frameworks. *Inorganic Chemistry* **2015,** *54* (15), 7142-7144

(103) Fei, H.; Cahill, J. F.; Prather, K. A.; Cohen, S. M. Tandem Postsynthetic Metal Ion and Ligand Exchange in Zeolitic Imidazolate Frameworks. *Inorganic Chemistry* **2013,** *52* (7), 4011-4016

(104) Jiang, J.-Q.; Yang, C.-X.; Yan, X.-P. Postsynthetic ligand exchange for the synthesis of benzotriazole-containing zeolitic imidazolate framework. *Chemical Communications* **2015,** *51* (30), 6540-6543

(105) Lewis, D. W.; Ruiz-Salvador, A. R.; Gomez, A.; Rodriguez-Albelo, L. M.; Coudert, F.-X.; Slater, B.; Cheetham, A. K.; Mellot-Draznieks, C. Zeolitic imidazole frameworks: structural and energetics trends compared with their zeolite analogues. *CrystEngComm* **2009,** *11* (11), 2272-2276

(106) Morabito, J. V.; Chou, L. Y.; Li, Z.; Manna, C. M.; Petroff, C. A.; Kyada, R. J.; Palomba, J. M.; Byers, J. A.; Tsung, C. K. Molecular encapsulation beyond the aperture size limit through dissociative linker exchange in metal-organic framework crystals. *J Am Chem Soc* **2014,** *136* (36), 12540-3

(107) Morabito, J. V.; Chou, L.-Y.; Li, Z.; Manna, C. M.; Petroff, C. A.; Kyada, R. J.; Palomba, J. M.; Byers, J. A.; Tsung, C.-K. Molecular Encapsulation beyond the Aperture Size Limit

through Dissociative Linker Exchange in Metal–Organic Framework Crystals. *Journal of the American Chemical Society* **2014,** *136* (36), 12540-12543

(108) Deria, P.; Mondloch, J. E.; Karagiaridi, O.; Bury, W.; Hupp, J. T.; Farha, O. K. Beyond post-synthesis modification: evolution of metal-organic frameworks via building block replacement. *Chemical Society Reviews* **2014,** *43* (16), 5896-5912

(109) Irving, H.; Williams, R. J. P. 637. The stability of transition-metal complexes. *Journal of the Chemical Society (Resumed)* **1953,** (0), 3192-3210

(110) Pearson, R. G. Hard and Soft Acids and Bases. *Journal of the American Chemical Society* **1963,** *85* (22), 3533-3539

(111) Brown, A. J.; Brunelli, N. A.; Eum, K.; Rashidi, F.; Johnson, J. R.; Koros, W. J.; Jones, C. W.; Nair, S. Interfacial microfluidic processing of metal-organic framework hollow fiber membranes. *Science* **2014,** *345* (6192), 72

(112) Pan, Y.; Lai, Z. Sharp separation of C2/C3 hydrocarbon mixtures by zeolitic imidazolate framework-8 (ZIF-8) membranes synthesized in aqueous solutions. *Chemical Communications* **2011,** *47* (37), 10275-10277

(113) Hara, N.; Yoshimune, M.; Negishi, H.; Haraya, K.; Hara, S.; Yamaguchi, T. Effect of Solution Concentration on Structure and Permeation Properties of ZIF-8 Membranes for Propylene/Propane Separation. *JOURNAL OF CHEMICAL ENGINEERING OF JAPAN* **2016,** *49* (2), 97-103

(114) Hara, N.; Yoshimune, M.; Negishi, H.; Haraya, K.; Hara, S.; Yamaguchi, T. Effect of Temperature on Synthesis of ZIF-8 Membranes for Propylene/propane Separation by Counter Diffusion Method. *Journal of the Japan Petroleum Institute* **2015,** *58* (4), 237-244

(115) Gutov, O. V.; Hevia, M. G.; Escudero-Adán, E. C.; Shafir, A. Metal–Organic Framework (MOF) Defects under Control: Insights into the Missing Linker Sites and Their Implication in the Reactivity of Zirconium-Based Frameworks. *Inorganic Chemistry* **2015,** *54* (17), 8396-8400

(116) Fang, Z.; Bueken, B.; De Vos, D. E.; Fischer, R. A. Defect-Engineered Metal–Organic Frameworks. *Angewandte Chemie International Edition* **2015,** *54* (25), 7234-7254

(117) Choi, J.; Jeong, H.-K.; Snyder, M. A.; Stoeger, J. A.; Masel, R. I.; Tsapatsis, M. Grain Boundary Defect Elimination in a Zeolite Membrane by Rapid Thermal Processing. *Science* **2009,** *325* (5940), 590

(118) Tian, F.; Cerro, A. M.; Mosier, A. M.; Wayment-Steele, H. K.; Shine, R. S.; Park, A.; Webster, E. R.; Johnson, L. E.; Johal, M. S.; Benz, L. Surface and Stability Characterization of a Nanoporous ZIF-8 Thin Film. *The Journal of Physical Chemistry C* **2014,** *118* (26), 14449-14456

(119) Cheng, P.; Hu, Y. H. H2O-Functionalized Zeolitic Zn(2-methylimidazole)2 Framework (ZIF-8) for H2 Storage. *The Journal of Physical Chemistry C* **2014,** *118* (38), 21866-21872

(120) Zhang, C.; Han, C.; Sholl, D. S.; Schmidt, J. R. Computational Characterization of Defects in Metal–Organic Frameworks: Spontaneous and Water-Induced Point Defects in ZIF-8. *The Journal of Physical Chemistry Letters* **2016,** *7* (3), 459-464

(121) Moh, P. Y.; Cubillas, P.; Anderson, M. W.; Attfield, M. P. Revelation of the Molecular Assembly of the Nanoporous Metal Organic Framework ZIF-8. *Journal of the American Chemical Society* **2011,** *133* (34), 13304-13307

(122) Qiu, S.; Xue, M.; Zhu, G. Metal-organic framework membranes: from synthesis to separation application. *Chemical Society Reviews* **2014,** *43* (16), 6116-6140

(123) Li, Y. S.; Liang, F. Y.; Bux, H.; Feldhoff, A.; Yang, W. S.; Caro, J. Molecular sieve membrane: supported metal-organic framework with high hydrogen selectivity. *Angewandte Chemie International Edition* **2010,** *49* (3), 548-51

(124) Li, Y.; Liang, F.; Bux, H.; Yang, W.; Caro, J. Zeolitic imidazolate framework ZIF-7 based molecular sieve membrane for hydrogen separation. *Journal of Membrane Science* **2010,** *354* (1), 48-54

(125) Pan, Y.; Liu, Y.; Zeng, G.; Zhao, L.; Lai, Z. Rapid synthesis of zeolitic imidazolate framework-8 (ZIF-8) nanocrystals in an aqueous system. *Chemical Communications* **2011,** *47* (7), 2071-2073

(126) Chmelik, C.; Kärger, J. The predictive power of classical transition state theory revealed in diffusion studies with MOF ZIF-8. *Microporous and Mesoporous Materials* **2016,** *225*, 128-132

(127) Tsapatsis, M. Toward High-Throughput Zeolite Membranes. *Science* **2011,** *334* (6057), 767

(128) Kong, L.; Zhang, X.; Liu, H.; Qiu, J. Synthesis of a highly stable ZIF-8 membrane on a macroporous ceramic tube by manual-rubbing ZnO deposition as a multifunctional layer. *Journal of Membrane Science* **2015,** *490*, 354-363

(129) Drobek, M.; Bechelany, M.; Vallicari, C.; Abou Chaaya, A.; Charmette, C.; Salvador-Levehang, C.; Miele, P.; Julbe, A. An innovative approach for the preparation of confined ZIF-8 membranes by conversion of ZnO ALD layers. *Journal of Membrane Science* **2015,** *475*, 39-46

(130) Dumee, L.; He, L.; Hill, M.; Zhu, B.; Duke, M.; Schutz, J.; She, F.; Wang, H.; Gray, S.; Hodgson, P.; Kong, L. Seeded growth of ZIF-8 on the surface of carbon nanotubes towards self-supporting gas separation membranes. *Journal of Materials Chemistry A* **2013,** *1* (32), 9208-9214

(131) Yoo, J.; Lee, S.; Lee, C. K.; Kim, C.; Fujigaya, T.; Park, H. J.; Nakashima, N.; Shim, J. K. Homogeneous decoration of zeolitic imidazolate framework-8 (ZIF-8) with core-shell structures on carbon nanotubes. *RSC Advances* **2014,** *4* (91), 49614-49619

(132) Kong, L.; Zhang, X.; Liu, H.; Wang, T.; Qiu, J. Preparation of ZIF-8 membranes supported on macroporous carbon tubes via a dipcoating–rubbing method. *Journal of Physics and Chemistry of Solids* **2015,** *77*, 23-29

(133) Pan, Y.; Wang, B.; Lai, Z. Synthesis of ceramic hollow fiber supported zeolitic imidazolate framework-8 (ZIF-8) membranes with high hydrogen permeability. *Journal of Membrane Science* **2012,** *421-422*, 292-298

(134) Xu, G.; Yao, J.; Wang, K.; He, L.; Webley, P. A.; Chen, C.-s.; Wang, H. Preparation of ZIF-8 membranes supported on ceramic hollow fibers from a concentrated synthesis gel. *Journal of Membrane Science* **2011,** *385*, 187-193

(135) Huang, K.; Dong, Z.; Li, Q.; Jin, W. Growth of a ZIF-8 membrane on the inner-surface of a ceramic hollow fiber via cycling precursors. *Chemical Communications* **2013,** *49* (87), 10326-10328

(136) Tao, K.; Kong, C.; Chen, L. High performance ZIF-8 molecular sieve membrane on hollow ceramic fiber via crystallizing-rubbing seed deposition. *Chemical Engineering Journal* **2013,** *220*, 1-5

(137) Cacho-Bailo, F.; Seoane, B.; Téllez, C.; Coronas, J. ZIF-8 continuous membrane on porous polysulfone for hydrogen separation. *Journal of Membrane Science* **2014,** *464*, 119-126

(138) Hou, J.; Sutrisna, P. D.; Zhang, Y.; Chen, V. Formation of Ultrathin, Continuous Metal–Organic Framework Membranes on Flexible Polymer Substrates. *Angewandte Chemie International Edition* **2016,** *55* (12), 3947-3951

(139) Hu, Y.; Wei, J.; Liang, Y.; Zhang, H.; Zhang, X.; Shen, W.; Wang, H. Zeolitic Imidazolate Framework/Graphene Oxide Hybrid Nanosheets as Seeds for the Growth of Ultrathin Molecular Sieving Membranes. *Angewandte Chemie International Edition* **2016,** *55* (6), 2048-2052

(140) Hu, Y.; Wu, Y.; Devendran, C.; Wei, J.; Liang, Y.; Matsukata, M.; Shen, W.; Neild, A.; Huang, H.; Wang, H. Preparation of nanoporous graphene oxide by nanocrystal-masked etching: toward a nacre-mimetic metal-organic framework molecular sieving membrane. *Journal of Materials Chemistry A* **2017,** *5* (31), 16255-16262

(141) Wang, Z.; Cohen, S. M. Postsynthetic modification of metal-organic frameworks. *Chemical Society Reviews* **2009,** *38* (5), 1315-1329

(142) Han, S. H.; Kwon, H. J.; Kim, K. Y.; Seong, J. G.; Park, C. H.; Kim, S.; Doherty, C. M.; Thornton, A. W.; Hill, A. J.; Lozano, A. E.; Berchtold, K. A.; Lee, Y. M. Tuning microcavities in thermally rearranged polymer membranes for CO2 capture. *Physical Chemistry Chemical Physics* **2012,** *14* (13), 4365-4373

(143) Takaishi, S.; DeMarco, E. J.; Pellin, M. J.; Farha, O. K.; Hupp, J. T. Solvent-assisted linker exchange (SALE) and post-assembly metallation in porphyrinic metal-organic framework materials. *Chemical Science* **2013,** *4* (4), 1509-1513

(144) Lalonde, M.; Bury, W.; Karagiaridi, O.; Brown, Z.; Hupp, J. T.; Farha, O. K. Transmetalation: routes to metal exchange within metal–organic frameworks. *Journal of Materials Chemistry A* **2013,** *1* (18), 5453

(145) Huang, A.; Caro, J. Covalent Post-Functionalization of Zeolitic Imidazolate Framework ZIF-90 Membrane for Enhanced Hydrogen Selectivity. *Angewandte Chemie International Edition* **2011,** *50* (21), 4979-4982

(146) Gadipelli, S.; Travis, W.; Zhou, W.; Guo, Z. A thermally derived and optimized structure from ZIF-8 with giant enhancement in CO2 uptake. *Energy & Environmental Science* **2014,** *7* (7), 2232-2238

(147) Zhang, C.; Koros, W. J. Tailoring the Transport Properties of Zeolitic Imidazolate Frameworks by Post-Synthetic Thermal Modification. *ACS Applied Materials & Interfaces* **2015,** *7* (42), 23407-23411

(148) Schneider, C. A.; Rasband, W. S.; Eliceiri, K. W. NIH Image to ImageJ: 25 years of image analysis. *Nat Meth* **2012,** *9* (7), 671-675

(149) ACE/JChem ACE and JChem acidity and basicity calculator. https://epoch.uky.edu/ace/public/pKa.jsp (accessed June 20).

(150) Cravillon, J.; Nayuk, R.; Springer, S.; Feldhoff, A.; Huber, K.; Wiebcke, M. Controlling Zeolitic Imidazolate Framework Nano- and Microcrystal Formation: Insight into Crystal Growth by Time-Resolved In Situ Static Light Scattering. *Chemistry of Materials* **2011,** *23* (8), 2130-2141

(151) Shekhah, O.; Eddaoudi, M. The liquid phase epitaxy method for the construction of oriented ZIF-8 thin films with controlled growth on functionalized surfaces. *Chemical Communications* **2013,** *49* (86), 10079-10081

(152) Shah, M. N.; Gonzalez, M. A.; McCarthy, M. C.; Jeong, H.-K. An Unconventional Rapid Synthesis of High Performance Metal–Organic Framework Membranes. *Langmuir* **2013,** *29* (25), 7896-7902

(153) Zhang, H.; Liu, D.; Yao, Y.; Zhang, B.; Lin, Y. S. Stability of ZIF-8 membranes and crystalline powders in water at room temperature. *Journal of Membrane Science* **2015,** *485*, 103-111

(154) Liu, C.; Liu, Q.; Huang, A. A superhydrophobic zeolitic imidazolate framework (ZIF-90) with high steam stability for efficient recovery of bioalcohols. *Chemical Communications* **2016,** *52* (16), 3400-3402

(155) Zhang, K.; Lively, R. P.; Zhang, C.; Koros, W. J.; Chance, R. R. Investigating the Intrinsic Ethanol/Water Separation Capability of ZIF-8: An Adsorption and Diffusion Study. *The Journal of Physical Chemistry C* **2013,** *117* (14), 7214-7225

(156) Chen, B.; Yang, Z.; Zhu, Y.; Xia, Y. Zeolitic imidazolate framework materials: recent progress in synthesis and applications. *Journal of Materials Chemistry A* **2014,** *2* (40), 16811-16831

(157) Rangnekar, N.; Mittal, N.; Elyassi, B.; Caro, J.; Tsapatsis, M. Zeolite membranes - a review and comparison with MOFs. *Chemical Society Reviews* **2015,** *44* (20), 7128-7154

(158) Biswal, B. P.; Bhaskar, A.; Banerjee, R.; Kharul, U. K. Selective interfacial synthesis of metal-organic frameworks on a polybenzimidazole hollow fiber membrane for gas separation. *Nanoscale* **2015,** *7* (16), 7291-7298

(159) Marti, A. M.; Wickramanayake, W.; Dahe, G.; Sekizkardes, A.; Bank, T. L.; Hopkinson, D. P.; Venna, S. R. Continuous Flow Processing of ZIF-8 Membranes on Polymeric Porous Hollow Fiber Supports for CO2 Capture. *ACS Applied Materials & Interfaces* **2017,** *9* (7), 5678-5682

(160) Woo, K. T.; Lee, J.; Dong, G.; Kim, J. S.; Do, Y. S.; Jo, H. J.; Lee, Y. M. Thermally rearranged poly(benzoxazole-co-imide) hollow fiber membranes for CO2 capture. *Journal of Membrane Science* **2016,** *498*, 125-134

(161) McCarthy, M. C.; Varela-Guerrero, V.; Barnett, G. V.; Jeong, H.-K. Synthesis of Zeolitic Imidazolate Framework Films and Membranes with Controlled Microstructures. *Langmuir* **2010,** *26* (18), 14636-14641

(162) Thompson, J. A.; Blad, C. R.; Brunelli, N. A.; Lydon, M. E.; Lively, R. P.; Jones, C. W.; Nair, S. Hybrid Zeolitic Imidazolate Frameworks: Controlling Framework Porosity and Functionality by Mixed-Linker Synthesis. *Chemistry of Materials* **2012,** *24* (10), 1930-1936

APPENDIX A

SUPPLEMENTARY INFORMATION OF CHAPTER III

A.1. Binary gas permeation test

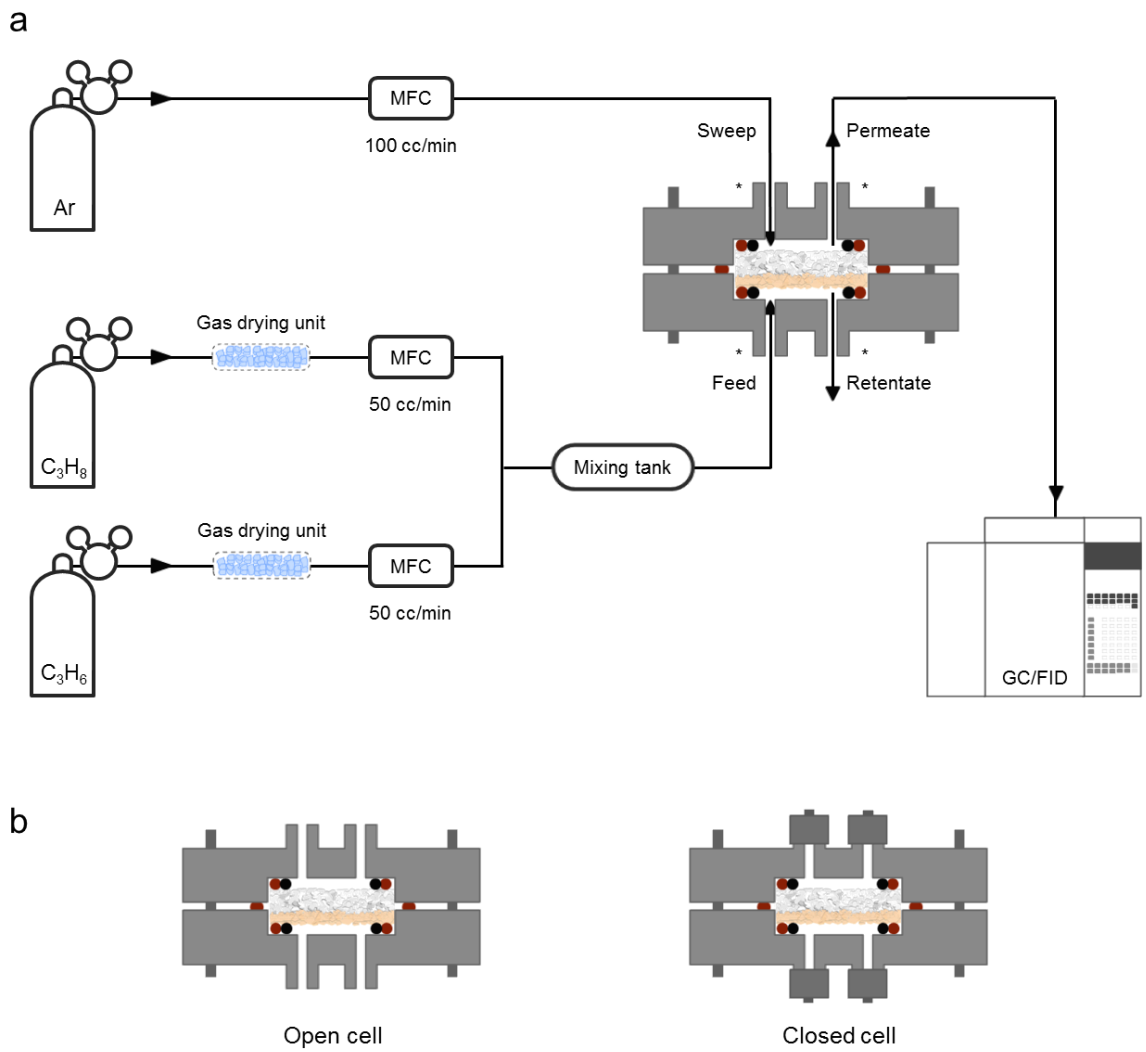

Figure A-1 Schematic diagram of binary gas permeation in Wicke-Kallenbach technique (a) and different permeation cell arrangements (b). The permeation cell is connected to feed, sweep, and permeate lines, accordingly to start measurement. After measurement, the cell is disconnected, marked with asterisks, and kept with membrane inside the cell remained opened, exposed to ambient atmosphere (18~21 °C, RH: 30~ 80%). For thermal activation studies, for controlled measurements, the selected cell remained closed after each permeation measurement until next measurement.

A.2 Comparison of microstructure of CD and MW-ZIF-8 membranes

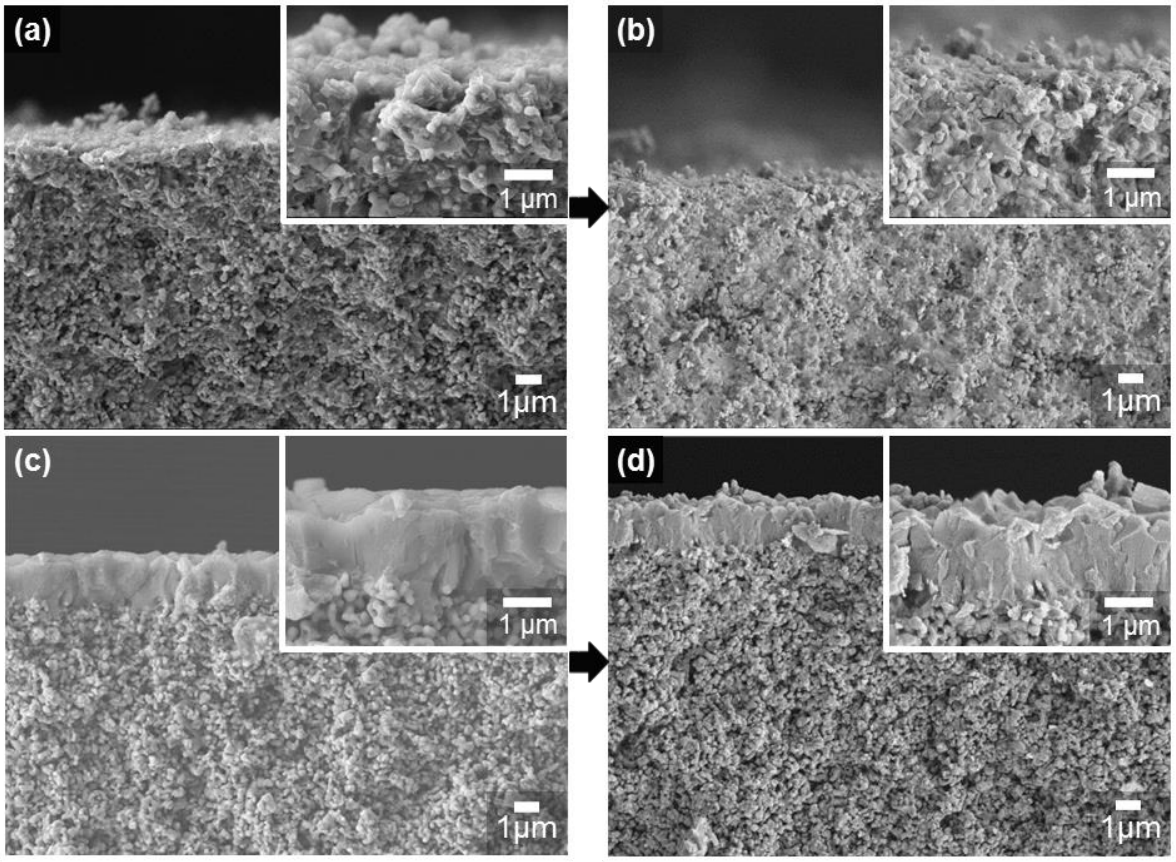

Figure A-2 SEM images of cross-sectional views of as-synthesized (a) CD-ZIF-8 and (c) MW-ZIF-8 membranes and after 60days of off-stream measurement (b, d), respectively.

A. 3 Absolute values of the off-stream measurements of as-synthesized CD-ZIF-8 and MW-ZIF-8 membranes

Table A-1 Permeances and separation factors of ZIF-8 membranes presented in Figure III-3

Day	Separation factor		Propylene permeance (10^{-10} mol/Pa·m^2 · s)	
	CD-ZIF-8	MW-ZIF-8	CD-ZIF-8	MW-ZIF-8
0	14.97	207.57	296.14	157.84
0.25	19.02	212.14	288.66	159.58
0.5	20.01	212.64	280.22	162.57
1	21.41	210.44	272.07	160.89
3	24.06	216.32	252.20	166.27
5	27.40	219.80	282.53	161.74
10	32.48	215.99	256.94	148.31
15	51.90	222.23	109.89	137.11
30	88.88	236.40	81.07	129.37
60	95.14	231.84	75.47	121.18

A. 4 Defects of ZIF-8 membranes

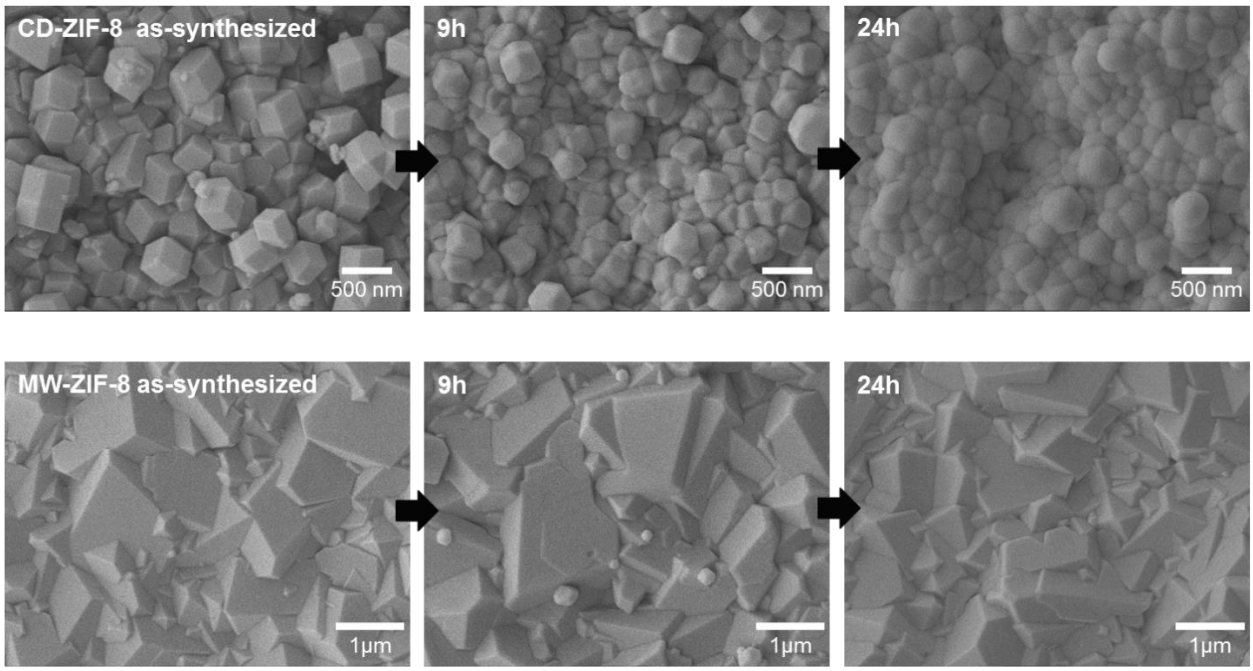

Figure A-3 SEM images of CD-ZIF-8 and MW-ZIF-8 membranes hydrothermally treated in the presence of ligand at 145 ºC for 9 and 24 hrs. Each membrane was inserted in Teflon-lined autoclaves with 1.5g of 2-methylimidazole and 1ml of water without direct contacting with any solvent and incubated in preheated convection oven at 145°C. After post-synthetic hydrothermal treatments in vapor phase, CD-ZIF-8 membrane lost crystal facets, whereas, MW-ZIF-8 membrane showed negligible changes even after 24 hrs at 145 °C. This work is from recent publication of Kwon et al.[1]

A. 5 Thermal activation of CD-M-ZIF-8 prior to off-stream measurement

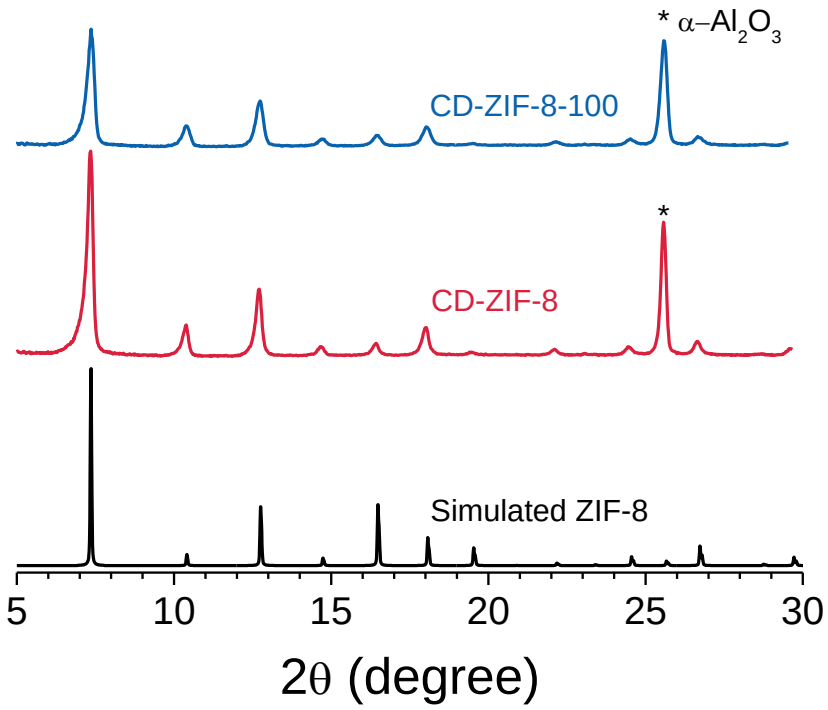

Figure A-4 XRD patterns of simulated ZIF-8 pattern, CD-ZIF-8 and CD-ZIF-8-100 membranes.

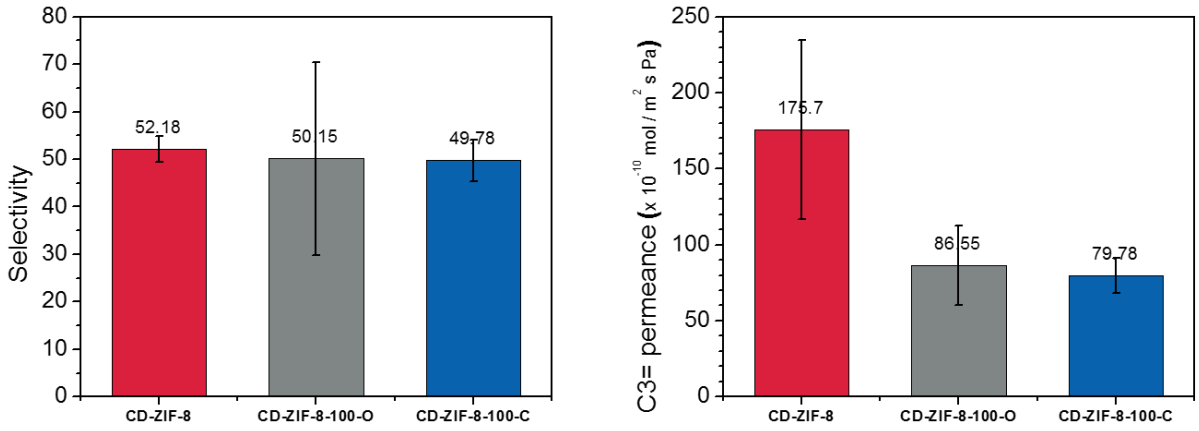

Figure A-5 Off-stream measurement of CD-ZIF-8 and CD-ZIF-8-100-O, CD--ZIF-8-100-C membranes.

Table A-2 Table of absolute values of the off-stream measurements in Figure III-6

Day	Separation factor			Propylene permeance (10^{-10} mol/Pa·m^2 · s)		
	CD-M-ZIF-8	CD-M-ZIF-8-100-O	CD-M-ZIF-8-100-C	CD-M-ZIF-8	CD-M-ZIF-8-100-O	CD-M-ZIF-8-100-C
0	54.06	63.56	52.90	134.18	66.03	71.67
5	64.24	84.28	51.39	105.47	55.80	66.47
10	N/A	N/A	49.33	N/A	N/A	57.53
15	80.11	82.68	49.14	88.5	53.05	54.29
30	83.01	86.13	43.39	84.9	52.78	49.93

A. 6 Post-synthetic ligand treatment to stabilize membrane performance

Hydrothermal ligand treatment was conducted post-synthetically to stabilize CD- ZIF-8 membranes. Ligand solution is prepared by dissolving 3 mg and 5 mg 2-methylimidazole in 20 ml water to prepare 15 wt% and 25 wt% ligand solutions, respectively. As-synthesized CD-ZIF-8 membranes were inserted vertically using house-made Teflon holder in Teflon-lined autoclave with 20 ml of aqueous ligand solution. Autoclaves were incubated in pre-heated convection oven at 60 and 120 °C for 4 hours followed by cool down to room temperature. Membranes were washed in 30 ml fresh methanol for 1 day followed by drying at room temperature for 12 hours.

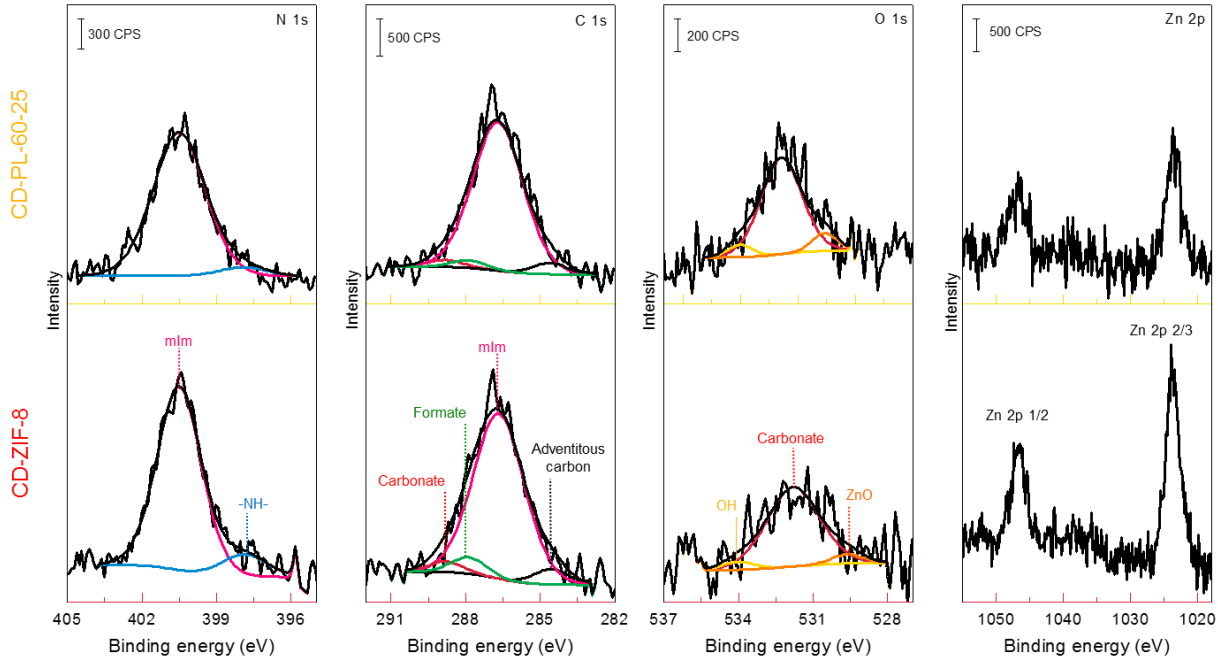

Figure A-6 Comparison of high resolution XPS spectra of CD- ZIF-8 and CD-PL-60-25 membranes

A.7 References

(1) Kwon, H. T.; Jeong, H.-K.; Lee, A. S.; An, H. S.; Lee, T.; Jang, E.; Lee, J. S.; Choi, J. Defect-induced ripening of zeolitic-imidazolate framework ZIF-8 and its implication to vapor-phase membrane synthesis. *Chemical Communications* **2016,** *52* (78), 11669-11672

APPENDIX B

SUPPLEMENTARY INFORMATION OF CHAPTER IV

B. 1 Binary gas permeation test

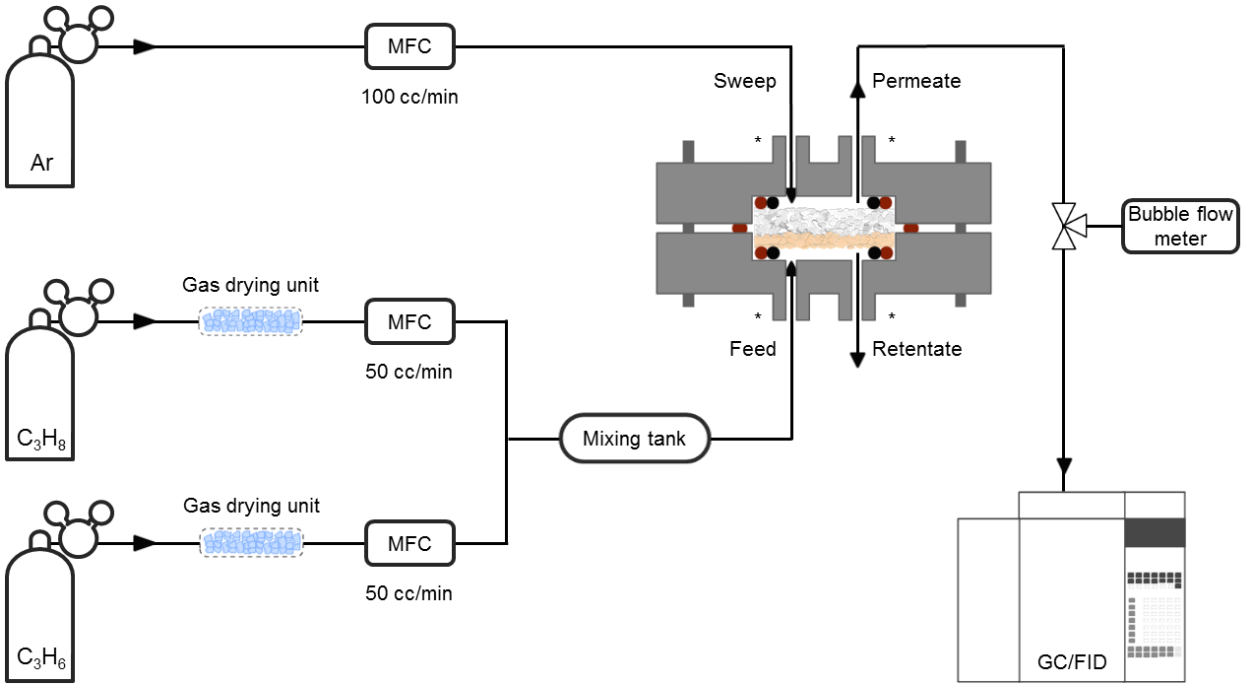

Figure B-1 The propylene/propane binary gas permeation measurement set up using Wicke-Kallenbach technique

B. 2 Post-synthetic linker exchange on CD-ZIF-8 membranes

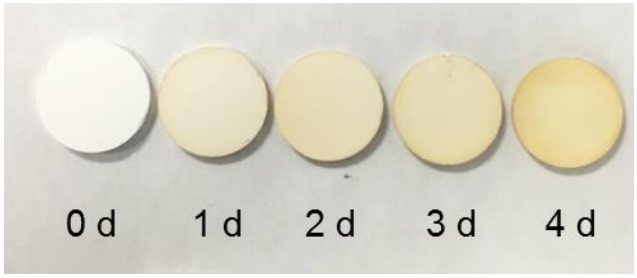

Figure B-2 Optical micrograph of as-synthesized CD-ZIF-8 and Ica-CD-ZIF-8 membranes.

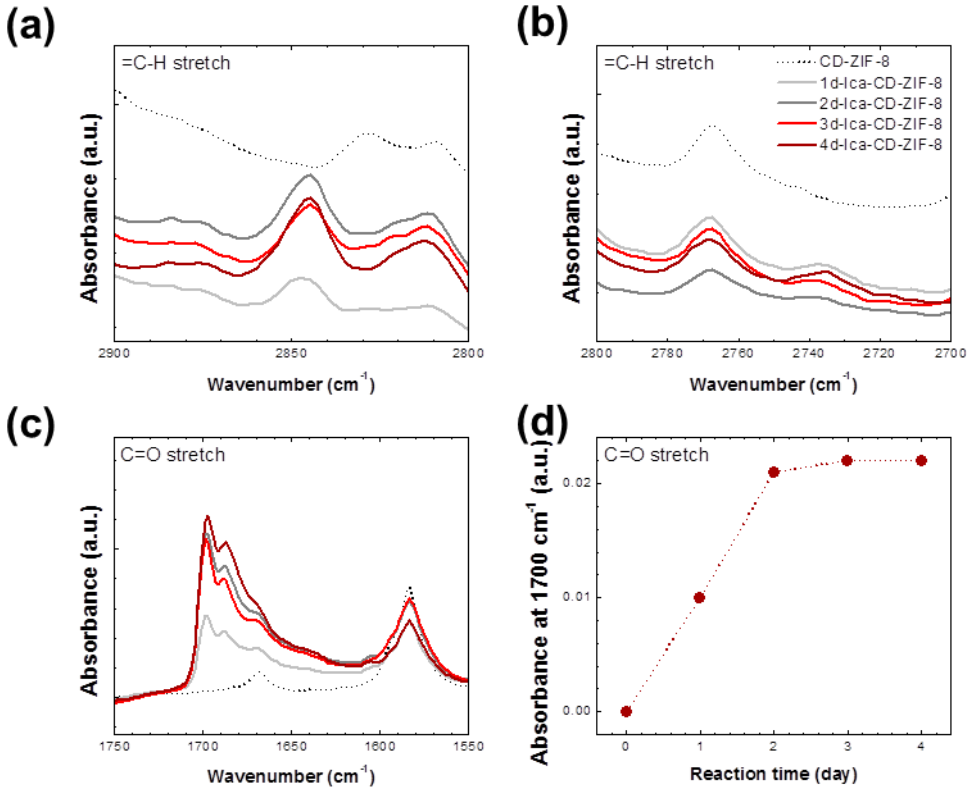

Figure B-3 ATR-IR spectra of CD-ZIF-8 and PSLE treated membranes over time. The Ica incorporation was found by the appearance of =C-H stretches (a) at 2850 cm^{-1} and (b) at 2740 cm^{-1}, (c) the C=O stretch at 1700 cm^{-1} and (d) the exchange reaction time-dependent absorbances at 1700 cm^{-1}. The absorbances were measured by the OMNIC™ software.

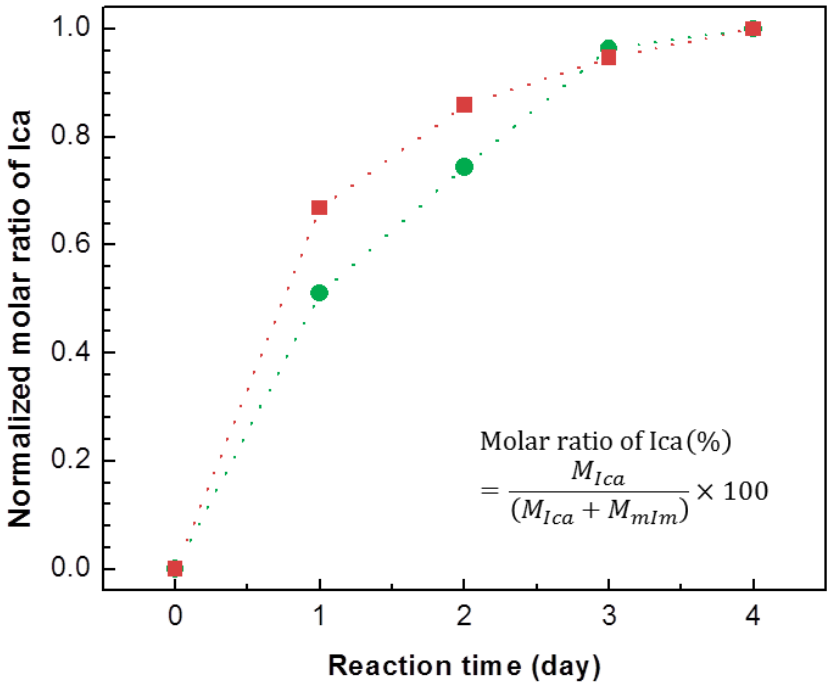

Figure B-4 Normalized molar ratio of Ica in the (··■··) CD- and (··●··) MW-ZIF-8 membranes after PSLE reaction over time. The molar ratio was first calculated based on ^{1}H solution NMR results and then normalized by the value of the 4d-Ica-ZIF-8 membrane.

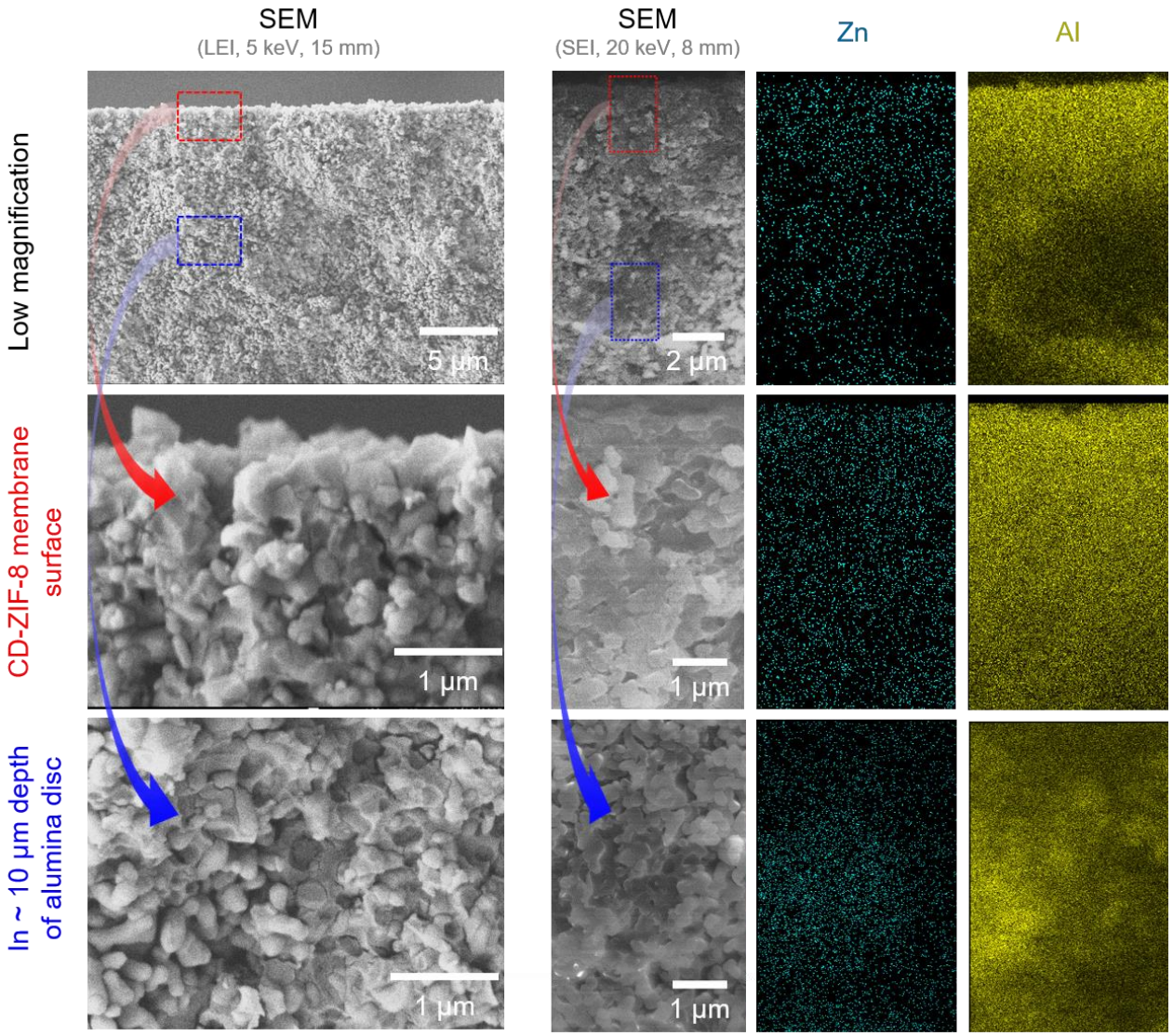

Figure B-5 SEM images and EDX mappings of the CD-ZIF-8 membrane were taken at cross-sectional views. The images of columns are SEM images in different working distance (15 vs. 8mm) with different detector (LEI vs SEI), and at different electron voltage. For elemental mapping, zinc and aluminum, the second column of SEM images was used. The first, second, and third rows are the images and mappings taken at lower magnification, near CD-ZIF-8 membrane surface, and near ~ 10 µm in depth of the alumina disc, respectively. As can be seen in the SEM images and elemental mapping, ZIF-8 crystals were formed in the alumina disc at ~10 µm depth from the surface. Note that uneven mappings of aluminum are because of surface roughness of the alumina disc upon cutting.

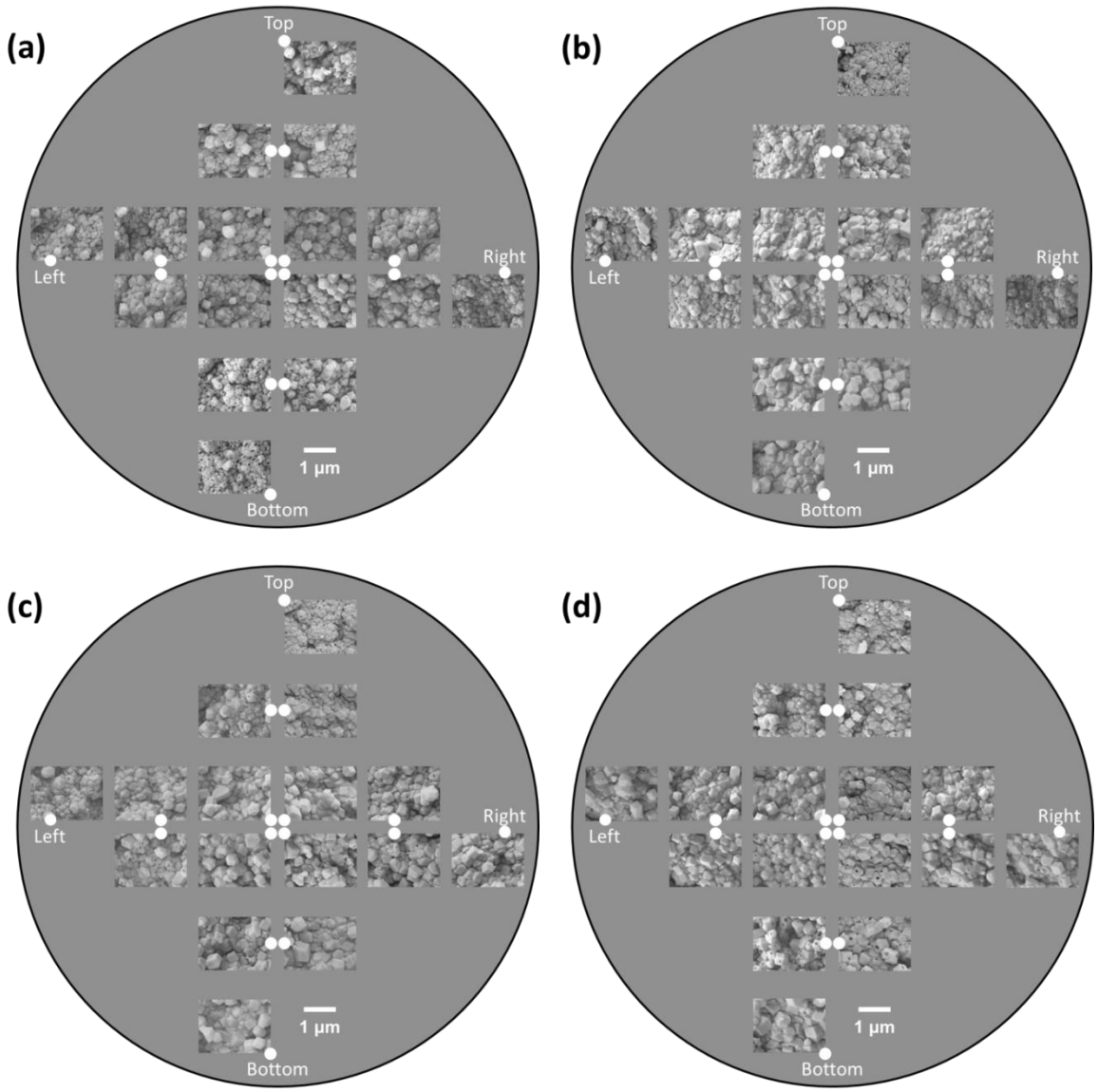

Figure B-6 SEM images of top of CD-ZIF-8 membranes after PSLE for (a) 1 day, (b) 2 days, (c) 3 days, and (d) 4 days. The grey circle and white circles are representing the surface of CD-ZIF-8 membrane on an alumina disc and locations of SEM images taken, respectively. Directions such as top and bottom are designated accordingly upon synthesis condition.

B. 3 Post-synthetic modification on CD-ZIF-8 membranes

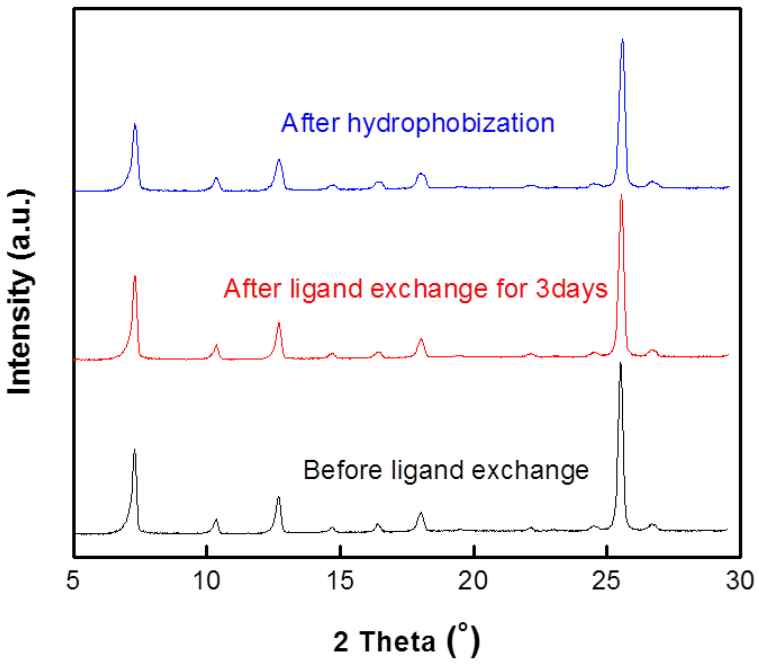

Figure B-7 XRD patterns of CD-ZIF-8 membranes after PSM. The introduction of dodecylamine on the surface of 3d-Ica-CD-ZIF-8 membrane did not compromised the crystallinity of the membrane.

Table B-1 A summary of contact angle measurements of CD-ZIF-8 and MW-ZIF-8 membranes as-synthesized, after 3days of PLSE, and subsequent surface modification. Contact angles were measured by ImageJ with drop analysis plug-in.

Contact angle (°)	As-synthesized	After PSLE for 3 days	After PSM
CD-ZIF-8	23.6 ±3.6 Hydrophilic	8.3 ±.3.0 Hydrophilic	100.5 ± 0.5 Hydrophobic
MW-ZIF-8	95.0 ± 5.0 Hydrophobic	74.4 ± 4.4 Hydrophilic	111.1 ± 2.8 Hydrophobic

B. 4 MW-ZIF-8 membranes

ZIF-8 membranes were fabricated by using our previously reported microwave method[1] and, hereafter, are referred to as MW-ZIF-8 membranes. Briefly, to prepare a ZIF-8 seed crystal layer, an alumina disk was first saturated with Zn^{2+} by immersing in 2.43 g of zinc nitrate hexahydrate in 40 ml of methanol for 1 hr. Subsequently, the Zn^{2+} satruated support was placed in the microwave-resistant tube containing 30 ml of ligand solution (2.59 g of mIm and 0.125 g of sodium formate in 40 ml methanol) and then treated under microwave (100W) for 1.5 min. The seeded alumina support was washed in 35 ml of fresh methanol for 1 day under gentle rocking followed by dried at 60 °C for 4 hrs. The subsequent secondary growth was carried out based on the aqueous recipe reported elsewhere[2]. Aqueous metal and ligand precursor solutions were prepared by dissolving 0.11 g of zinc nitrate hexahydrate and 2.27 g of mIm in 20 ml of DI water, respectively. The metal solution was added rapidly to the ligand solution and continued for stirring for 2 min. The resulting growth solution was poured into a beaker with the seeded support placed vertically using a custom-made Teflon holder. The hydrothermal reaction was conducted in a vacuum oven at 30 °C for 6 hrs under ambient pressure. After the reaction, the membrane was washed in 35 ml of fresh methanol for 5 days and then dried in an oven at 60 °C for 6 hrs.

The PSLE and PSM were conducted on MW-ZIF-8 membranes as described previously in the section A, supplementary information.

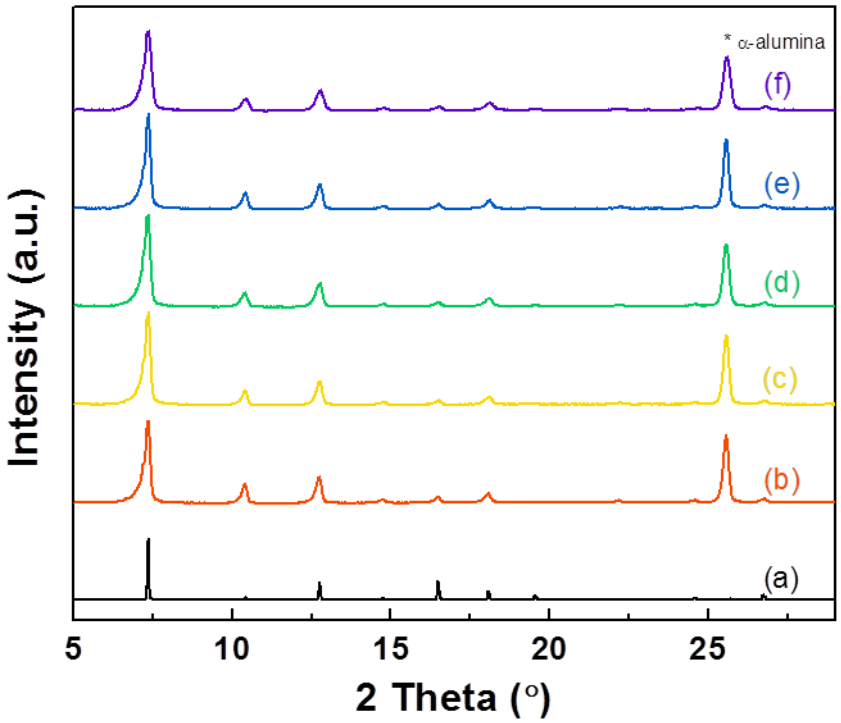

Figure B-8 Reaction-time-dependent X-ray diffranction patterns of (a) ZIF-8 simulated pattern, (b) MW-ZIF-8 as-synthesized, (c) 1d-Ica-MW-ZIF-8, (d) 2d-Ica-MW-ZIF-8, (e) 3d-Ica-MW-ZIF-8, and (f) 4d-Ica-MW-ZIF-8 membranes.

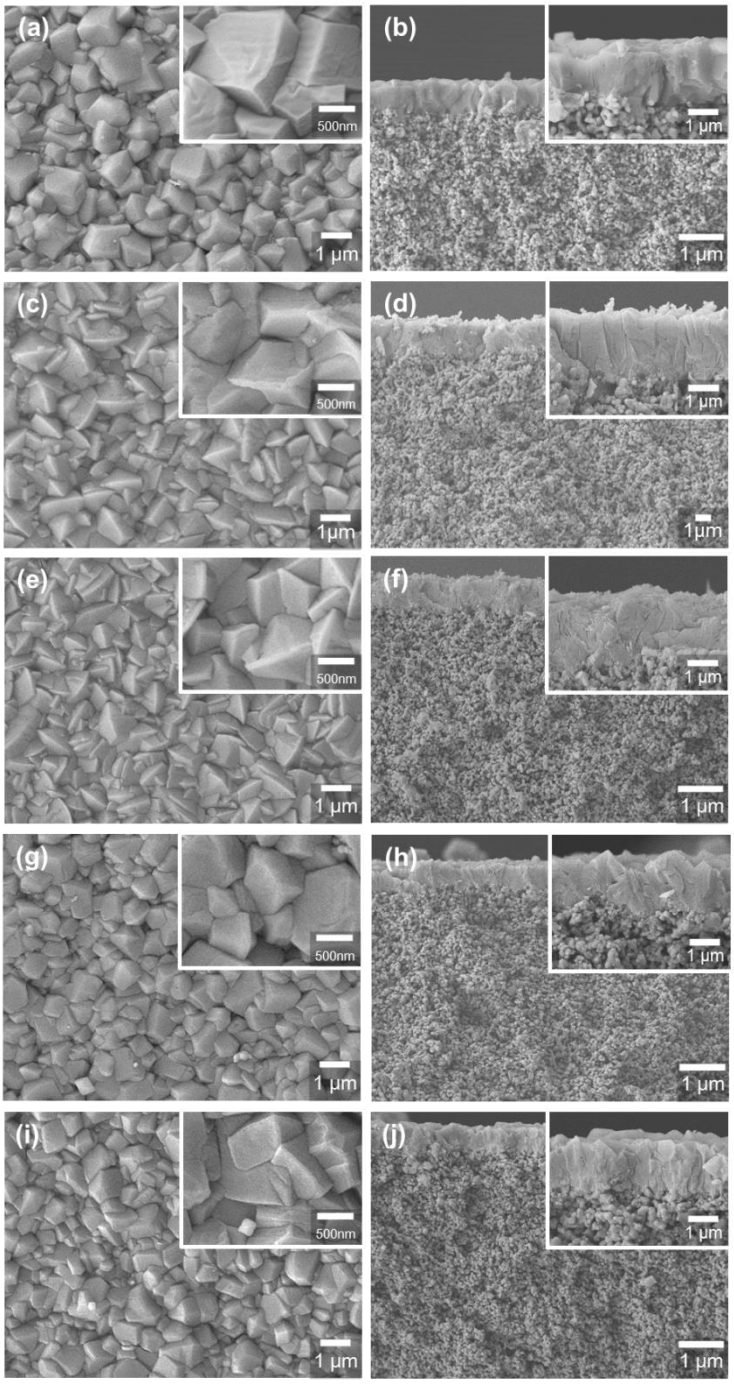

Figure B-9 SEM images of top and cross-section of (a), (b) as-synthesized MW-ZIF-8, (c), (d) 1d-Ica-MW-ZIF-8, (e), (f) 2d-Ica-MW-ZIF-8, (g), (h) 3d-Ica-MW-ZIF-8, and (i), (j) 4d-Ica-MW-ZIF-8 membranes.

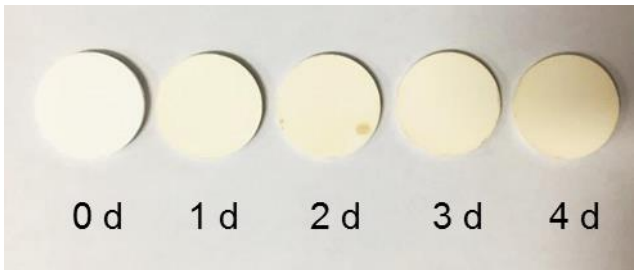

Figure B-10 A digital photo of MW-ZIF-8 as synthesized, 1d-, 2d, 3d, and 4d-Ica-MW-ZIF-8 membranes.

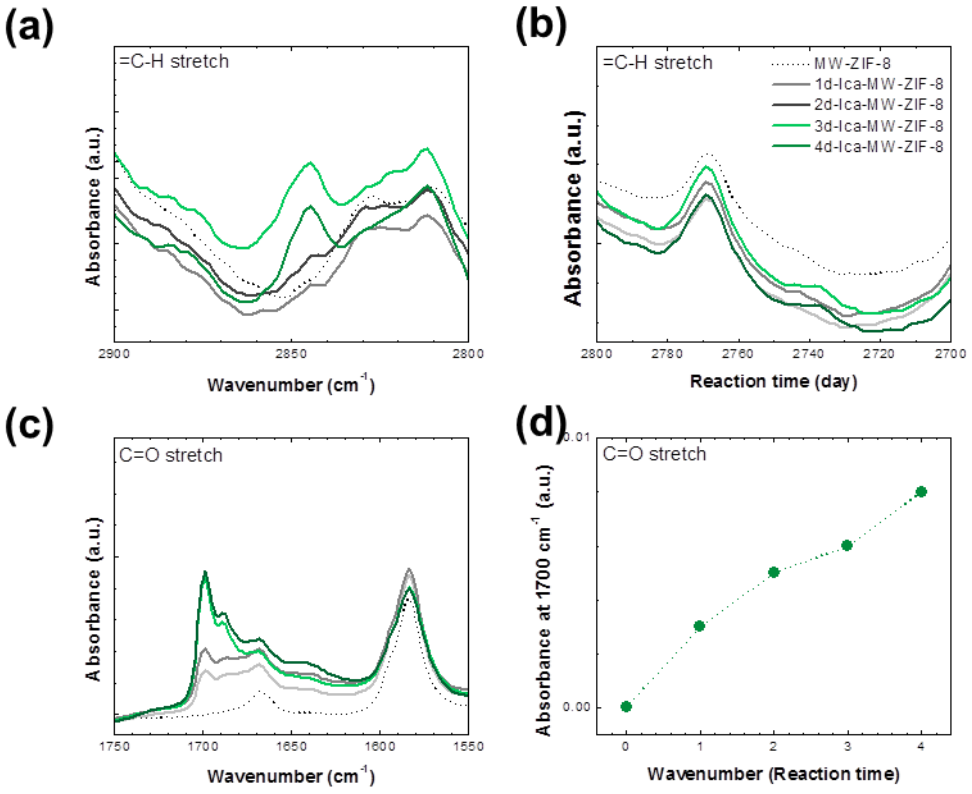

Figure B-11 ATR-IR spectra of MW-ZIF-8 and PSLE treated membranes over time. The presence of Ica linker was confirmed by the =C-H stretches (a) at 2850 cm^{-1} and (b) at 2740 cm^{-1}, (c) the C=O stretch at 1700 cm^{-1} and (d) the exchange reaction time-dependent absorbances at 1700 cm^{-1}. The absorbances were measured by the OMNIC™ software.

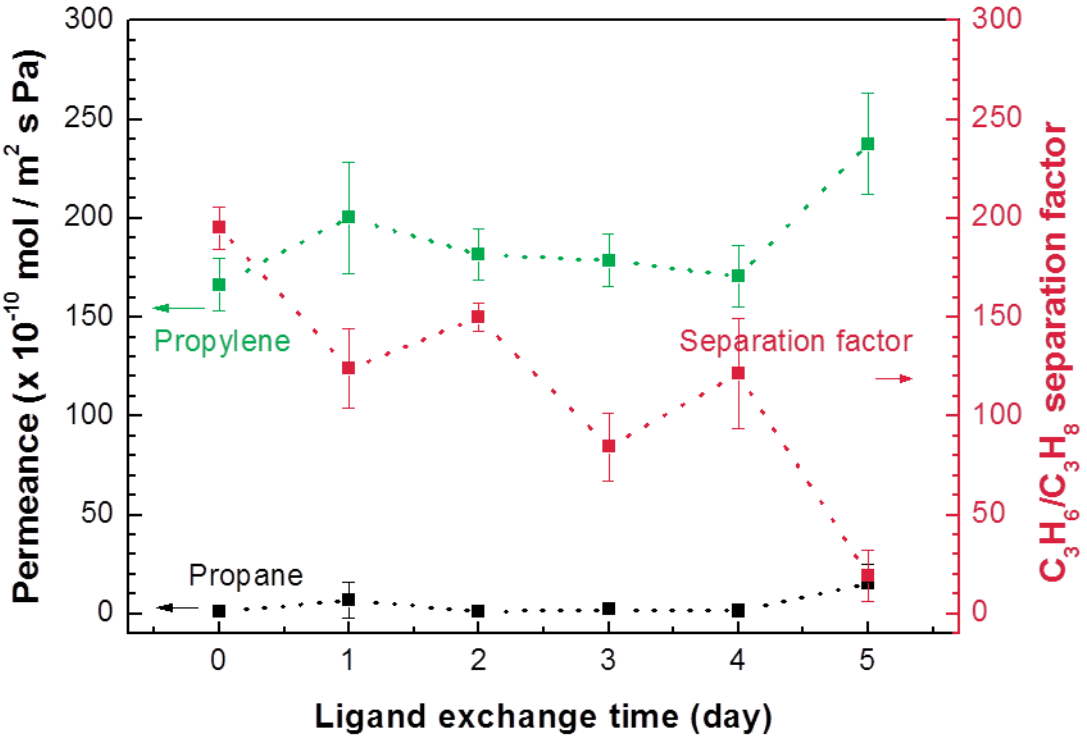

Figure B-12 Binary permeation results of propylene/propane separation of post-synthetic ligand exchanged MW-ZIF-8 membranes with different reaction time. Permeation measurements were conducted at room temperature (18 ~ 21 °C).

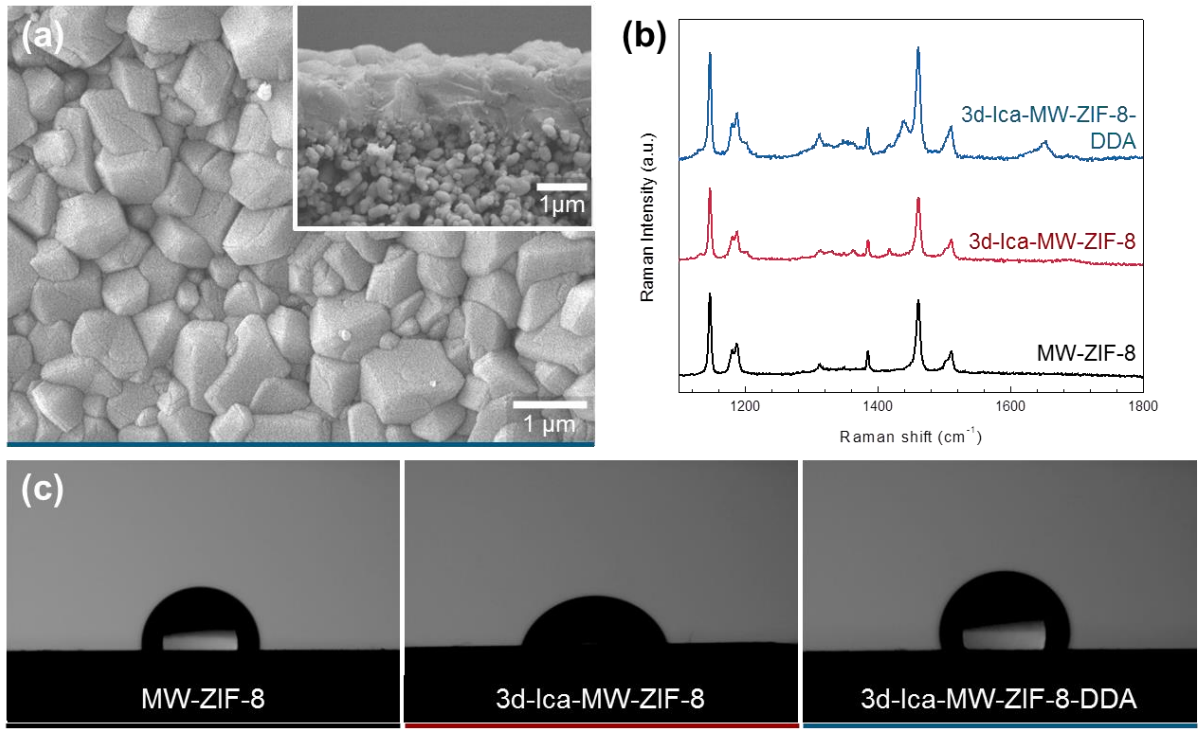

Figure B-13 (a) SEM image of 3d-Ica-MW-ZIF-8-DDA membrane, (b) Raman spectra, and (c) water droplet measurement of as synthesized MW-ZIF-8, 3d-Ica-MW-ZIF-8, and 3d-Ica-MW-ZIF-8-DDA membranes. Summary of contact angle data is in Table B-1.

B. 6 References

(1) Kwon, H. T.; Jeong, H.-K. Highly propylene-selective supported zeolite-imidazolate framework (ZIF-8) membranes synthesized by rapid microwave-assisted seeding and secondary growth. *Chemical Communications* **2013,** *49* (37), 3854-3856
(2) Pan, Y.; Liu, Y.; Zeng, G.; Zhao, L.; Lai, Z. Rapid synthesis of zeolitic imidazolate framework-8 (ZIF-8) nanocrystals in an aqueous system. *Chemical Communications* **2011,** *47* (7), 2071-2073

APPENDIX C

SUPPLEMENTARY INFORMATION OF CHAPTER X

C. 1 Experimental

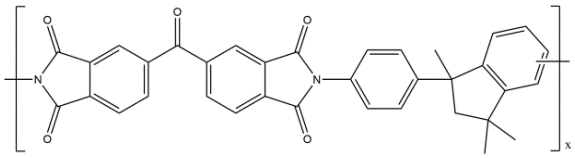

Figure C-1 Chemical structure of Matrimid® 5218.

Table C-1 Parameters of Matrimid® hollow fiber fabrication.

Parameters	Values
Dope solution composition (P/S) (wt.%)	20/80
Bore solution composition (NMP/water) (wt.%)	70/30
Dope and bore solution temperatures (°C)	60
Spinneret temperature (°C)	60
Air-gap distance (cm)	0-5
Dope and bore flow rates (ml/min)	0.5-1.5
Coagulation bath temperature (water) (°C)	80
Washing temperature (^{o}C)	35
Washing time (day)	3

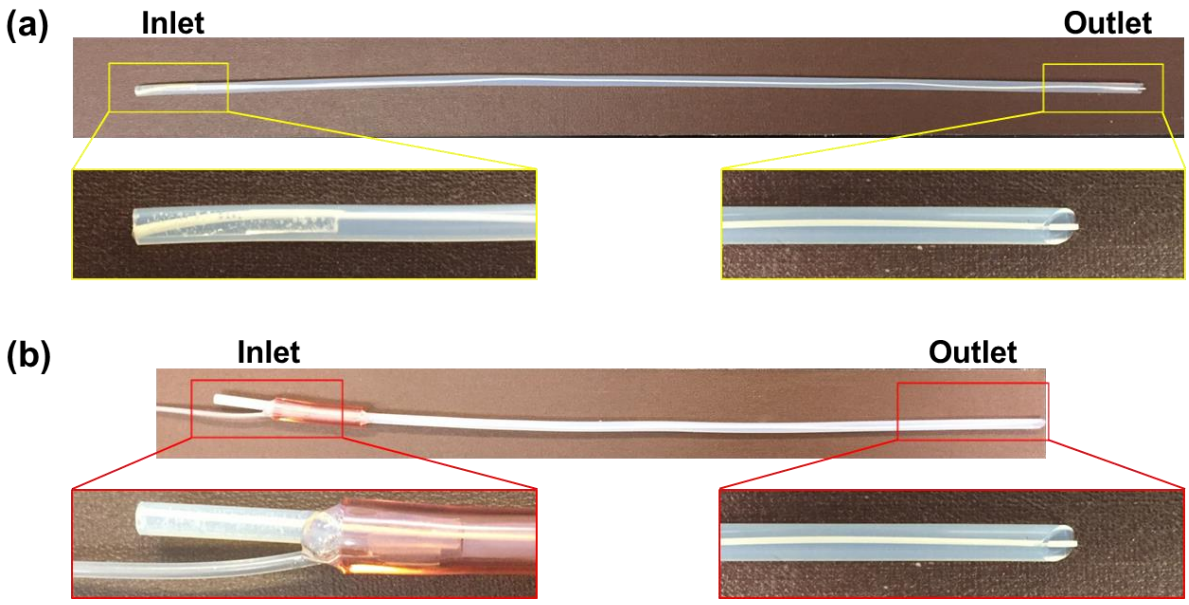

Figure C-2 Optical photographs of protective PTFE tubing for flow synthesis on (a) bore side and (b) shell side.

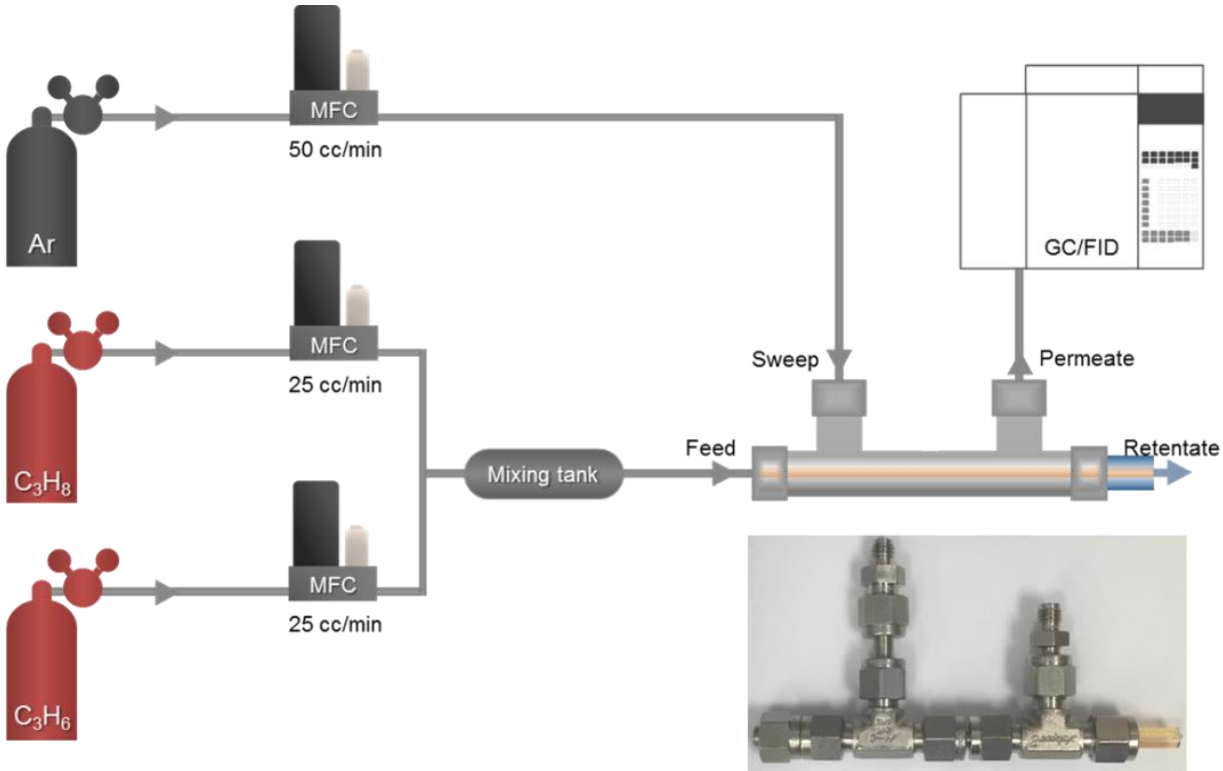

Figure C-3 Schematic illustration of the Wicke-Kallenbach set up for binary gas separation of propylene/propane using ZIF-8 membranes on pHF substrate.

C. 2 Spun hollow fibers: gas permeance and morphology

Table C 2 Gas permeance data of spun hollow fiber.

Sample	P(He)/l (GPU)	$P(H_2)/l$ (GPU)	$P(O_2)/l$ (GPU)	$P(N_2)/l$ (GPU)	$P(CO_2)/l$ (GPU)	$P(CH_4)/l$ (GPU)
1	23242	34342	10220	11224	9553	15081
2	26180	40346	11922	12988	11025	17453
3	24465	37463	11034	12045	10300	15797
Average	24711	37344	11071	12106	10289	16267

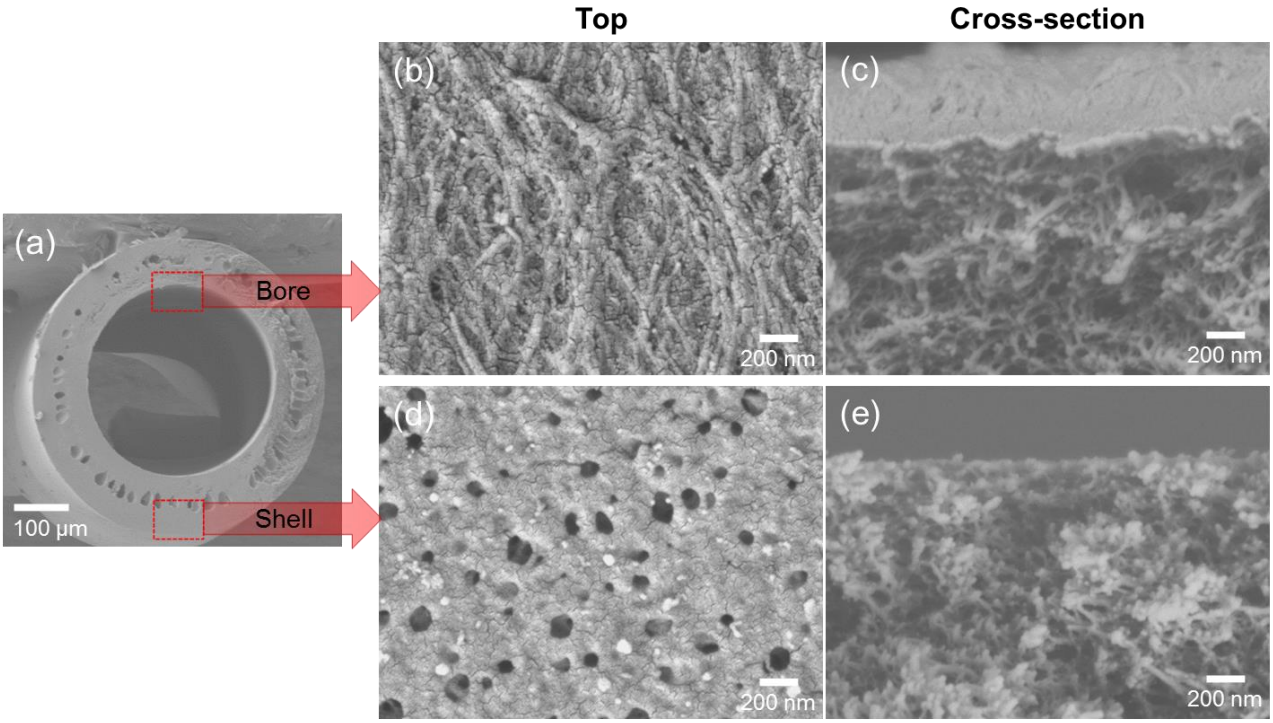

Figure C-4 SEM images of (a) porous Matrimid® hollow fiber in cross-sectional view in low magnification, (b) top and (c) cross-sectional views of bore sides, and (d) top and (e) cross-sectional views of shell sides in higher magnification.

C. 3 ZIF-8 seeding and secondary growth on the shell side of hollow fibers

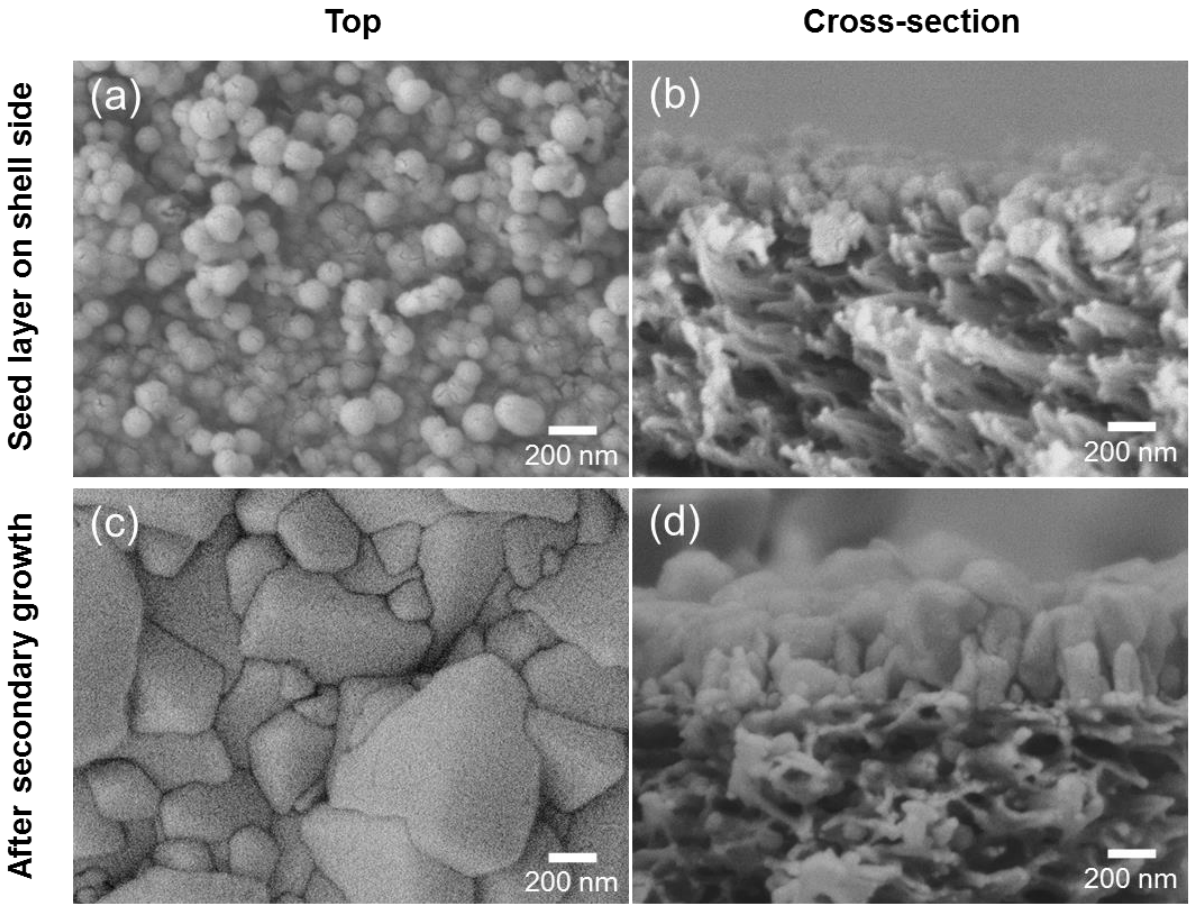

Figure C-5 SEM images of ZIF-8/pHF seed layer prepared on shell side by microwave seeding: (a) top and (b) cross-section and ZIF-8/pHF membrane after secondary growth: (c) top and (d) cross-section. SEM images of the shell side of bare hollow fibers are shown in Figure 9-4 (d, e).

C. 4 Microfluidic seeding and secondary growth on the bore side of hollow fibers

ZIF-8 nanocrystals were synthesized following method reported by Cravillon et al.[1] with minor modification. In brief, metal precursor solution was prepared by dissolving 2.936 g of zinc nitrate hexahydrate in 140 ml of methanol. On the other hand, ligand precursor solution was prepared by dissolving 6.477 g of 2-methylimidazole in 140 ml of methanol. The metal precursor solution was then poured into the ligand precursor solution followed by continuous mixing for 1 hr. Next, ZIF-8 nanocrystals were separated by centrifugation and thoroughly washed with fresh methanol. ZIF-8 yield is 28% based on zinc. Sizes of the nanocrystals were comparable to size of ZIF-8 crystals on seeded pHF (~ 70 nm vs. ~ 60 nm). ZIF-8 seed layers were deposited on bore side of pHF by flowing ZIF-8 nanocrystals suspension in methanol (ZIF-8 concentration ~ 2.7 mg/ml) at flow rate of 0.11 ml/min for total of 1 min. Then, the seeded pHF was dried in a convective oven for 60 °C for 1 hr. The seed layers were secondarily grown to form continuous membrane following similar procedure described in experimental section.

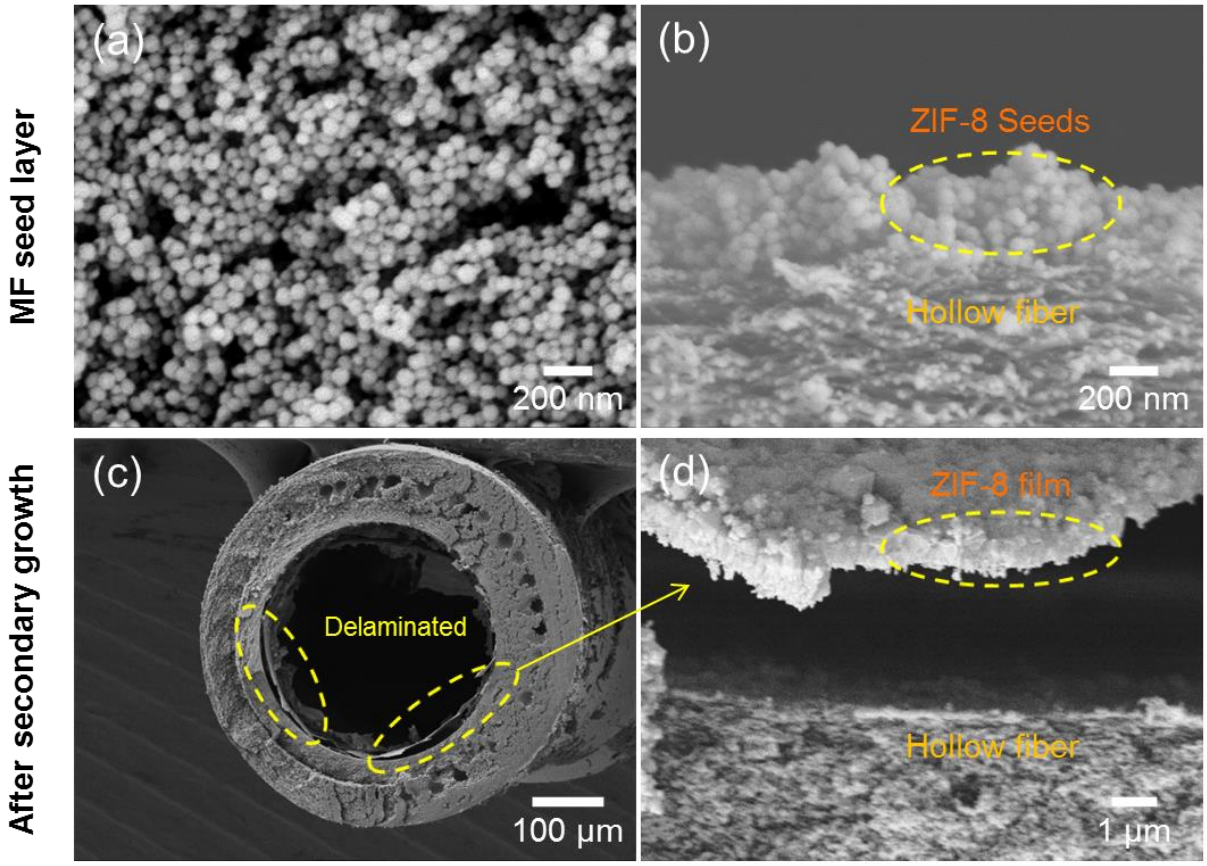

Figure C-6 SEM images of ZIF-8/pHF seed layer prepared on bore side by microfluidic (MF) seeding: (a) top and (b) cross-section and ZIF-8/pHF membrane after secondary growth: in cross-sectional view at (c) lower magnification and (d) higher magnification.

C. 5 ZIF-8 in situ growth on the bore side of hollow fibers

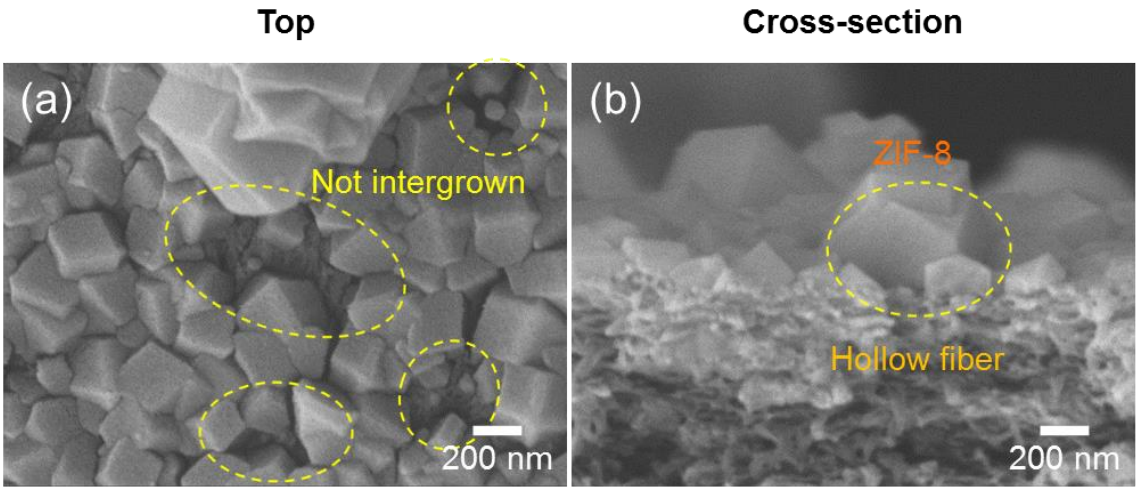

Figure C-7 SEM images of ZIF-8 crystals grown *in situ* on the bore side of a pHF without seed crystals: (a) top and in (b) cross-sectional views. The film is not well-intergrown.

C. 6 Literature review

Table C-3 Summary of literatures of ZIF-8 membranes prepared on different substrates by using various synthesis methods and their gas separation performances.

Support	Synthesis Method[1]	Bore/Shell	ID/OD (μm)	Thickness (μm)	C_3H_6/C_3H_8 Separation[2]		Ref
					Separation Factor	C_3H_6 Permeance[3]	
α-alumina disk	Liquid phase epitaxy	N/A	N/A	1.6	3	0.44	2
α-alumina disk	Seeding (slip coating) and hydrothermal secondary growth	N/A	N/A	2.5	21	164	3
α-alumina disk	Seeding (slip coating) and hydrothermal secondary growth	N/A	N/A	5.0	36	220	4
α-alumina disk	Seeding (slip coating) and hydrothermal secondary growth	N/A	N/A	2.2	35 ± 6	278 ± 57	5
α-alumina disk	Seeding (slip coating) and hydrothermal secondary growth	N/A	N/A	3.0	65 ± 15	120 ± 44	6
α-alumina disk	Seeding (slip coating) and hydrothermal secondary growth followed by PDMS coating	N/A	N/A	2.0	89 ± 5	213 ± 17	7
α-alumina disk	Counter-diffusion	N/A	N/A	1.5	50	200	8
α-alumina disk	Microwave seeding and hydrothermal secondary growth	N/A	N/A	1.5	40	207	9
α-alumina disk	Counter-diffusion in situ growth and post-synthetic linker exchange	N/A	N/A	< 1.0	40	780	10

Table C-3 Continued

Support	Synthesis Method[1]	Bore/Shell	ID/OD (μm)	Thickness (μm)	C_3H_6/C_3H_8 Separation[2]		Ref
					Separation Factor	C_3H_6 Permeance[3]	
α-alumina disk	Microwave seeding and hydrothermal secondary growth	N/A	N/A	1.6	208	158	[11]
α-alumina disk	Microwave seeding and heteroepitaxial growth of ZIF-67 membranes	N/A	N/A	1.0	209	370	[12]
α-alumina disk	Microwave seeding and secondary growth of ZIF-67 membranes	N/A	N/A	1.2	120	204	[13]
α-alumina disk	Rapid microwave seeding and solvent-assisted recrystallization technique	N/A	N/A	0.4	120	125	[14]
BPPO asymmetric support	Counter diffusion method	N/A	N/A	2.0	16	150	[15]
α-alumina tube	Counter-diffusion method	Shell	3000 (OD)	80	59	25	[16]
α-alumina tube	Counter-diffusion method	Shell	3000 (OD)	M2: 30 M3: 20	7.2 20	52 120	[17]
Torlon hollow fiber	Interfacial microfluidic membrane processing (IMMP)	Bore	300 (OD)	8.8	12.1	89	[18]
PBI-BuI-HF	IMMP ZIF-8	Bore/Shell	460/780 (ID/OD)	10 – 25	N/A	N/A	[19]

Table C-3 Continued

Support	Synthesis Method[1]	Bore/Shell	ID/OD (μm)	Thickness (μm)	C_3H_6/C_3H_8 Separation[2]		Ref
					Separation Factor	C_3H_6 Permeance[3]	
Polysulfone hollow fiber	Microfluidic growth method	Bore	315/520 (ID/OD)	3.6	N/A	N/A	20
PVDF hollow fiber	*In situ* growth with immersion technique	Shell	500 /1100 (ID/OD)	1.0	N/A	N/A	21
Torlon hollow fiber	IMMP ZIF-8	Bore	200/300 (ID/OD)	4.5	65	221	22
Torlon hollow fiber	IMMP	Bore	N/A	8.1	180	151	23
PVDF hollow fiber	Gel-vapor deposition	Shell	1400/1600 (ID/OD)	0.087	73	2800	24
Matrimid hollow fiber	Microwave seeding and microfluidic secondary growth	Bore	344/545 (ID/OD)	0.8	45.5	183	This work

[1]Synthesis methods of ZIF-8 membranes are described if otherwise stated (*i.e.*, ZIF-67 or ZIF-90)

[2]Performance data reported by the literature are individually plotted in the Fig. 4 but average and stdev values are only shown in Table S4

[3]Permeance unit: $\times 10^{-10}$ mol m^{-2} s^{-1} Pa^{-1} , unless stated otherwise

C.7 References

(1) Cravillon, J.; Münzer, S.; Lohmeier, S.-J.; Feldhoff, A.; Huber, K.; Wiebcke, M. Rapid Room-Temperature Synthesis and Characterization of Nanocrystals of a Prototypical Zeolitic Imidazolate Framework. *Chemistry of Materials* **2009,** *21* (8), 1410-1412
(2) Shekhah, O.; Swaidan, R.; Belmabkhout, Y.; du Plessis, M.; Jacobs, T.; Barbour, L. J.; Pinnau, I.; Eddaoudi, M. The liquid phase epitaxy approach for the successful construction of ultra-thin and defect-free ZIF-8 membranes: pure and mixed gas transport study. *Chemical Communications* **2014,** *50* (17), 2089-2092
(3) Pan, Y.; Lai, Z. Sharp separation of C2/C3 hydrocarbon mixtures by zeolitic imidazolate framework-8 (ZIF-8) membranes synthesized in aqueous solutions. *Chemical Communications* **2011,** *47* (37), 10275-10277
(4) James, J. B.; Wang, J.; Meng, L.; Lin, Y. S. ZIF-8 Membrane Ethylene/Ethane Transport Characteristics in Single and Binary Gas Mixtures. *Industrial & Engineering Chemistry Research* **2017,** *56* (26), 7567-7575
(5) Pan, Y.; Li, T.; Lestari, G.; Lai, Z. Effective separation of propylene/propane binary mixtures by ZIF-8 membranes. *Journal of Membrane Science* **2012,** *390*, 93-98
(6) Pan, Y.; Liu, W.; Zhao, Y.; Wang, C.; Lai, Z. Improved ZIF-8 membrane: Effect of activation procedure and determination of diffusivities of light hydrocarbons. *Journal of Membrane Science* **2015,** *493*, 88-96
(7) Sheng, L.; Wang, C.; Yang, F.; Xiang, L.; Huang, X.; Yu, J.; Zhang, L.; Pan, Y.; Li, Y. Enhanced C3H6/C3H8 separation performance on MOF membranes through blocking defects and hindering framework flexibility by silicone rubber coating. *Chemical Communications* **2017,** *53* (55), 7760-7763
(8) Kwon, H. T.; Jeong, H.-K. In Situ Synthesis of Thin Zeolitic–Imidazolate Framework ZIF-8 Membranes Exhibiting Exceptionally High Propylene/Propane Separation. *Journal of the American Chemical Society* **2013,** *135* (29), 10763-10768
(9) Kwon, H. T.; Jeong, H.-K. Highly propylene-selective supported zeolite-imidazolate framework (ZIF-8) membranes synthesized by rapid microwave-assisted seeding and secondary growth. *Chemical Communications* **2013,** *49* (37), 3854-3856
(10) Lee, M. J.; Kwon, H. T.; Jeong, H.-K. Toward high-flux zeolitic-imidazolate framework ZIF-8 membranes for propylene/propane separation via post-synthetic linker exchange. *Angewandte Chemie International Edition*,
(11) Lee, M. J.; Kwon, H. T.; Jeong, H.-K. Defect-dependent stability of highly propylene-selective zeolitic-imidazolate framework ZIF-8 membranes. *Journal of Membrane Science* **2017,** *529*, 105-113
(12) Kwon, H. T.; Jeong, H.-K.; Lee, A. S.; An, H. S.; Lee, J. S. Heteroepitaxially Grown Zeolitic Imidazolate Framework Membranes with Unprecedented Propylene/Propane Separation Performances. *Journal of the American Chemical Society* **2015,** *137* (38), 12304-12311
(13) Hillman, F.; Zimmerman, J. M.; Paek, S.-M.; Hamid, M. R. A.; Lim, W. T.; Jeong, H.-K. Rapid microwave-assisted synthesis of hybrid zeolitic-imidazolate frameworks with mixed metals and mixed linkers. *Journal of Materials Chemistry A* **2017,** *5* (13), 6090-6099
(14) Kwon, H. T.; Jeong, H.-K.; Lee, A. S.; An, H. S.; Lee, T.; Jang, E.; Lee, J. S.; Choi, J. Defect-induced ripening of zeolitic-imidazolate framework ZIF-8 and its implication to vapor-phase membrane synthesis. *Chemical Communications* **2016,** *52* (78), 11669-11672

(15) Shamsaei, E.; Lin, X.; Low, Z.-X.; Abbasi, Z.; Hu, Y.; Liu, J. Z.; Wang, H. Aqueous Phase Synthesis of ZIF-8 Membrane with Controllable Location on an Asymmetrically Porous Polymer Substrate. *ACS Applied Materials & Interfaces* **2016,** *8* (9), 6236-6244
(16) Hara, N.; Yoshimune, M.; Negishi, H.; Haraya, K.; Hara, S.; Yamaguchi, T. Diffusive separation of propylene/propane with ZIF-8 membranes. *Journal of Membrane Science* **2014,** *450*, 215-223
(17) Hara, N.; Yoshimune, M.; Negishi, H.; Haraya, K.; Hara, S.; Yamaguchi, T. ZIF-8 membranes prepared at miscible and immiscible liquid–liquid interfaces. *Microporous and Mesoporous Materials* **2015,** *206*, 75-80
(18) Brown, A. J.; Brunelli, N. A.; Eum, K.; Rashidi, F.; Johnson, J. R.; Koros, W. J.; Jones, C. W.; Nair, S. Interfacial microfluidic processing of metal-organic framework hollow fiber membranes. *Science* **2014,** *345* (6192), 72
(19) Biswal, B. P.; Bhaskar, A.; Banerjee, R.; Kharul, U. K. Selective interfacial synthesis of metal-organic frameworks on a polybenzimidazole hollow fiber membrane for gas separation. *Nanoscale* **2015,** *7* (16), 7291-7298
(20) Cacho-Bailo, F.; Catalán-Aguirre, S.; Etxeberría-Benavides, M.; Karvan, O.; Sebastian, V.; Téllez, C.; Coronas, J. Metal-organic framework membranes on the inner-side of a polymeric hollow fiber by microfluidic synthesis. *Journal of Membrane Science* **2015,** *476*, 277-285
(21) Hou, J.; Sutrisna, P. D.; Zhang, Y.; Chen, V. Formation of Ultrathin, Continuous Metal–Organic Framework Membranes on Flexible Polymer Substrates. *Angewandte Chemie International Edition* **2016,** *55* (12), 3947-3951
(22) Eum, K.; Rownaghi, A.; Choi, D.; Bhave, R. R.; Jones, C. W.; Nair, S. Fluidic Processing of High-Performance ZIF-8 Membranes on Polymeric Hollow Fibers: Mechanistic Insights and Microstructure Control. *Advanced Functional Materials* **2016,** *26* (28), 5011-5018
(23) Eum, K.; Ma, C.; Rownaghi, A.; Jones, C. W.; Nair, S. ZIF-8 Membranes via Interfacial Microfluidic Processing in Polymeric Hollow Fibers: Efficient Propylene Separation at Elevated Pressures. *ACS Applied Materials & Interfaces* **2016,** *8* (38), 25337-25342
(24) Li, W.; Su, P.; Li, Z.; Xu, Z.; Wang, F.; Ou, H.; Zhang, J.; Zhang, G.; Zeng, E. Ultrathin metal–organic framework membrane production by gel–vapour deposition. *Nature Communications* **2017,** *8* (1), 406